**Université de la Méditerranée
Aix-Marseille II**

Ecole Doctorale Sciences de l'Environnement

THESE

présentée par

ZiYuan HU
pour obtenir le grade de
DOCTEUR DE L'UNIVERSITE AIX-MARSEILLE II
Discipline : Océanographie Physique

Structures tourbillonnaires à l'ouest du Golfe du Lion : modélisation numérique et mesures en mer

Soutenue le 24 Février 2011 devant le jury composé de :

Mme Claude Estournel	Présidente du jury	LA, Toulouse
Mme Sabrina Speich	Rapporteur	LPO, Brest
Mme Anne Molcard	Rapporteur	LSEET, Toulon
M Ivan Dekeyser	Directeur de thèse	COM, Marseille
Mme Anne Petrenko	Directeur de thèse	LOPB, Marseille
M Andrea Doglioli	Directeur de thèse	LOPB, Marseille

Centre d'Océanologie de Marseille (COM), OSU
Laboratoire d'Océanographie Physique et Biogéochimique (LOPB),
UMR 6535
Campus de Lumniy - Case 901, 13288 Marseille Cedex 09, France

Table des matières

Introduction

Contents

L'océan côtier se joint à l'océan hauturier à travers les marges continentales. Ces marges continentales, malgré leur faible surface et volume (8% et 0,05%) comparés à celles de l'océan global, sont caractérisées par une forte productivité biologique en raison d'un enrichissement en nutriments lié aux apports des fleuves ou à l'anthropisation importante du littoral et suite aux urbanisations croissantes. Les marges continentales, tampons entre les zones côtières et l'océan profond, pourraient contribuer de façon importante aux échanges d'énergie, de carbone et de production biologique entre les deux zones, et ainsi présentent des enjeux scientifiques cruciaux. Divers processus physiques agissant sur la marge continentale, moteurs dans les échanges côte-large, ont été cités par *Huthnance* [1995] : les ondes piégées à la côte, les courants de pente longeant le talus continental, les instabilités des méandres, les fronts et les filaments, les remontées et les descentes d'eau, les marées, les ondes d'inertie et les tourbillons.

En Méditerranée Nord Occidentale, le Golfe du Lion est un site privilégié pour étudier les processus d'échange côte-large impactés par les caractéristiques suivantes présentes sur la marge continentale : une morphologie caractérisée par un large plateau continental suivi d'une pente continentale abrupte intersectée par de nombreux canyons ; des vents continentaux forts induisant des remontées d'eau côtières et des ondes d'inertie ; un apport important d'eau douce par le Rhône ; le Courant Nord Méditerranéen qui longe la pente continentale avec des intrusions et des instabilités ; des tourbillons

de sub-méso à mésoéchelle. Parmi tous ces phénomènes qui participent aux processus d'échange côte-large, les tourbillons ont subi un regain d'intérêt ces dernières années en raison du manque de connaissance de leur influence potentielle sur la distribution des flux biogéochimiques et des flux de CO_2 [*Mémery et al.* 2005]. Les tourbillons anticycloniques de mésoéchelle qui se développent près de la côte du Roussillon, à l'ouest du Golfe du Lion, peuvent induire des transports d'eau importants à travers les talus continentaux et favoriser les processus de mélange. Les courants forts associés aux mouvements rotationnels des tourbillons entraînent vers le large des éléments nutritifs venant de la zone côtière du Roussillon et exportent par un mouvement descendant la matière organique vers les profondeurs. Par ailleurs, les tourbillons sont potentiellement influencés par l'extension distale du panache du Rhône qui peut atteindre cette région sous certaines conditions de vent [*Estournel et al.* 1997] et amener des nutriments dans les tourbillons [*Minas and Minas* 1989; *Ludwig et al.* 2009]. En effet, les interactions entre les tourbillons et le Courant Nord, présentes sur le bord sud-est des tourbillons, peuvent revêtir une importance capitale pour leurs influences sur les échanges côte-large. L'étude du rôle des tourbillons sur les échanges côte-large, nécessite une bonne compréhension de la dynamique des structures tourbillonnaires, en particulier le mécanisme de leur génération qui reste, à notre connaissance, encore mal connu. Cette méconnaissance provient essentiellement de la difficulté à acquérir des mesures *in situ* qui donneraient une vision entière de la structure et rendraient

compte simultanément de la variabilité spatiale et temporelle des processus en jeu. De plus, étant donné la grande variabilité en milieu côtier par rapport au milieu hauturier, les observations *in situ* en zone côtière sont parfois très complexes à interpréter. Par la suite, la modélisation numérique constitue un outil privilégié utilisé par la communauté océanographique depuis une vingtaine d'années.

Le projet LATEX (Lagrangian Transport EXperiment) (2008-2011), dans lequel s'inscrit ce travail de thèse, a été initialisé afin d'étudier les tourbillons côtiers à (sub) mésoéchelle et d'évaluer leur rôle dynamique et leur influence sur les processus biogéochimiques dans les échanges de matière et d'énergie entre les zones côtières et hauturières avec, comme zone d'étude, le Golfe du Lion. La stratégie de ce projet est fondée sur une utilisation combinée de modélisation numérique, d'observations *in situ* et d'observations satellitales. Le modèle 3D côtier à surface libre SYMPHONIE est utilisé afin d'approfondir la connaissance des structures tourbillonnaires dans le Golfe du Lion. SYMPHONIE a été utilisé de façon fort satisfaisante pour l'étude d'un certain nombre de processus présents sur le talus continental du golfe, par exemple : les circulations induites par le vent [Auclair et al. 2003; Estournel et al. 2003; Petrenko et al. 2005, 2008] ; les intrusions du Courant Nord sur le plateau [Auclair et al. 2001; Gatti et al. 2006] ; la formation et les plongées d'eau dense sur le plateau [*Dufau-Julliand et al.* 2004; *Ulses et al.* 2008a,b] ; la propagation du panache du Rhône [Marsaleix et al. 1998; *Estournel et al.* 2001].

La présente thèse est une des premières utilisations du modèle SYMPHO-NIE pour reproduire les tourbillons qui apparaissent dans la partie ouest du Golfe du Lion et d'étudier les différents processus à l'origine de ces structures. Un des objectifs du présent travail est de développer une configuration optimale pour reproduire de façon plus réaliste des tourbillons côtiers de (sub) mésoéchelle dans cette région. Ensuite, à partir des résultats numériques sur les tourbillons et leur présence spatiale et temporelle, des campagnes en mer ont été réalisées. Réciproquement, des observations *in situ*, combinées avec des observations satellitales, ont été utilisées pour valider la modélisation. La combinaison de l'ensemble des données numériques et expérimentales permettra d'évaluer les impacts physiques-bio-géochimiques des structures tourbillonnaires sur les échanges côte-large dans le Golfe du Lion.

Le présent mémoire s'articule autour de cinq chapitres. Le chapitre I donne une description des principales caractéristiques, des processus physiques dans le Golfe du Lion ainsi qu'un bilan des études des structures tourbillonnaires présentes dans cette région. Le chapitre II est consacré au développement d'une configuration idéale, avec des paramétrisations et une résolution appropriées, pour reproduire de façon la plus réaliste possible les tourbillons côtiers de (sub) mésoéchelle dans le golfe. Dans le chapitre III, la stratégie d'échantillonnage et les observations *in situ* des tourbillons sont présentées. Les tourbillons sont mis en évidence et caractéristisés à partir de la modélisation numérique et des observations *in situ*. Dans le chapitre IV,

les mécanismes de génération des tourbillons sont investigués. Finalement, les

conclusion et les perspectives sont présentées dans le chapitre V.

1.1 Le Golfe du Lion et ses forçages

Situation géographique
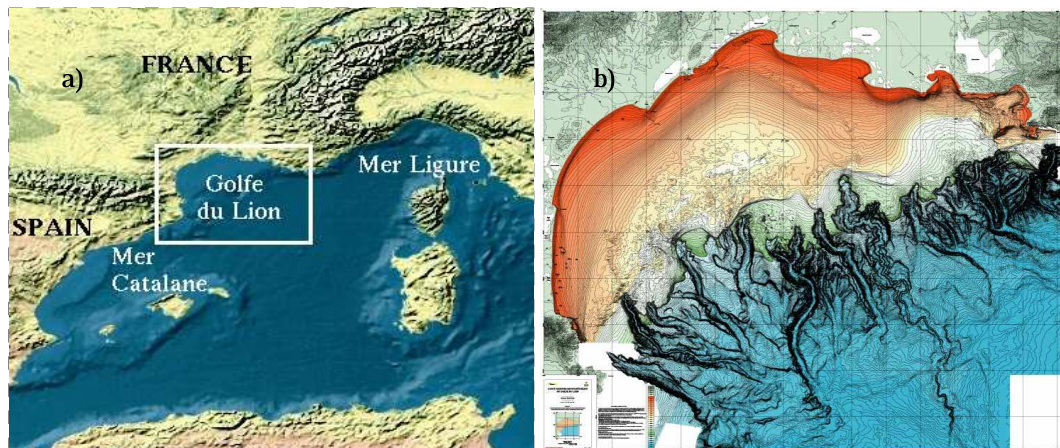
FIG. 1.1 – Localisation (a) et topographie (b) du Golfe du Lion.

Le Golfe du Lion est situé sur la façade méditerranéenne française au nord-ouest du bassin Méditerranéen. C'est le plus grand plateau continental du bassin nord. Il est constitué d'un large plateau en forme de demi-disque qui s'ouvre au sud-ouest sur la Mer Catalane et à l'est sur la Mer Ligure. Il s'étend sur 220 kilomètres d'ouest en est et sur 150 kilomètres du nord au sud (Fig. 1.1-a). Le plateau a une profondeur moyenne de 80 mètres, ce qui est faible. Le talus continental est entaillé par de nombreux canyons sous-marins (Fig. 1.1-b). Ces canyons jouent un rôle important dans l'hydrodynamique du Golfe du Lion car ils influencent la circulation dans le golfe. La plaine abyssale, dont la profondeur dépasse les 2500 mètres, s'étend au pied du talus.

Le Golfe du Lion, zone de transition entre le continent et la mer du large, est une zone d'étude riche et complexe. La circulation est essentiellement influencée par les apports fluviaux, les vents et le Courant Nord (Fig. 1.2).
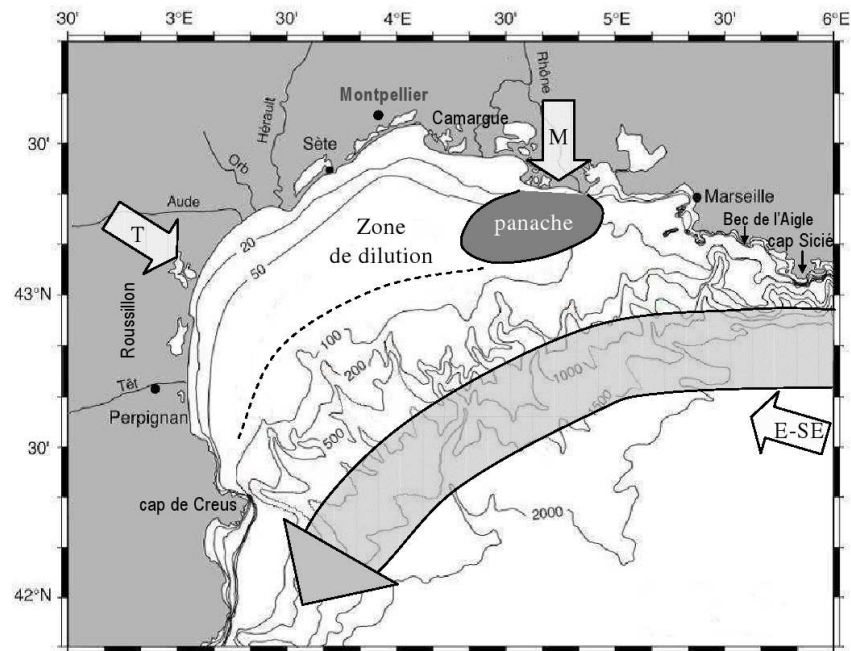
Fig. 1.2 – Carte du Golfe du Lion (Extrait de [*Gatti* 2008]) sur laquelle sont indiqués : les 3 secteurs principaux de vent(flèches blanches) : E-SE, le Mistral (M) et la Tramontane (T) ; le panache (zone grise foncée) ; la zone de dilution (délimitée par des pointillés) du Rhône ; le Courant Nord (flèche grise).

Apports fluviaux

Les apports fluviaux du Golfe du Lion proviennent de 5 fleuves principaux : le Rhône, l'Aude, l'Hérault, l'Orb et la Têt, classés par ordre décroissant de débit [*Ludwig et al.* 2009]. Le Rhône avec un débit moyen de l'ordre de 1700 m^3s^{-1} [*Thill et al.* 2001], pouvant dépasser 5000 m^3s^{-1} en période de crue au

printemps et à l'automne, est le principal fleuve de la Méditerranée. C'est la source majeure d'eau douce depuis la construction du barrage d'Assouan sur le Nil. Le Rhône constitue 90% des apports d'eau douce du Golfe du Lion. Ces eaux continentales apportent des éléments nutritifs favorables à la production biologique dans le milieu marin où il est oligotrophe. Le Rhône joue donc de ce point de vue un rôle important et majeur dans cette région. Près de son embouchure, les eaux du Rhône forment dans le bassin récepteur un panache qui, sauf conditions météorologiques particulières, se dirige vers l'ouest sous l'effet de la force de Coriolis. L'extension horizontale et l'épaisseur de la couche d'eau formant le panache dépendent des conditions météorologiques et des circulations environnantes. Lors d'un épisode de Mistral et de Tramontane, le panache s'étend vers le sud-ouest et se mélange intensément avec les couches sous-jacentes [*Broche et al.* 1998]. La zone de dilution peut s'étendre jusqu'aux côtes Roussillonnaises. Lorsque le vent de sud-est souffle, le panache du Rhône est confiné et plaqué à la côte [*Estournel et al.* 1997]. Lorsque les vents sont relativement faibles, le panache s'arrondit et suit la côte vers l'ouest. Gatti et al. [2006] ont montré que, lors de la présence des vents d'est, le panache du Rhône peut se diriger vers l'est, remontant jusqu'à la région marseillaise.

Les vents

Le Golfe du Lion, région la plus ventée de toute la Méditerranée, est soumis

à trois régimes de vents dominants. Les deux premiers sont des vents contientaux : le Mistral et la Tramontane, qui sont canalisés par les reliefs alentours. Le Mistral est un vent du nord, formé dans l'axe de la vallée du Rhône entre le Massif Central et les Alpes, tandis que la Tramontane est un vent du nordouest, canalisé entre les Pyrénées et le Massif Central. Ces deux vents soufflent en moyenne un jour sur deux pour la Tramontane et un jour sur trois pour le Mistral avec grande variabilité saisonnière. En hiver, ils sont plus intenses avec une vitesse moyenne de 15 à 25 ms^{-1} et durent plus longtemps. En été, leur vitesse moyenne est de 10 à 15 ms^{-1} et ils durent rarement plus de 4 jours [*Millot* 1990; *Guénard* 2004]. Le troisième vent est un vent de secteur est, sud-est d'origine marine, qui peut souffler violemment de l'automne jusqu'au printemps. Il est moins fréquent que les vents continentaux et souvent amène nuages et pluies sur le Golfe du Lion.

Ces vents locaux ont de fortes influences sur la variabilité de la dynamique côtière avec des échelles de temps allant de quelques heures à quelques jours. Le Mistral et la Tramontane engendrent des remontées d'eau (upwellings) et de descentes d'eau (downwellings) le long de la côte du golfe [*Millot* 1979]. Lorsque le milieu marin est stratifié, les forts épisodes de Mistral et de Tramontane, qui ont des directions stables mais dont la vitesse a une variation temporelle très intense, peuvent générer des oscillations d'inertie sur le plateau [*Millot and Crépon* 1981; *Broche et al.* 1998; Petrenko 2003]. En hiver, ces vents continentaux secs, froids et violents entraînent une forte

évaporation et un refroidissement important qui augmentent la densité de l'eau de surface [*Dufau-Julliand et al.* 2004; *Ulses et al.* 2008a,b].

Le Courant Nord

Le Golfe du Lion est bordé par un courant permanent s'écoulant en profondeur de la Mer Ligure vers la Mer Catalane le long du talus continental. Branche nord de la circulation générale dans le bassin méditerranéen occidental, ce courant précédemment appelé courant Liguro-Provençal-Catalan a été nommé Courant Nord par *Millot* [1991]. C'est un courant de densité en équilibre géostrophique. Il sépare les eaux plus légères du plateau des eaux plus denses du large et présente une forte variabilité saisonnière [*Albérola et al.* 1995; *Conan and Millot* 1995; *Albérola and Millot* 2003; Petrenko 2003]. En hiver, le Courant Nord est plus étroit (environ 25 kilomètres), rapide (0.6-0.8 ms^{-1}), plus profond (environ 250-300 mètres) et s'approche de la côte. En été, il est plus au large (environ 30-50 kilomètres), plus lent (0.3-0.5 ms^{-1}) et moins profond (inférieur à 250 mètres).

Le Courant Nord présente une grande variabilité mésoéchelle en hiver quand le courant devient plus instable. Des études sur ces phénomènes mésoéchelles ont été effectuées : au large de Nice par *Albérola et al.* [1995] et *Sammari et al.* [1995] ; au large de Marseille par *Conan and Millot* [1995] et dans le Golfe du Lion par *Flexas et al.* [2002] et Petrenko [2003]. Le développement de méandres à l'interface d'un courant avec le milieu océanique

environnant est généralement lié à des deux types d'instabilités : les instabilités barotropes liées au cisaillement horizontal du courant et dues à une transformation en l'énergie cinétique du courant en énergie de perturbation à mésoéchelle ; les instabilités baroclines liées au cisaillement vertical du courant et dues à un transfert d'énergie potentielle du courant. La loi de conservation de la vorticité potentielle implique que la variation topographique induit une variation de la vorticité relative du fluide qui peut permettre le développement d'instabilités barotropes et/ou baroclines au sein du courant.

Suite à l'interaction avec l'un ou plusieurs des forçages précédemment évoqués, associé à la morphologie du talus continental, le Courant Nord peut se séparer en deux branches. La branche principale suit la pente continentale et la branche secondaire pénètre sur le plateau en franchissant les isobathes. Ces intrusions du Courant Nord ont été observées à l'entrée est du Golfe du Lion [Millot and Wald 1980; *Albérola and Millot* 2003; Petrenko 2003; Petrenko et al. 2005; Gatti et al. 2006], au centre du golfe [Estournel et al. 2003; Petrenko 2003; Petrenko et al. 2005; *Leredde et al.* 2007] et à l'ouest du golfe [Petrenko 2003; Petrenko et al. 2008]. Les mécanismes des intrusions sont associées aux conditions de vent, de stratification et à l'effet bathymétrique [Petrenko 2003; Petrenko et al. 2005; *Echevin et al.* 2003; Estournel et al. 2003; *Langlais* 2007].

1.2   Les tourbillons dans le Golfe du Lion

Des structures tourbillonnaires cycloniques et anticycloniques ont été observées dans le Golfe du Lion par divers moyens : images satellitales (Sea-WiFs, MODIS et AVHRR), radars, flotteurs Lagrangiens, courantomètres. Elles sont aussi mises en évidence par des simulations numériques.

Tourbillons au nord
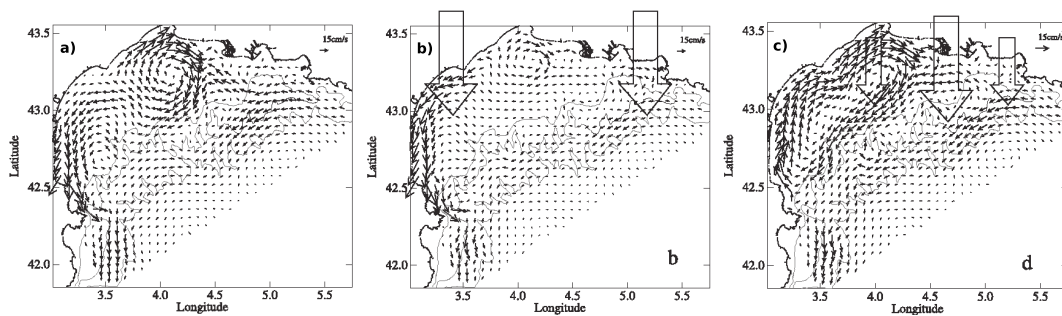
FIG. 1.3 – Champs de courant moyenné en profondeur : a) réaliste, 16 Mars, 1998 ; b) académique avec un vent du nord homogène sur tout le domaine ; c) académique avec un vent du nord non-homogène (Mistral). (Extrait de [Estournel et al. 2003])

Estournel et al. [2003] ont observé, dans les résultats numériques issus de la modélisation de l'expérience FETCH (Mars 1998), un tourbillon anticyclonique au nord du plateau et une circulation cyclonique à l'ouest (Fig. 1.3-a). Elle a par ailleurs mis en évidence, à l'aide de simulations académiques, que des vents du nord, homogènes et non-homogènes, pouvaient

créer des structures anticycloniques au nord du plateau. Des vents du nord homogènes (Fig. 1.3-b) favorisent le développement d'un upwelling le long de la côte nord, et d'un downwelling le long de la côte ouest. Une petite circulation tourbillonnaire anticyclonique au nord se produit pour compenser la forte divergence de la vitesse du courant entre les deux zones upwelling et downwelling. Le Mistral (Fig. 1.3-c) avec son rotationnel négatif sur le plateau, quant à lui induit une circulation tourbillonnaire de type anticyclonique dans la partie nord du Golfe du Lion.

Tourbillons à l'est

A l'est du Golfe du Lion, au sud de Marseille, pendant les campagnes ECOLOPHY, *Allou et al.* [2010] ont observé des tourbillons anticycloniques entre le Courant Nord et la côte en utilisant des données *in situ* de courantométrie, des données fournies par des radars HF (haute fréquence) installés à la côte, ainsi que des données de télédétection de SST (Sea Surface Temperature) (Fig. 1.4-a). *Allou et al.* [2010] ont montré que ces tourbillons sont souvent dissymétriques, avec une taille allant de 12 à 28 km en diamètre, et une vitesse tangentielle maximale de l'ordre de grandeur de la vitesse du Courant Nord durant la période d'observation. L'extension verticale des tourbillons s'étend sur toute l'épaisseur d'eau. Ces structures barotropes sont partiellement advectées par le Courant Nord vers l'ouest du plateau avec
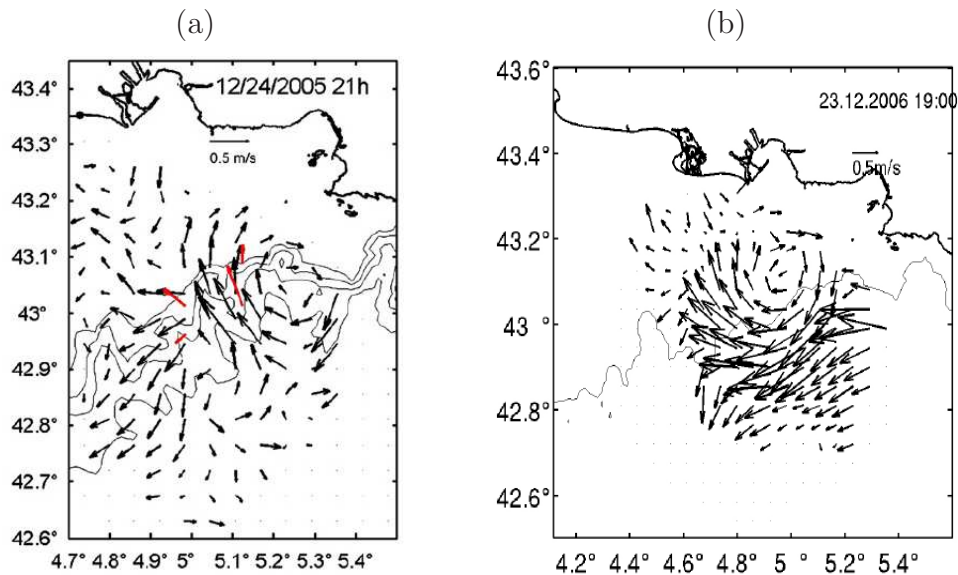
FIG. 1.4 – (a) : courants mesurés par radars HF (flèches noires) et par mouillages (flèches rouges) à 50 mètres, le 24 décembre 2005 ; lignes fines : isobathes à 150, 200, 500, 1000 mètres (Extrait de *Allou et al.* [2010]) ; (b) : courants de surface mesurés par radars HF ; isobathe à 130 mètre (Extrait de *Schaeffer* [2010]).

des vitesses de dérive de l'ordre 0.2 ms^{-1}, vitesses plus faibles que celles présentes dans le cœur du Courant Nord. Les études de *Flexas et al.* [2002] suggèrent que ces tourbillons anticycloniques sont générés par les instabilités du Courant Nord à l'est du Golfe du Lion. Dans les études de *Rubio et al.* [2005] sur les tourbillons au large de l'Espagne, une des hypothèses sur l'origine des tourbillons anticycloniques en mer Catalane est qu'ils seraient formés à l'est du Golfe du Lion puis advectés par le Courant Nord dans la mer Catalane. Cette hypothèse a été rejetée par la suite [*Rubio et al.* 2009]. *Schaeffer* [2010] a aussi observé des tourbillons anticycloniques dans le Golfe
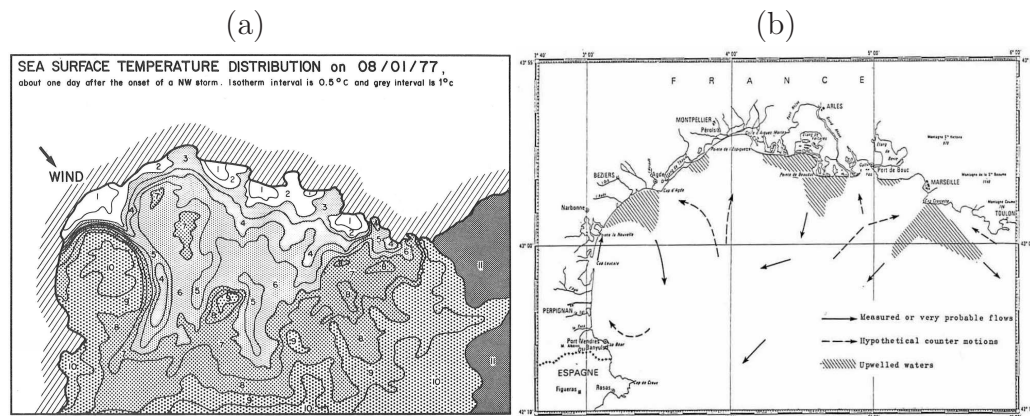
FIG. 1.5 – (a) : Température de surface le 1er Août 1977 à 09 00 TU (Extrait de *Millot* [1982]) ; (b) : Schéma de la circulation de surface induite par le vent d'après l'analyse des vues satellitales et de mesures *in situ* ; les flèches pleines représentent des courants mesurés par courantomètrie ; les flèches discontinues sont des courants hypothétiques (Extrait de *Millot* [1979]).

du Lion au large de Marseille à l'aide des radars HF (Fig. 1.4-b) et dans les résultats de simulations numériques. Elle a montré que les mécanismes de leur génération sont fortement liées aux conditions de vent.

Tourbillons à l'ouest

Une circulation tourbillonnaire anticyclonique à l'ouest du Golfe du Lion a été évoquée pour la première fois par *Millot* [1979, 1982] à partir de données satellitales (Fig. 1.5-a) et courantologiques (Fig. 1.5-b). L'apparition de cette structure fait suite à la présence d'un upwelling au sud du Cap d'Agde après une forte Tramontane. *Millot and Wald* [1981] suggèrent qu'un épisode de Tramontane créant un upwelling à l'ouest du Golfe du Lion, une circulation

de type anticyclonique pourrait se développer dans la couche de surface afin de compenser le transport off-shore. Petrenko et al. [2008] ont montré, à l'aide de simulations numériques académiques, que les rotationnels d'une Tramontane favorisent le développement d'une circulation anticyclonique dans la partie nord et une circulation cyclonique sur la partie ouest du plateau du Golfe du Lion.

Parmi toutes les structures tourbillonnaires précédemment étudiées dans le Golfe du Lion, ce sont les tourbillons anticycloniques qui durent le plus longtemps. Cela est probablement du au fait que, lorsque le Courant Nord s'écoule d'est en ouest le long du talus du plateau du Golfe du Lion, les instabilités présentes sur son bord interne favorisent le développement des vorticités anticycloniques [*Flexas et al.* 2002]. Les structures anticycloniques présentes sur le plateau du golfe pourraient être alimentées par ce phénomène et, par conséquence, avoir des durées de vie plus longues que les tourbillons cycloniques.

Par la suite, dans le cadre des travaux de cette thèse, nous nous intéressons aux tourbillons anticycloniques présents dans la partie ouest du Golfe du Lion. Par rapport aux tourbillons observés à l'est et au nord sur le plateau, les structures tourbillonnaires localisées à l'ouest ont en général une taille plus grande. Comme mentionné précédemment, ils peuvent intéagir avec l'extension distale du panache du Rhône et le Courant Nord. Ils pourraient avoir un impact im-

portant sur les échanges côte-large dans le Golfe du Lion. Il est donc nécessaire d'avoir une bonne connaissance de leur dynamique, ainsi que des mécanismes de leur génération.

1.3 Objectifs et stratégies

Les objectifs de la présente thèse sont de caractériser les tourbillons anti-cycloniques à l'ouest du Golfe du Lion et de comprendre les processus de leur génération, en utilisant à la fois la modélisation numérique et les données *in situ*.

La première partie de ce travail a été de développer une meilleure configuration du modèle SYMPHONIE pour reproduire les tourbillons de (sub) mésoéchelle dans le Golfe du Lion. Les résultats des tests de sensibilité effectués sur la résolution du modèle et les termes de diffusion horizontale, connus pour leur rôle clé dans la dissipation d'énergie et les instabilités numériques, sont présentés. Les images satellitales seront utilisées pour valider les résultats du modèle et choisir la meilleure paramétrisation. L'analyse des résultats du modèle permetd'avoir une connaissance améliorée des tourbillons. Cette partie de travail fait l'objet du chapitre 2.

Puis, la deuxième partie a consisté en l'analyse des données acquises pendant la campagne en mer *Latex08*, qui s'est déroulée au début du mois de septembre 2008 et qui était dédiée à l'observation des tourbillons anticyclo-

niques à l'ouest du Golfe du Lion (chapitre 3). Cette campagne a été orga-
nisée en fonction des caractéristiques des tourbillons révélés par les simulations
numériques. Les caractéristiques du tourbillon observé *in situ* sont confrontées
à celles déduites des résultats du modèle. L'utilisation conjointe de ces deux
types d'approche servent à améliorer et approfondir notre connaissance sur
les tourbillons présents dans la partie ouest du Golfe du Lion.

Enfin, la dernière partie de ce travail est de comprendre les processus
de génération des tourbillons anticycloniques présents à l'ouest du Golfe du
Lion (chapitre 4). Les simulations numériques, avec la meilleure configuration
retenue pour le modèle, ont été réalisées sur une longue période allant de 2001
à 2008. La reproductibilité des tourbillons sera analysée afin de comprendre le
mécanisme de leur génération. Les différences interannuelles observées seront
analysées et discutées (chapitre 4).

Numerical simulations of eddies

in the Gulf of Lion

Contents

Résumé

L'objet de cette première partie de thèse a deux objectifs : i) trouver une configuration appropriée du modèle numérique *SYMPHONIE* pour une reproduction réaliste des structures tourbillonnaires anticycloniques de mésoéchelle, qui ont été observées assez souvent dans les images satellitales, dans la partie ouest du Golfe du Lion ; ii) accroitre notre connaissance sur leurs caractéristiques. Une simulation à haute résolution (1km) restreinte au Golfe du Lion, imbriquée dans une simulation à basse résolution (3km) étendue sur toute la région nord-ouest du bassin Méditerranéen, avec un forçage de la simulation à basse résolution vers celle à haute résolution (one-way nesting) a été effectuée. Le schéma d'advection-diffusion utilisé est un schéma de type "upwind centré" dont le terme diffusif est ajusté par un coefficient d'atténuation qui varie entre 0 et 1. Plusieurs tests de sensibilité sur la résolution du modèle et sur la valeur du coefficient d'atténuation ont été effectués afin d'optimiser la reproduction des tourbillons côtiers observés dans la partie ouest du Golfe du Lion. Une technique d'analyse en ondelettes a été appliquée aux champs de vorticité relative calculés à partir des sorties du modèle pour identifier et suivre les structures tourbillonnaires dans le Golfe du Lion. Elle permet d'obtenir la surface, la position, en particulier le centre, et la durée de vie des tourbillons étudiés. Une comparaison quantitative entre les surfaces des tourbillons simulés numériquement et celles des tourbillons observés dans les

images satellitales a permis de valider les résultats du modèle et de choisir la meilleure configuration pour reproduire les structures tourbillonnaires de mésoéchelle dans la partie ouest du Golfe du Lion. La description de la configuration d'étude et les résultats obtenus ont fait l'objet d'une publication dans *Ocean Modelling*. Le texte de l'article est reproduit ci-après.

Numerical simulations of eddies in the Gulf of Lion

Hu, Z. Y., Doglioli, A. M. Petrenko, A. A., Marsaleix, P., Dekeyser, I., 2009 : **Numerical simulations of eddies in the Gulf of Lion**. Ocean Model. 28 (4), 203 - 208.

Abstract

We present realistic simulations of mesoscale anticyclonic eddies, present in the western side of the Gulf of Lion and generally observed in satellite imagery during July and August. A nested model of 1-km resolution covering the Gulf of Lion is implemented from a coarse model of 3-km resolution. The models use an upwind-type advection-diffusion scheme, in which the numerical diffusion term is adjusted by an attenuation coefficient. Sensitivity tests have been carried out, varying the model spatial resolution and the attenuation coefficient to reproduce the (sub)mesoscale structures. A wavelet technique is applied to analyze the modelled horizontal relative vorticity in order to define the area, position and tracking duration of the eddy structures. Comparisons between the modelled eddies and those observed by satellite have allowed us to choose the best model setup. With this setup, the studied anticyclonic eddy lasted for 60 days.

2.1 Introduction

The Gulf of Lion (hereafter GoL), is located in the northwestern Mediterranean Sea (Fig. 2.2). This large continental shelf has approximatively the shape of a semi-circle with a 100 km radius. Its continental slope is cut by numerous canyons. Three main forcings of the shelf circulation are : i) the strong northerly and northwesterly continental winds (the Mistral and the Tramontane) ; ii) the Northern Current (hereafter NC) which represents the northern branch of the cyclonic circulation of the western Mediterranean basin and flows along the continental slope from the Ligurian Sea to the Catalan Sea [*Millot* 1990] ; iii) the Rhône River which is the main fresh water source of the GoL. A general description of the hydrodynamics of the GoL is provided by *Millot* [1990]. He was the pioneer in describing an anticyclonic circulation in the western part of the gulf following upwelling phenomena and an offshore drift of surface water (Fig. 2.1) [*Millot* 1979, 1982]. In both data and model, Estournel et al. [2003] showed an anticyclonic eddy located at the center of the GoL continental shelf or an anticyclonic circulation covering the western and center parts of the GoL. The eddy-like structures in the western part of the GoL, potentially influenced by the distal plume extension of the Rhône river, could play an important role in the shelf-offshore transport of nutrients and phytoplankton because of the presence of the NC nearby. However, to our knowledge, no one has yet studied and modelled the dynamics of the
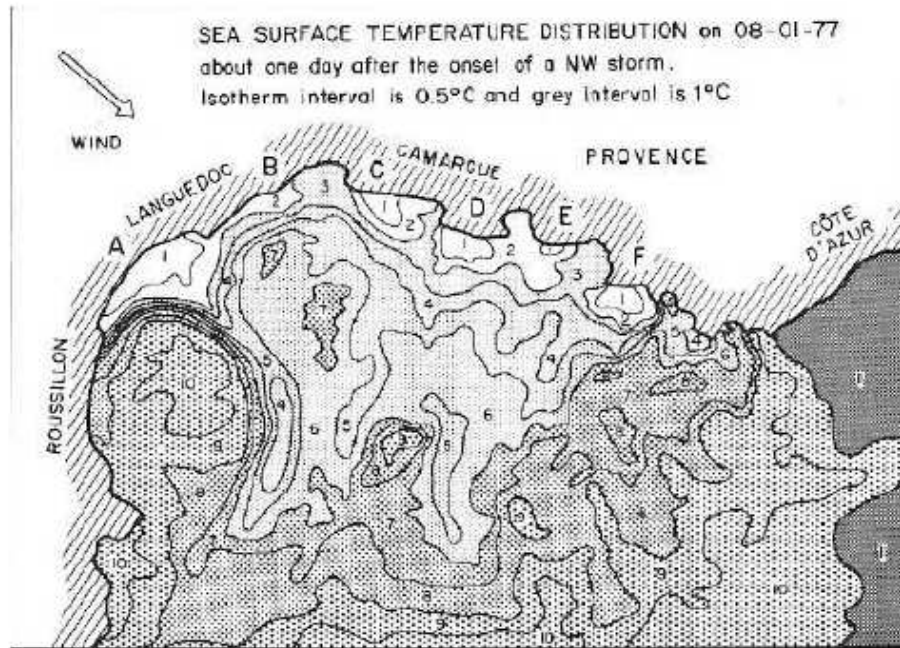
FIG. 2.1 – Infrared thermography on the August 1, 1977 at about 09 00 TU. [From *Millot* 1982]

eddy structures in this area. Hence, the LAgrangian Transport EXperiment (LATEX) projet (2008-2011) has been initiated in order to study the role of (sub)mesoscale (5-25 km) structures on shelf-offshore exchanges in this area. The LATEX strategy combines use of data from an inert tracer release (SF_6), Lagrangian drifters, satellites and Eulerian moorings with numerical modelling. In this framework, starting from regional numerical model [Estournel et al. 2007; Bouffard et al. 2008], we implemented a nested high-resolution shelf-scale model to reproduce accurately the processes on the shelf at the (sub)mesoscale. We paid special attention to two aspects of the model : the spatial grid resolution and the diffusion numerical scheme. The latter is known
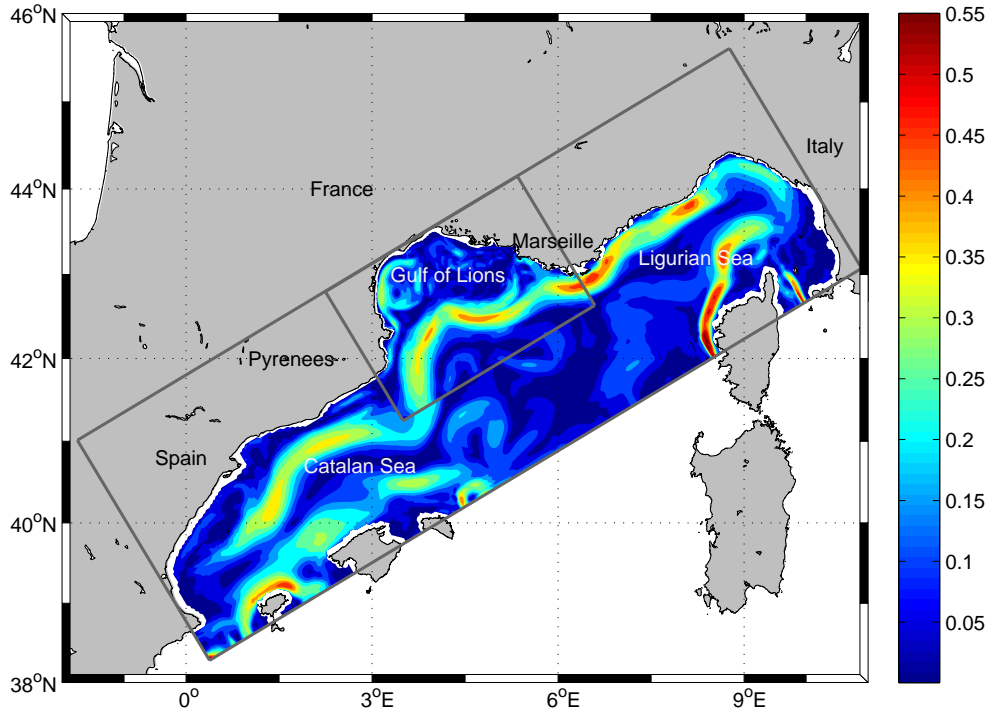
FIG. 2.2 – Model domains. The larger (smaller) rectangle represents the model domain of the 3-km (1-km) resolution. Shaded color represents the intensity of the modelled horizontal current [m s^{-1}] at 20-m depth on July 25, 2001.

to play a key role because it controls the dissipation of the model energy and prevents the generation of numerical instabilities.

In this paper we present the first results of a sensitivity study that allow us to find the best model setup to reproduce anticyclonic eddies in the western side of the GoL. Our numerical results are validated by a qualitative comparison with satellite imagery.

2.2   Methods

Symphonie, the model used for the present study, is a 3-D primitive equation, free surface, sigma coordinate ocean model, based on Boussinesq and hydrostatic approximations. Components of current, temperature and salinity are computed on an Arakawa-C grid using a classic finite difference method detailed in *Marsaleix et al.* [2006]; Marsaleix et al. [2008]. The vertical turbulence closure is achieved through a prognostic equation for the turbulent kinetic energy and a diagnostic equation for the mixing and dissipation length scales [Gaspar et al. 1990]. During the last ten years, the Symphonie has been used widely and successfully by the coastal ocean modeling community. The realistic simulations of this model have contributed to the study of : i) the wind-induced circulations in the GoL [Auclair et al. 2003; Estournel et al. 2003; Petrenko et al. 2005, 2008] ; ii) the intrusion of the NC onto the continental shelf [Auclair et al. 2001; *Gatti* 2008] ; iii) dense-water formation and cascading phenomena over the continental shelf [*Dufau-Julliand et al.* 2004; *Herrmann and Somot* 2008; *Herrmann et al.* 2008; *Ulses et al.* 2008a,b] and iv) the Rhône river plume circulation [Marsaleix et al. 1998; *Estournel et al.* 2001].

For this work, a coarse model extends throughout the northern part of the western basin of the Mediterranean sea with a horizontal resolution of 3 km, while a nested model focuses on the GoL with a horizontal resolution

of 1 km (Fig. 2.2). These values respect the grid ratio proposed by *Spall and Holland* [1991] and are smaller than the Rossby radius of this area (15 km suggested by *Grilli and Pinardi* [1998]). A one-way nesting, described in [*Ulses et al.* 2005], is adopted. Realistic simulations are run over the whole 2001 year, which is of special interest since both satellite data used in this paper (Fig. 2.3a) and cruise data (not shown in this paper) are available. Data from the weather-forecast model Aladin with a high spatial (0.1° x 0.1°) and temporal (3h) resolution are used as meteorological forcings. The air-sea fluxes are estimated thanks to bulk formulae [Estournel et al. 2007]. The large scale field from a general circulation model of the mediterranean sea (OGCM) is applied as an inital state of the presented simulations and is used to force the Symphonie model. Daily fluxes of fresh water supplied by the major rivers (Rhône, Hérault, Aude and Orb) constitute the river input (data from the *Compagnie Nationale du Rhône* and the *Directions Départementales de l'Équipement*).

In the following, a short description of the advection-diffusion scheme is given to introduce the reader to the meaning of our sensitivity study. Momentum equations use an upwind advection scheme. As shown by *James* [1996], the standard upwind scheme can be written as the combination of a centered advection scheme and a Laplacian type dissipation term, in which the viscosity coefficient is given by :

$$A = |u|\frac{\Delta x}{2} \tag{2.1}$$

where u and Δx are respectively the current component and the grid mesh size related to the Ox axis.

Combined with a Leapfrog time-stepping technique, the advection-diffusion scheme becomes :

$$\frac{\phi_i^{t+\Delta t} - \phi_i^{t-\Delta t}}{2\Delta t} = -\frac{u_{i+1/2}^t}{\Delta x}\frac{\phi_i^t + \phi_{i+1}^t}{2} + \frac{u_{i-1/2}^t}{\Delta x}\frac{\phi_i^t + \phi_{i-1}^t}{2}$$
$$+ \frac{A_{i+1/2}}{\Delta x}\frac{\phi_{i+1}^{t-\Delta t} - \phi_i^{t-\Delta t}}{\Delta x} - \frac{A_{i-1/2}}{\Delta x}\frac{\phi_i^{t-\Delta t} - \phi_{i-1}^{t-\Delta t}}{\Delta x} \tag{2.2}$$

where ϕ is any of the two horizontal current components, Δt the model time step and i the horizontal Ox grid index (for the sake of clarity, discretization related to the Oy and Oz grid axes is intentionally omitted). The first two terms of the right hand of Eq.(2.2) correspond to advection processes and the last two terms to diffusion processes. In the diffusion terms, we use the values obtained at the previous time step $(t - \Delta t)$ for numerical stability reasons, while, in the advection terms, we use the current time step (t) for energy conservation reasons [Marsaleix et al. 2008]. The value of the horizontal viscosity coefficient provided by Eq.(2.1) can be quite large. With the size of the coarse horizontal mesh (3 km), a current of only 0.01 ms^{-1} induces a viscosity

coefficient of 15 m^2s^{-1}. In a realistic context with much stronger currents, the energy dissipation using an upwind advection scheme probably becomes excessive. However, the opportunity to prevent the development of numerical instabilities through an increase of energy dissipation is rather attractive and pleads for an upwind-type advection-diffusion scheme. A compromise can be found in using an attenuated value of Eq.(2.1), namely :

$$\tilde{A} = \delta \cdot |u| \frac{\Delta x}{2} \qquad (2.3)$$

The value of the non-dimensional coefficient δ varies between 0 and 1. When $\delta = 0$, the dissipative effect is cancelled ; when $\delta = 1$, the dissipation is totally taken into account.

Table 1 summarizes the numerical experiments. *exp0*, *exp1* and *exp2* represent the simulations of the northern part of the western basin of the Mediterranean Sea with 3-km resolution. *exp3* and *exp4* are the nested simulations of GoL with 1-km resolution. In the first experiment(*exp0*), the horizontal viscosity coefficient has been fixed equal to 15 m^2s^{-1} following *Dufau-Julliand et al.* [2004] and Estournel et al. [2007]. Then, we performed two experiments in which, for a fixed resolution of 3 km, we varied the δ value : 0.2 in *exp1* and 0.8 in *exp2*. Analogously, we performed two experiments for a fixed resolution of 1 km with $\delta = 0.2$ in *exp3* and $\delta = 0.8$ in *exp4*. For the sake of simplicity, in *exp3* and *exp4*, the two nested models are forced by the same coarse model :

exp1.

Then, to objectively analyze all simulation results, we use wavelet analysis, which is a useful and powerful tool. Indeed, wavelets have been applied, for the ocean, to the numerical resolution of Kelvin and Rossy waves [*Jameson and Miyama* 2000] and to time-evolving structures such as eddies and fronts described by numerical modeling or by satellite data [*Luo and Jameson* 2002]. In this work we applied the method developed by *Doglioli et al.* [2007], based on wavelet analysis of horizontal slices of modelled relative vorticity, to identify and to track the localized structures. First, the wavelet technique extracts eddy structures from model gridcells. The area of identified structure is calculated as the sum of gridcell areas. The center of eddies is defined as the gridpoint of local maximum in absolute relative vorticity over the eddy area. Then, for an eddy identified at a specific time (*t*), time tracking can be performed both backward (*t-1*) and forward (*t+1*) in time until a certain criterion cannot be satisfied, which stops the analysis. The reader is referred to *Doglioli et al.* [2007] for more details. The 'birth' and 'death' of the eddy correspond to the last instant of the backward and forward tracking respectively. The eddy life is computed in this way and a time series of eddy area is obtained to provide useful information on the evolution of the shape of the eddy. In this present work, analysis is performed at 20-m depth because it is the operational depth (SF_6 release and Lagrangian drifters anchoring) chosen for the future LATEX cruises scheduled to take place in September. Indeed,

experiment code	resolution [km]	δ [non-dimensional]	eddy area mean $\pm$ std [km^2]	tracking duration [days]
exp0	3	* $\tilde{A} = 15$ [m^{2}s^{-1}]	1035 $\pm$ 407	42
exp1	3	0.2	950 $\pm$ 398	33
exp2	3	0.8	1853 $\pm$ 1753	45
exp3	1	0.2	694 $\pm$ 446	70
exp4	1	0.8	1193 $\pm$ 543	56

TAB. 2.1 – Summary of numerical experiment setups and results.
* N.B : here, the horizontal viscosity coefficient is taken as a fixed value and, hence, does not contain the attenuation coefficient δ.

this depth generally corresponds to half the depth of the mixed layer at that period. The eddy area at 20-m is averaged and the corresponding standard deviation is calculated over the tracking duration (Table 1). The latter is not only used as a mean error but also provides insight on the variability of the eddy.

2.3 Results and discussions

Figure 2.2 shows imbricated horizontal slices of the modelled current intensity on July 25, 2001 at 20-m depth for *exp1* (3 km) over the large domain minus the GoL and *exp4* (1 km), in the GoL. The continuation of the NC at the northeastern and southwestern boundary edges of the nested model shows that the nesting works very well. The major features in the GoL such as the NC, eddies and filaments are reproduced very well. Indeed, the NC's width, depth, velocity and meanders with its seasonal variations (not shown here) are
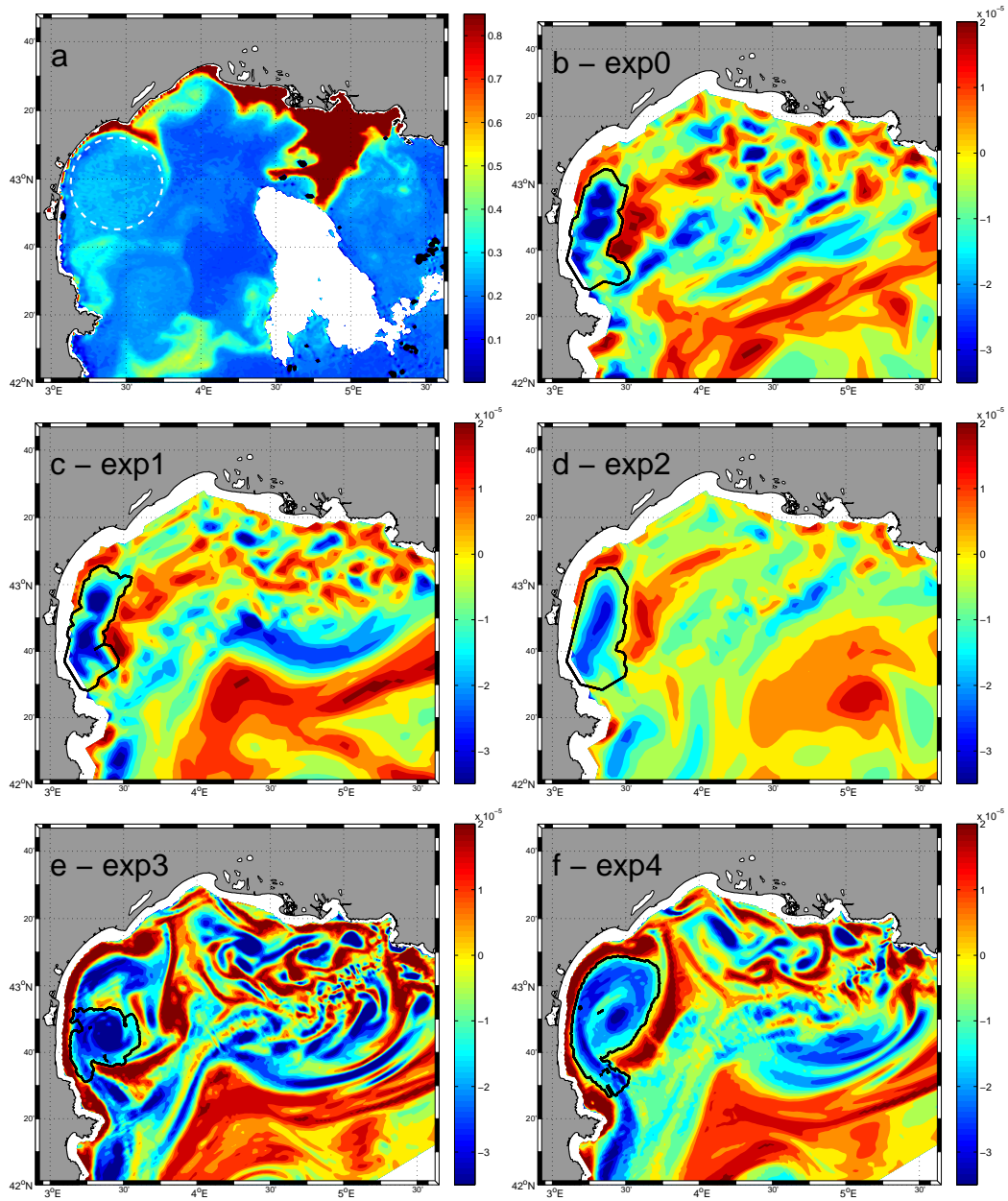
FIG. 2.3 – Comparison of the signature of the anticyclonic eddy on a chlorophyll a [mg m^{-3}] map and the eddy, as identified by the wavelet analysis (contour black) of simulated relative vorticity [s^{-1}] on July 25, 2001. a) Sea-WiFs image processed with OC4 (courtesy E.Bosc); the dashed white circle represents the eddy area. Relative vorticity at 20-m depth from simulations b) *exp0*, c) *exp1*, d) *exp2*, e) *exp3* and f) *exp4*. See text for more explanations.

comparable to previous measurements [*Millot* 1990; *Conan and Millot* 1995; *Albérola and Millot* 2003; Petrenko 2003; Petrenko et al. 2005]. In the relative vorticity field, anticyclonic (cyclonic) features appear in the NC's internal (external) edge (Fig. 2.3b-f). Among all the (sub)mesoscale structures reproduced in the model, special attention is given here to an intense anticyclonic eddy frequently observed in the western side of the GoL. This anticyclonic eddy is clearly observed in the chlorophyll *a* concentrations derived from satellite data (Fig. 2.3a). Moreover, this structure corresponds well, in position and size, to the one observed at the same period of the year in SST satellite images by *Millot* [1982] and reproduced here in Fig. 2.1.

Our simulations successfully reproduce this eddy. In all simulation results, the wavelet analysis tracks this eddy from its 'birth' (mid of July 2001 for 3-km simulations ; end of June 2001 for 1-km simulations), to its 'death' (mid of August 2001). In fact, the simulation results show that, at the middle of August (the end of the eddy's life), the anticyclonic eddy approaches the Northern Current and interacts with it. Such interaction can be considered fatal to the eddy and brings its collapse. The eddy has a much stronger signal throughout his life compared to other modelled structures of the shelf. Nevertheless non negligible differences appear between simulations. These differences are due to both the model spatial resolution and the attenuation coefficient δ. Hence, in the following, we will present : i) the influence of the model spatial resolution and ii) of the attenuation coefficient, and iii) the validation of the best model

configuration for eddies' simulation.

Firstly, we study the influence of the spatial resolution. Fig.2 shows that more small-scale processes are resolved, as expected, in the refined simulations. The intensity of the modelled relative vorticity in the 1-km simulations (*exp3* and *exp4*) is stronger than the one in the 3-km simulations (*exp0*, *exp1* and *exp2*). The site of the anticyclonic structure in the 1-km simulations is located more North than the site of the eddy in the 3-km simulations. Moreover (Table 1), the eddy in the 1-km simulations has a much longer tracking duration (56-70 days) than the eddy in the 3-km simulations (33-45 days). As we mentioned previously, since the 'death' of this eddy in each simulation is occurring at the same period, the differences in tracking duration are due to the differences in the starting date of the eddy. At the beginning of the eddy's life determined in the 1-km simulations, the eddy area is very small; hence the 3-km simulations can not reproduce it. Furthermore, the ring of cyclonic vorticity, indicating the outer edge of the anticyclonic circulation, is much better represented in the nested simulations than in the coarse model ones (Fig. 2.3b-f). We compared our numerical results with satellite data. Fig. 2.3a shows a chlorophyll *a* situation typical of the time period of interest. The eddy structure is identified by a relatively low chlorophyll *a* concentration (0.1 mg m^{-3}) contoured on its northern edge (43°15'N, 3°30'E) by a high chlorophyll *a* plume extending southeastward and indicating the clockwise rotation of the anticyclonic eddy. The large size and northern position of the

eddy in the satellite imagery match the high-resolution model results better than the low-resolution model ones. However, the size differences between the simulations (Table 1) are not obvious to interpret because of the high temporal variability of the eddy. This effect is probably due not only to the horizontal resolution but also to the horizontal diffusion.

For this reason, secondly, we study the influence of the coefficient δ in the horizontal diffusion term. We observed that the variation of the δ coefficient does not change the general position of the eddy in the 3-km simulations or in the 1-km ones (Fig. 2.3). Nevertheless, with increasing attenuation coefficient δ, the diffusion effect becomes more important. As shown in Table 1, for each resolution, the mean eddy area increases as the structure becomes more diffusive when δ increases from 0.2 to 0.8. Furthermore, the influence of the variation of δ is more important in the coarse-resolution simulations than in the fine-resolution ones. Visual analysis of all simulations with $\delta = 0.8$ show that (sub) mesoscale structures tend to completely disappear in the 3-km resolution simulations but not completely in the 1-km resolution ones. Moreover, for the 3-km simulations, when δ goes from 0.2 to 0.8, the standard deviation of *exp2* increases dramatically (Table 1), indicating the lack of realism of the *exp2* results. Whereas, for the 1-km simulations, the influence of the change of δ on the standard deviation is not significant, meaning that the eddy size and position do not change much. Moreover, we observed that the result of *exp3* (δ=0.2) displays considerable small-scale noise, or, in other words, that

the dissipative effect is too weak. At the same time a more realistic coherence of the eddy and a decrease in small-scale noise are gained with an increased diffusion (*exp4*). Indeed, the eddy structure in *exp3* (Fig. 2.3e) is more heterogeneous than the one in *exp4* (Fig. 2.3f). This heterogeneity separates the eddy into several substructures and complicates the wavelet identification. This heterogeneity, present in the modelled relative vorticity, does not have a counterpart in the satellite chlorophyll concentration (Fig. 2.3a).

Combining the effects of both the model resolution and the coefficient δ, and preliminary comparison of results to satellite observations, we can deduce that the best simulation to reproduce anticyclonic eddies in our study area has a 1-km resolution and an attenuation coefficient δ of 0.8 in the horizontal diffusion term, as in *exp4*.

Hence, thirdly, we are going to validate this chosen configuration. As explained before, we have compared the eddies' size in the results of simulation *exp4* and the satellite images. Despite the discontinuity in the satellite images due to cloud coverage, this anticyclonic structure has been observed very clearly 13 times during its lifetime, between the middle of July (July 11, 2005) and the middle of August (August15, 2001). The longest gap in the data - when we have no satellite observations - is 6 days. Before mid July, a small structure was also detected in the same area and period as the one reproduced by the 1-km simulations and detected by the wavelet analysis. Further study would be needed to verify its rotation direction and, if anticyclonic, whether

it corresponds or not to the origin of our eddy as suggested by the nested model. We tried to estimate the area of the eddy from the thirteen satellite images available during its lifetime. We subjectively contoured the eddy by a circle, which area is then compared to the corresponding area obtained by the wavelet analysis. The circle area of Fig. 2.3a is, for example, equal to 1950 km^2. It is in good agreement with the instantaneous value obtained from *exp4* (2103 km^2), knowing that this latter is slightly overestimated since a small 'tail' (high vorticity leaving the eddy on its south side) is included in the wavelet identification. In the satellite data, the minimum value is 1146 km^2 estimated on July 11, 2001, corresponding to the first satellite observation. The maximum value is 2223 km^2 estimated on July 30, 2001, corresponding to the half period of the satellite observations. In the last observation, the eddy area is 1962 km^2, and the averaged eddy area within the period of satellite observations is 1786 ± 384 km^2. These values fit nicely within the range 1193 ± 543 km^2 obtained with the *exp4* simulation (Table 1). Moreover, the agreement is even better when the values are compared to 1442 ± 598 km^2 obtained in averaging the corresponding thirteen *exp4* simulation. Despite the subjective character of this estimation, these values allow us to say that *exp4* is in good agreement with the observations.

2.4 Conclusions

In order to accurately simulate the (sub)mesoscale structures in the GoL, we have studied the impacts of the model resolution and of an attenuation coefficient in the advection-diffusion scheme. An anticyclonic eddy, in good agreement with satellite imagery as far as its size and position, is for the first time reproduced numerically, in the western side of the gulf of Lion, by choosing a model setup of 1-km spatial resolution and an attenuation coefficient of 0.8 for the horizontal diffusion. Its average area is about 1200 km^2 and it lasts about 60 days. It is also the first time that a wavelet technique is used to detect (sub)mesoscale structures in the coastal waters. As expected [*Nof 1999*], the model and wavelet analysis results show that this anticyclonic eddy is nearly constant in its position during its life time. Future work will focus on the study of the generating processes and mechanisms of these anticyclonic eddies, and will try to identify its potential impact on shelf-offshore exchanges. Furthermore, the numerical modeling will help us set up the sampling strategy of the main LATEX cruise, which plans to focus on this eddy structure. The in situ measurements combined with the modeling results will allow us to well understand the eddies' dynamics.

2.5   Acknowledgments

Study of coastal eddies : application in the Gulf of Lion

Contents

Résumé

Afin de vérifier *in situ* l'existence des structures tourbillonnaires anticy-
cloniques à l'ouest du Golfe du Lion mises en évidence par les simulations
numériques, la campagne en mer *Latex08* s'est déroulée pendant la première
semaine de septembre 2008. Ce chapitre permet de présenter l'exploitation
des données de la campagne *Latex08*, de confronter les mesures *in situ* avec
les résultats numeriques, et d'approfondir notre connaissance des tourbillons.

Au cours de cette campagne en mer des mesures ont été réalisées à l'aide
de l'ADCP (Acoustic Doppler Current Profiler) de coque du navire le *TéthysII*
et de sondes XBT (eXpendable Bathy Thermograph). Ces mesures, combinées
avec des images satellitales de SST et des trajectoires de bouées Lagran-
giennes, montrent la présence d'un tourbillon anticyclonique présentant un
fort rotationnel à l'ouest du golfe. Cette structure tourbillonnaire a une forme
elliptique avec un demi-grand axe et un demi-petit axe estimés à 21.5 et
15.5 km respectivement. Son extension verticale, limitée par la profondeur de
la couche de mélange saisonnière de cette zone, atteint 35 m. Vers la fin de
la campagne ce tourbillon interagit avec le Courant Nord. Ce dernier est pro-
bablement responsable de la déformation du tourbillon et du renforcement de
la partie sud-est de la structure. Des données complémentaires de trajectoires
de bouées suggèrent que cette structure était déjà présente au début du mois
d'août 2008. Par la suite, la durée de vie de ce tourbillon a été estimée de

l'ordre d'une cinquantaine de jours. Les caractéristiques du tourbillon observé pendant la campagne *Latex08* ont été comparées avec celles du tourbillon simulé par le modèle numérique. A la lumière des résultats numériques nous proposons quelques hypothèses sur la formation et le comportement de ce tourbillon. Ce travail fait l'objet d'un manuscrit soumis au *Journal of Marine System*, accepté par les co-éditeurs pour un numéro spécial et en attente de la décision finale de l'éditeur. Le texte de l'article est reproduit ci-après.

Study of coastal eddies : application in the Gulf of Lion

Abstract

Acoustic Doppler Current Profiler (ADCP) and Expendable Bathy Thermograph (XBT) data were collected during the Latex08 cruise (September 1 - 5, 2008) throughout the western part of the gulf of Lion. These data, combined with Sea Surface Temperature (SST) satellite images and Lagrangian drifter trajectories, show the presence of an intense anticyclonic eddy in the western side of the gulf. The eddy is elliptic in shape and the estimated radii are 21.5 (15.5) km for its major (minor) axis. The vertical extent of the eddy reached about 35 m depth and was limited by the bottom of the seasonal mixed layer. The eddy interacts with the Northern Current at the end of the cruise, maybe leading to its deformation. More-over complementary drifter data suggest that this anticyclonic eddy was already present at the beginning of August 2008. Hence the eddy lasted around 50 days in the same region. Some hypothesis about the formation and behaviour of the eddy are also discussed.

3.1 Introduction

Oceanic eddies may have an important impact on transfer and redistribution of heat, energy and matter. Several studies have previously focused on mesoscale eddies and their influences on biogeochemical distributions [e.g. *Garçon et al.* 2001; *Taupier-Letage et al.* 2003; *McGillicuddy et al.* 2007; *Benitez-Nelson et al.* 2007]. Nevertheless, questions remain, particularly in coastal waters where dynamical processes are very complex and fluxes of nutrients and sediments are high.

The Gulf of Lion (hereafter GoL) is a large continental margin with a semi-circle shape located in the northwestern Mediterranean Sea (Fig. 3.1). The hydrodynamics of the GoL are complex and highly variable, as described by *Millot* [1990]. Three main forcings coexist :

i) strong continental winds : the Mistral (northerly) and the Tramontane (northwesterly, sometimes westerly). They are cold and dry and can generate strong upwellings and downwellings along the entire coast of the GoL [*Millot* 1979] ;

ii) a quasi-geostrophic alongslope current : the Northern Current (hereafter NC). It is the northern part of the cyclonic gyre occurring in the western Mediterranean basin. The NC flows along the continental slope from the Ligurian Sea to the Catalan Sea [*Millot* 1990; Millot 1999]. As a first approximation, the NC can be considered in geostrophic balance, acting as a dynamical bar-

rier for coastal waters. Nevertheless, several studies have demonstrated the presence of transient ageostrophic processes [*Albérola et al.* 1995; *Sammari et al.* 1995; Petrenko 2003] ;

iii) important fresh waters inputs, bringing nutrients that enhance primary productivity on the shelf [e.g. *Minas and Minas* 1989; *Ludwig et al.* 2009]. The Rhone river on the north-eastern part of the gulf delivers about 80% of the total riverine water inputs and constitutes the main fresh water source of the GoL. The plume extension of the Rhone can extend offshore towards the southwest part of the GoL under certain meteorological conditions [*Estournel et al.* 1997].

Previous *in situ* studies suggested the presence of an anticyclonic circulation in the western part of the GoL, in September during stratified conditions [*Millot* 1979, 1982]. Estournel et al. [2003] have also shown with numerical modelling that an anticyclonic circulation can be present in this region in winter. These coastal eddies could potentially be influenced by the Rhone distal plume which could bring nutrients and phytoplankton inside the eddy. Numerical modelling suggests that the eddy can interact with the NC [*Hu et al.* 2009]. Such interactions, whether with the river plume or the neighboring current, indicate that these eddy structures could play an important role in the coastal-offshore transport of nutrients and phytoplankton, as well as heat and energy. To our knowledge, no experimental studies have been dedicated on the study of the eddy dynamics in this area since the early hypothesis

of *Millot* [1979, 1982] cited earlier.

The main objective of this paper is to investigate the dynamical characteristics of an anticyclonic eddy observed during the Latex08 cruise, adding cruise data to the previous numerical study by *Hu et al.* [2009], to better understand coastal mesoscale structures. The material and methods used in the experiment are described in Section 2 and the results are presented in Section 3. Eddy features and the possible mechanisms of its generation and its behaviour are discussed in Section 4. In the final section, we summarize the main results and briefly describe the perspective work.

3.2 Material and methods

The strategy of the LATEX project combines use of data from satellite observation, *in situ* measurements and numerical modelling. The Latex08 cruise was conducted from September 1 to 5, 2008 on board the RV *Téthys II*. The data collected during Latex08 came from satellite, ship-based and drifters observations.

A few days prior to the beginning of the Latex08 cruise, some eddy-like features appeared in the study region on SST satellite images provided by Météo-France (data not shown). Specifically, an eddy feature was present in the coastal waters east of Leucate. During the cruise, SST images were e-mailed to the RV *Téthys II* to help us track the eddy. Unfortunately, at
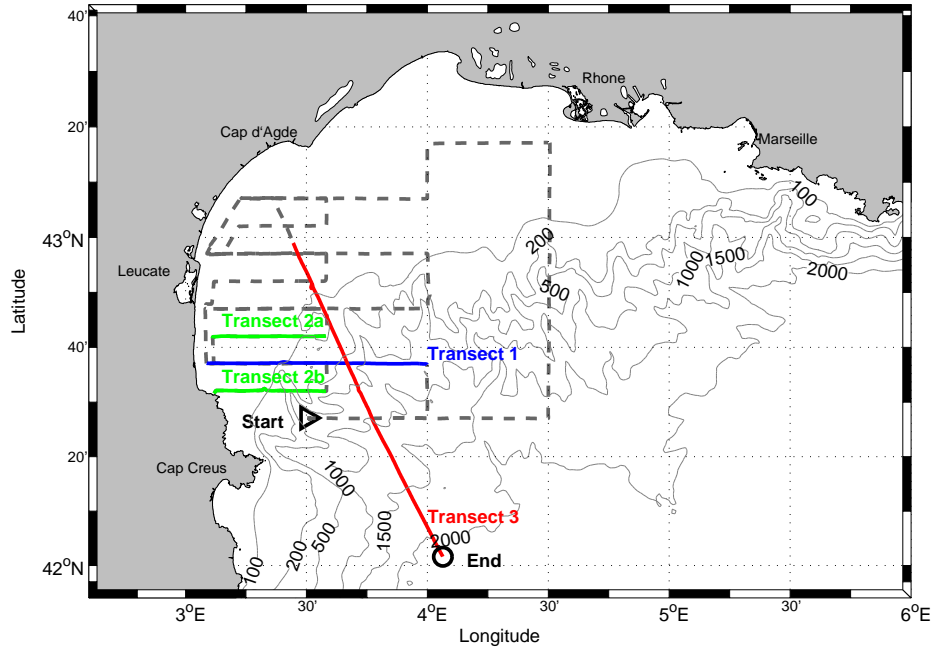
FIG. 3.1 – Map of the Gulf of Lion with the complete Latex08 ship trajectory. The transects used in the study are overlined in colors. Isobaths at 100, 200, 500, 1000, 1500 and 2000 m are plotted with thin lines.

the beginning of the cruise extensive cloud coverage limited our ability to determine the optimal sampling region for the eddy. Thus, based on numerical modelling results [*Hu et al.* 2009], we decided to start the sampling by doing a 10nm spaced radiator throughout the western region (Fig. 3.1).

Because of the complexity of the measured currents, we pursued with a reduced 5nm spaced radiator closer to the coast. Then, the image of September 2 showed us the presence of an eddy-like feature close to the continental slope (Fig. 3.2). Hence, at the end of the small radiator, we decided to cross through it diagonally from the northwest to the southeast direction (Transect 3 in Fig. 3.1). However, later in the cruise, the SST image was again distur-

bed by both clouds and the cold signature of surface waters upwelled by the Tramontane. Hence, the image on September 2 is the only informative image available during the cruise.

A ship-mounted VMBB-150 kHz ADCP, merged at 3 m below the water surface, was used to measure current velocity. Following Petrenko et al. [2005], the ADCP configuration used during the cruise was : 60 cells of 4 m depth, an ensemble average of 1 min and bottom tracking when possible. Consequently, the depth range of current data covers 11 to 243 m. The software for ADCP data analysis was provided by the French INSU (*Institut National des Sciences de l'Univers*) technical division. The measured ADCP horizontal currents were analyzed in near-real time during the entire cruise.

Since the sea state did not allow the use of the SeaBird SBE 19 CTD we had on board, temperature profiles were obtained by using XBTs. The reader can refer to Fig. 3.3 for the location of the XBT profile launched on September 5 at 04 :32 PM UTC. Two satellite-tracked drifters, equipped with a 6 m long holey-sock drogue, extending between 12m and 18m, were deployed in the eddy to track the fluid motion of the eddy at 15 m depth (Fig. 3.2, Fig. 3.3).

3.3 Results

The eddy is clearly apparent in ADCP, drifters and SST data. For the sake of clarity, we show the SST image in Fig. 3.2 and the ADCP measurements
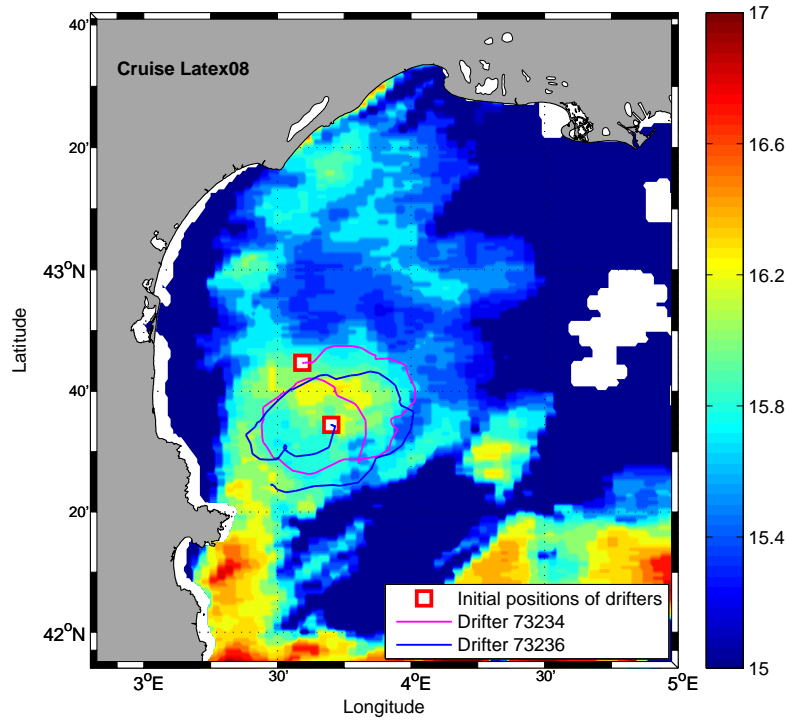
FIG. 3.2 – SST satellite image (Sept. 2) (data from Météo-France) and drifters trajectories (Sept. 5 - 11).

in Fig. 3.3. The drifters trajectories were added on both figures in order to obtain a synoptic view of the sampled eddy. Then, XBT data are combined with a vertical section of the ADCP data.

3.3.0.1 ADCP data

ADCP horizontal current velocity vectors at 15 m depth (corresponding to the same depth as the drifter measurements) for Transects 1, 2a, 2b and 3 clearly revealed the clockwise motion field associated with an anticyclonic eddy feature (Fig. 3.3). In Transects 1 and 3, the current speed increases gradually before reaching a peak and then decays until reaching its minimum
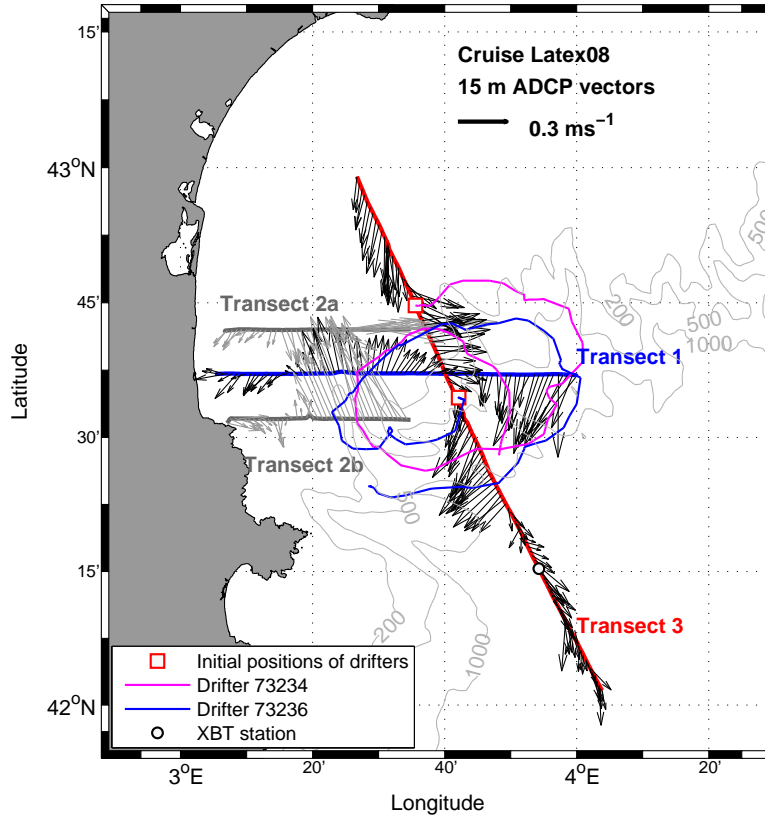
FIG. 3.3 – ADCP current vectors (plotted every 4 minutes) in the upper layer (15-m) for Transects 1 (Sept. 1), 2a and 2b (Sept. 3) and 3 (Sept. 5) ; blue and magenta lines represent the two drifters trajectories (Sept. 5 - 11). Isobaths at 200, 500 and 1000 m are plotted with thin lines.

values near the transect crossing, and increases again on the other side in the opposite direction. Transects 2a and 2b did not cross the eddy but showed the continuity of the anticyclonic circulation. Maximum velocity magnitude inside this eddy is about 0.6 ms^{-1}.

In order to accurately locate the geometric position of the eddy center for each transect, we followed the method described in *Nencioli et al.* [2008]. A square area 30 × 30 km (colored squares in Fig. 3.4) was defined around the

minimum velocity zone of each transect and then was divided into a grid of 30×30 points. Then, each point of that grid was tested as a possible location for the center of the eddy, decomposing ADCP velocities into tangential and radial components relative to the tested point. At all depths the center of the eddy was defined as the grid point for which the mean absolute value of tangential (radial) component was maximal (minimal). For Transect 1 (3) the above velocity decomposition was performed on the nearest 200 (155) records of ADCP measurements (black vectors in Fig. 3.4a and b). We used only these latter vectors in order that the estimation of the center location not be affected by the peripheral flow of the eddy which is more perturbed by the outer velocity field. We tested the sensivity to the numbers of vectors used (data not shown). The present result is considered to be the best estimation since it is least influenced by surrounding current fields. From now on, we choose to continue the analysis using the eddy centers determined with the tangential components of ADCP velocities since tangential velocities within the eddy are usually much higher in magnitude than radial velocities and hence are less sensitive to the variations due to background noise. Fig. 3.4 shows the estimated center positions for Transect 1 (a) and Transect 3 (b) at 15 m depth. The estimated location of the eddy center derived from ADCP vectors at 15 m depth was 42°36′N, 3°40′W (42°37′N, 3°43′W) for Transect 1 by using the tangential (radial) components ; and 42°34′N, 3°37′W (42°33′N, 3°37′W) for Transect 3, with an incertitude of about 1 km which is the size
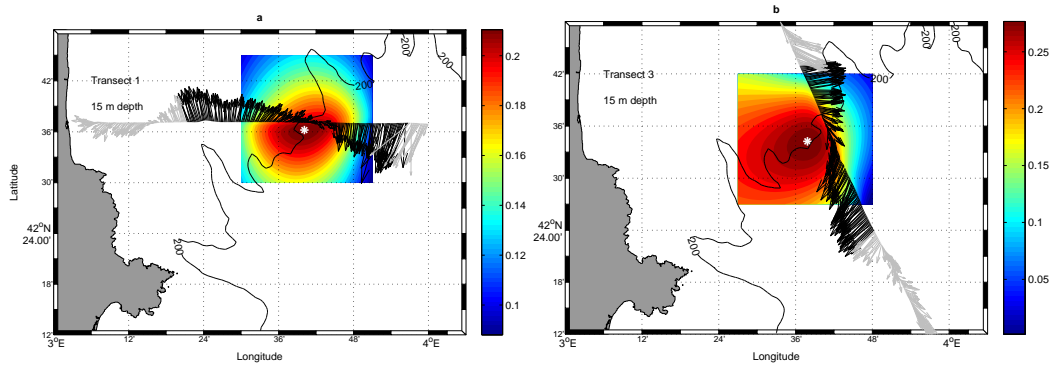
FIG. 3.4 – Estimated center location of anticyclonic eddy (white asterisk) for Transect 1 (left) and Transect 3 (right) at 15 m depth. Tangential components of the black vectors were computed for each point within the grids. For each transect, the center of the eddy was defined as the point for which the mean absolute value of tangential velocity was maximal. The contours in the square areas indicate values of equal mean absolute tangential velocity (ms^{-1}). Isobath at 200 m is plotted with black line.

of the grid within the square area. The differences between the two methods in the present case are relatively small. Analysis shows that the survey line of Transect 1 was very close to the eddy's center while Transect 3 was a few km to the east. The estimated position of the eddy center at 15 m depth moved 5 km southwest during the 4 days separating these two transects. The resulting drifting velocity of the eddy is 0.01 ms^{-1}. Moreover, we estimated the variation of the eddy center location with depth and we obtained $2'$ of latitude and $3'$ of longitude for Transect 1 and $1'$ of latitude and $1'$ of longitude for Transect 3.

In Fig. 3.5 we plotted the radial and tangential velocities at 15 m depth computed for both Transects 1 and 3 versus the radial distance from the esti-
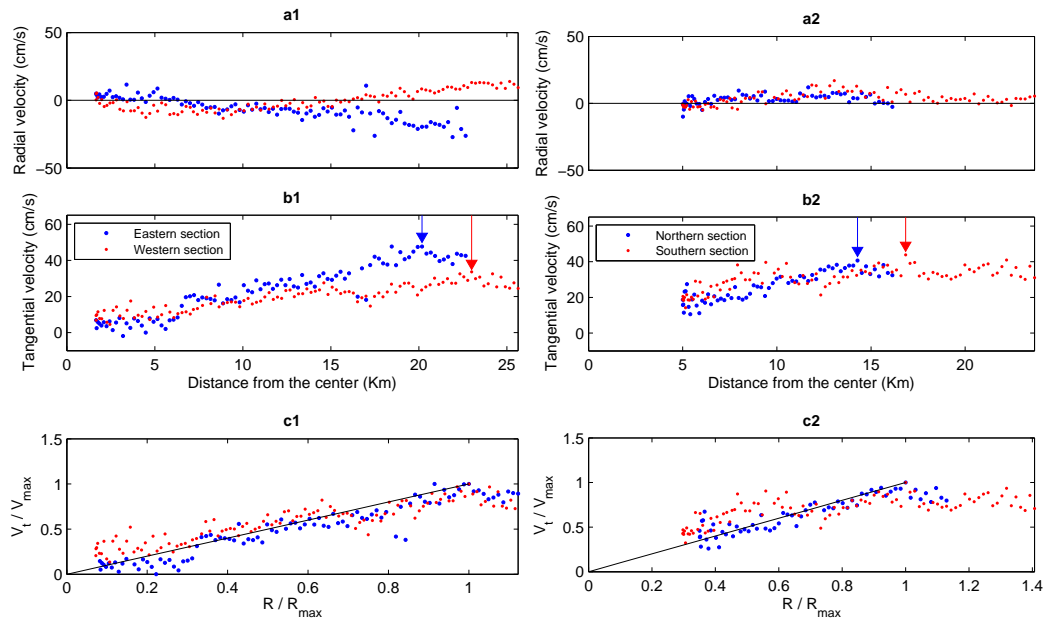
FIG. 3.5 – Distribution of (a) radial and (b) tangential velocities with respect to radial distance from the center ; (c) distribution of normalized tangential velocity with respect to normalized radial distance for both Transect 1 (left column) and Transect 3 (right column). Arrows in (b) indicate the locations of maximum velocity magnitude for two sections ; the solid lines in (c) indicate values of equal angular velocity (V_{max}/R_{max}).

mated eddy center. The blue dots in the figures correspond to the data from the section before crossing the center of the eddy (western part for Transect 1 and northern part for Transect 3) while the red ones represent the data from the section after crossing the center. The eddy center is at a distance of 1.7 km from Transect 1, and at about 5 km from Transect 3 (Fig. 3.5a and b). For each transect, the values of radial velocities are near zero within the eddy and become greater with radial distance due to the influence of the outer circulation field (Fig. 3.5a1 and a2). The tangential velocities are smallest near the eddy center. During Transect 1, they increased roughly linearly outward with radial distance until their maximum magnitude (V_{max}), and then decayed (Fig. 3.5b1). However this linearity was not so clear for Transect 3, since Transect 3 was further away from the eddy center (Fig. 3.5b2) than Transect 1. Furthermore, for both transects, the tangential velocities of the two radial sections reached their maximum value at different distances R_{max} from the center. R_{max} equals 20 (23) km for the eastern(western) section of Transect 1; R_{max} equals 14 (17) km for the northern(southern) section of Transect 3. The fact that the maximum tangential magnitudes of both radial sections were different and were reached at different radial distances from the center, suggests that the sampled anticyclonic eddy was asymmetric. Following *Olson* [1980], angular velocity can be computed as the tangential velocity (V_t) divided by the radial distance (R) from the determined center of the eddy. In Fig. 3.5c, we plotted the normalized tangential velocities (V_t/V_{max}) against

the normalized radial distances (R/R_{max}). The solid lines in the Fig. 3.5c thus represent a constant value of the angular velocity (V_{max}/R_{max}). The part of the eddy with a constant angular velocity is roughly considered as a solid body in which the rotation of the eddy is isolated from the surrounding waters. This confirms that the solid body rotation is included in the elliptical shape whose dimensions are detailed previously.

3.3.0.2 Drifter data

Drifter trajectories obtained six days after their launch during the Latex08 cruise are displayed in Fig. 3.2 and Fig. 3.3. The two drifters were deployed on September 5. Drifter N°73234 was deployed on Transect 3 near the northern outer edge of the eddy and drifter N°73236 was deployed at the center of the eddy, according to the ADCP data. Both drifters made one full loop around the eddy in about 5 days. The trajectories of these two drifters followed the outer edge of the eddy indicated in the SST satellite image, and clearly revealed the well developed warm-core anticyclonic feature of the eddy (Fig. 3.2). These trajectories further confirmed the asymmetric nature of the eddy and suggested that it has an elliptical shape with its major axis being oriented southwest (SW) to northeast (NE). The time-averaged translational velocity of each drifter was calculated as the distance covered by the drifter divided by the corresponding time interval. This velocity can be considered as the drifter-based tangential velocity $V_t^{Drifter}$ of the eddy at its outer edge and at
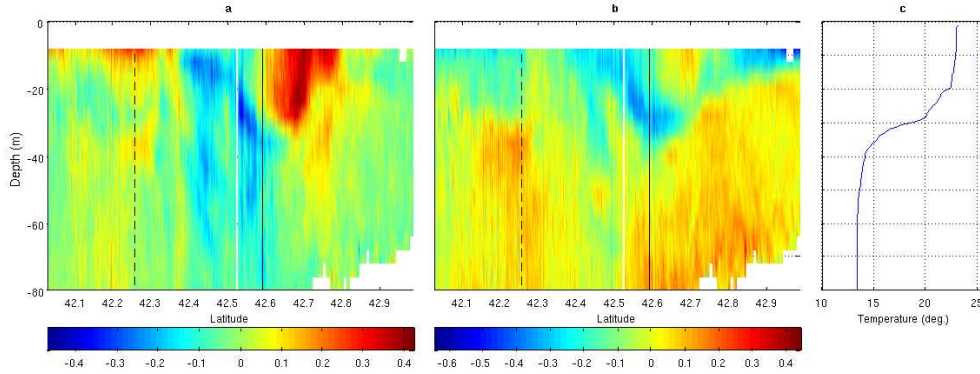
FIG. 3.6 – Vertical sections (depth vs. latitude) of the horizontal currents (colors ; ms^{-1}) for Transect 3 : a) the observed west-east component (eastward, positive) ; b) : the observed south-north component (northward, positive) ; c) : the temperature profile measured by XBT at the location marked by dotted line ; the solid line indicates the nearest position to the estimated eddy center using 15 m ADCP data.

15 m depth. For the drifter N°73234 (N°73236) we obtained V$_t^{Drifter}$ = 0.48 (0.41) ms^{-1}. Moreover, we considered the distance between the two drifter positions near the endpoints of the SW-NE (NW-SE) axis as the major (minor) diameter of the elliptical eddy. Then, the estimated eddy major (minor) radii R^{Drifter} are equal to 25 (18) km for the drifter N°73234 and 24 (17) km for the drifter N°73236.

3.3.0.3   Vertical profiles

The vertical sections of the ADCP derived east-west (U) and south-north (V) current components show the whole eddy extension (Fig. 3.6a and b respectively). U (V) is defined as positive when the current is eastward (northward). The solid lines indicate the projection, on the transect, of the estimated

eddy center using the 15 m ADCP data (section 3.1). Two areas with oppo-site directions on both sides of the eddy center and with relatively high value in magnitude, represent a typical eddy. Here the northern section (Fig. 3.6a) of the eddy reveals a clear red (positive) spot since the current vectors - in this section - are almost eastward. The eddy signature is less obvious in the southern part. This reinforces the observation that the eddy is not circular. Vertical current distribution shows that the horizontal extent of the eddy de-creases with depth increasing, and that there is no eddy at depths deeper than 35 m. The temperature profile measured with an XBT at the location marked by the dotted line is shown in Fig. 3.6c. The temperature is about 23°C at the surface and decreases progressively with depth to the value of 13.4°C at about 60 m depth, which is the typical temperature of the Modified Atlantic Water (MAW) in this area [*Albérola and Millot* 2003]. The marked thermocline depth is about 35 m, suggesting that the vertical extent of the anticyclonic feature was limited by the bottom of the mixed layer.

3.4   Discussions

The combined analysis of the ADCP and drifter data revealed that the eddy was approximately elliptical and elongated along the southwest to nor-theast direction. In order to fix a unique value for the two radii of the eddy solid body rotation, we averaged the values of ADCP-based R_{max} and obtai-
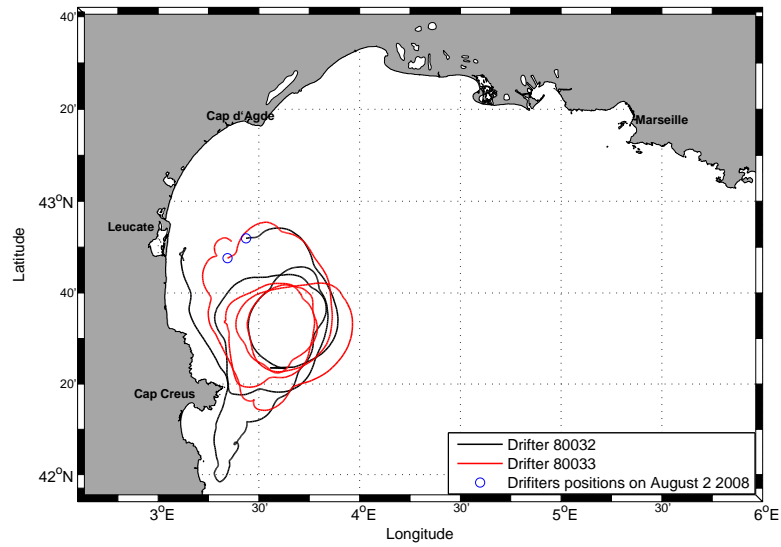
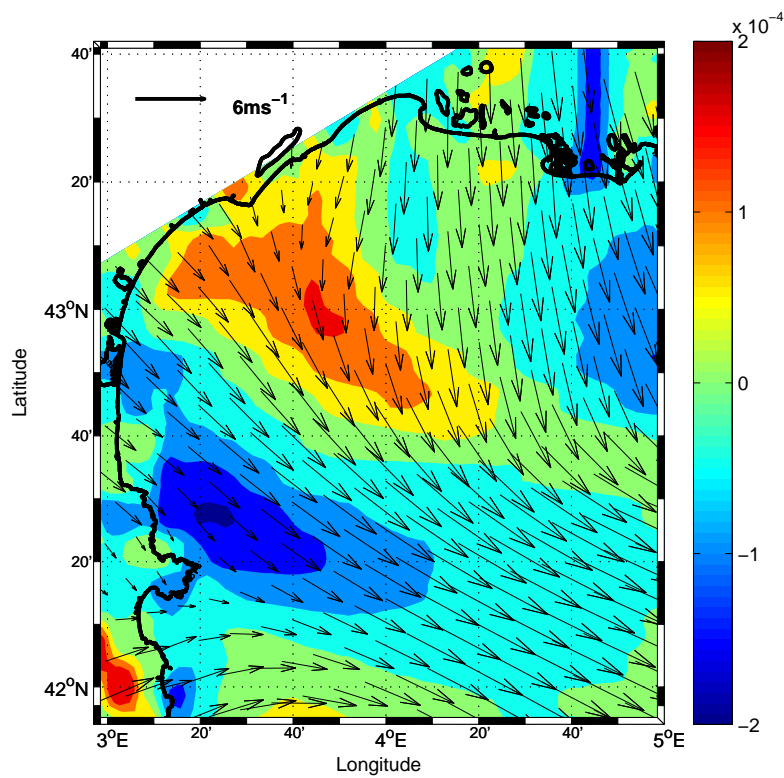FIG. 3.7 – Additional Argos drifters trajectories (August 2 - 19, 2008).

FIG. 3.8 – Wind vectors at 10 m altitude in ms^{-1} and wind stress curl in s^{-1} on September 2, 2008. Results from the Météo-France ALADIN meteorological model.

ned a major radius of 21.5±1.5 km and a minor radius of 15.5±1.5 km. These values are slightly smaller than the radii estimated from drifter trajectories. In fact, averaging the values for the two drifters N°73234 and N°73236, we obtained a major radius of 24.5±0.5 km and a minor radius of 17.5±0.5 km. We explain these differences by the fact that both drifters looped in the outer edge of the eddy, just outside of the solid body rotation, as suggested by their $V_t^{Drifter}$ smaller than V_{max} and by the overlappings of the drifter trajectories with ADCP vectors (Fig. 3.3) and SST contours (Fig. 3.2). Moreover, the eddy radius values agree with our previous study. Indeed, in *Hu et al.* [2009], a numerical eddy simulated for the year 2001 had a time-averaged area during its life duration of about 1193 km². Assuming a circular shape for the eddy, the radius corresponding to this area value is hence about 20 km. These values of the estimated radius of the eddy are comparable with the Rossby radius of this area, suggested to be 15 km by *Grilli and Pinardi* [1998]. The magnitude and direction of current vectors derived from drifters trajectories were in a good agreement with the ADCP velocities at 15 m depth. The maximum velocity within the eddy is 0.6 ms⁻¹, indicating that it is an intense coastal eddy. Compared to the position of the eddy simulated for the year 2001 [*Hu et al.* 2009], the eddy observed during the Latex08 cruise in 2008 is farther offshore and more to the south.

In order to estimate the life duration of the Latex08 eddy, we need more information. On one hand, on July 21, 2008, two Argos drifters with an an-

chor depth of 15 m were launched in the GoL (drifter data can be found at http://www.coriolis.eu.org/default.htm as numbers 80032 and 80033). Both drifters were entrained simultaneously (August 2) into an anticyclonic eddy, which had a similar shape and was located in the same position as the one sampled during the experiment Latex08. The drifters spun up nearly four times in the eddy until the middle of August (Fig. 3.7). Then, the two Argos drifters moved northward along the coast. In addition, in the SST satellite images without cloud coverage, a similar eddy-like structure was observed in the western part of the GoL in August (data not shown). On the other hand, *Hu et al.* [2009] showed that, in the same region, an anticyclonic eddy persisted for more than a month in 2001 (56 days) both in simulation results and in satellite observations. Hence, it is quite possible that the eddy evidenced in August 2008 by the drifters N°80032 and N°80033 was the same as the one sampled during the Latex08 cruise. Since the drifter trajectories in the beginning of August show that the eddy was already well developed, the 'birth' of the eddy is assumed to be at least one to two weeks earlier, between the middle and the end of July. The life of this eddy is thus reasonably assumed to be at least 50 - 60 days.

In the numerical experiments of *Hu et al.* [2009], the 'death' of the eddy in 2001 happened in the middle of August when the anticyclonic eddy approached the NC and interacted with it. Such interaction was considered fatal to the eddy and brought its collapse. The present analysis of the ADCP data

shows that R_{max} on the southern section of Transect 3 is greater than R_{max} on the northern section and that the maximum of current velocity along Transect 3 is also found on the southern section. Hence, we suppose that, at the end of the cruise, this anticyclonic eddy interacted at its southeastern side with the NC and was stretched and accelerated by it, as along Transect 1 and 3, where the current stayed intense with depth. Instead, the amplitude of the current vectors along Transect 2b decreased quickly with depth, were halved at 23 m depth, and became even weaker below 31 m (data not shown) probably due to a local wind effect. Whether these hypotheses are true or not remains an open question until future modelling experiments provide more information. Unfortunately, no available data can help us verify whether or not the eddy still existed after this interaction with the NC.

Regarding the formation of such an anticyclonic eddy, we consider the following mechanism, based on the work by *Millot* [1982]. During a Tramontane event, a southeastward wind-driven current appears south of Cap d'Agde. Coastal waters pushed offshore are partly compensated by upwelled waters. The deficit part is compensated by a northward coastal jet near Leucate. Under the Coriolis effect, the wind-driven offshore current shifts southwestly onshore to Cap Creus. There, it joins the beginning of the northward current along the coast and as such, closes the loop forming the anticyclonic circulation. Once the eddy is generated, we think, based on model simulations, that it can survive longer than a month. Different mechanisms probably intervene

as fueling processes maintaining this eddy. We propose here two mechanisms. The first one is the direct effect of wind stress curl on the west part of the GoL. The wind time series (data from the ALADIN meteorological model, provided by Météo-France) over the GoL show that, near the Roussillon coast, the gradients in the wind velocity fields favor an anticyclonic wind stress curl, such as on September 2, 2008 (Fig. 3.8). Transmission of the anticyclonic wind momentum to the sea surface could feed the anticyclonic vorticity of the eddy after its generation. The second potential fueling mechanism is the baroclinic instability of the NC. Indeed, during the MATER HFF experiment, *Flexas et al.* [2002] observed from satellite SST images that, when the NC propagates to the western part of the GoL, anticyclonic motions due to baroclinic instability may occur on the inner edge of the NC. The possible mechanisms for this baroclinic instability may result from diverse factors such as the wind stress, topographic irregularities (canyons) and along-shelf variations, etc. Otherwise, in the numerical experiments, *Hu et al.* [2009] also showed the appearance of anticyclonic features on the inner edge of the NC.

The estimated drifting velocity of 0.01 ms^{-1} of the observed eddy is 10 times smaller than the previously reported drifting velocity of eddies in the studied region. In *Allou et al.* [2010], the eddies located in the eastern part of the GoL shifted at 0.1-0.2 ms^{-1}; while in *Rubio et al.* [2005], the eddies located downstream of the GoL shifted at 9 km/day (i.e. 0.1 ms^{-1}). In these two latter cases, the eddies are instabilities of the NC meanders in the eastern part of the

GoL as we mentioned earlier, and are (partially) advected by the NC. Hence, the drifting velocities of these eddies have values which are comparable to the one of the NC which propagates at speeds of 10-20 km/day (i.e. 0.1-0.2 ms^{-1}), as documented by *Crépon et al.* [1982]; Millot [1999]; *Sammari et al.* [1995]; Petrenko et al. [2005]. *Ginzburg et al.* [2002] proposed a value of 0.043 ms^{-1} for eddy's drifting velocity in the shelf area of the Black Sea where hydrodynamic conditions are similar to the NWM (the Rossby radius of deformation in the Black Sea is of the order of 20-30 km, according to *Stanev et al.* [2002]; *Stanev* [2005]).

3.5 Conclusions and perspectives

During the Latex08 cruise, a coastal mesoscale anticyclonic eddy was sampled in the western part of the GoL. SST satellite images suggested presence of a structure at the surface, while ADCP current data not only confirmed the presence of the eddy, but also gave us the dynamic characteristics of the eddy structure. Furthermore, the time series of the fluid motion associated with the eddy derived from drifter data provided complementary information on the eddy characteristics. From these data, we have greatly increased our knowledge on these eddy features, which was previously mainly based on numerical modellingf. The studied anticyclonic eddy may have lasted 50 - 60 days. It was characterized by an elliptical shape with radius about 21.5 (15.5) km for

its major (minor) axis and by a maximum tangential velocity of about 0.6 ms^{-1}. The vertical extent of the eddy has been estimated to be 35 m, which was also the bottom depth of the thermocline. Analysis results suggested that the eddy interacted with the NC at the end of the cruise. The generation of the eddy in this region is considered to be due to an enclosed anticyclonic circulation linked to an upwelling phenomena. Moreover the eddy is suspected to be fueled by two additional processes : the direct wind stress curl and anticyclonic baroclinic instabilities of the NC.

Ongoing numerical modelling work focuses on a 10-year (2001-2010) simulation with the same model configuration discussed in *Hu et al.* [2009]. The numerical modelling may allow us to verify the assumption on the eddy's life duration ; to explain the difference in the eddies' locations in 2001 and 2008 ; to study the eddy's evolution throughout its lifetime and to investigate whether the eddy dies after its interaction with the NC at the beginning of September 2008. During the second cruise of the LATEX project (Latex09, August 25-30, 2009), three Eulerian ADCPs were moored to constitute an on-offshore eddy-crossing transect between the coast and the area where the eddy has been observed, and will provide us a one-year time series (August 2009 - September 2010) of horizontal current measurements through the water column. These data will allow us to systematically evaluate the circulation in this key area where eddies regularly form, in order to detect the presence of eddy structures and, furthermore, to study the phenomena associated with the wind variation

near the coast. Such data, as well as meteorological data and future numerical modelling work, will help us test our hypotheses regarding eddy generation and fueling. The third LATEX project cruise (Latex10, planned for September 6-30, 2010) will add, to the strategy used in the present work, an inert tracer release and glider measurements with the objective of better understanding the remaining open questions about the coupled physical and biogeochemical dynamics at mesoscale and their role in the transfers between the GoL coastal zone and the northwestern Mediterranean open ocean.

3.6   Acknowledgments

Numerical study of eddy generation in the western part of the Gulf of Lion

Contents

Résumé

La dernière partie de ce travail a été d'étudier la reproductibilité, la variabilité des tourbillons et d'appréhender leur processus de génération. Une simulation pluri-annuelle a été réalisée de 2001 à 2008 avec la configuration optimisée retenue précédemment (chapitre II) et un forçage météorologique issu des sorties du modèle Aladin de Météo-France (Annexe 1). Des tourbillons anticycloniques apparaissent régulièrement à l'ouest du Golfe du Lion. Les tourbillons qui perdurent plus de 15 jours sont appelés 'tourbillons de longue durée de vie'. Ils apparaissent pendant la saison stratifiée de juillet jusqu'à début octobre. Ceux qui ont une durée de vie inférieure à 15 jours sont qualifiés de transitoires. La présence d'un vent du nord-ouest fort et persistant et d'une forte stratification sont les deux conditions nécessaires pour engendrer un tourbillon de longue durée de vie. Pendant la saison où le milieu marin est stratifié, un vent fort du nord-ouest soufflant 2-3 jours dans la partie ouest du golfe engendre un upwelling au sud du cap d'Agde avec un courant de surface s'éloignant de la côte nord. Ce courant vers le large tourne sous l'effet des forces de Coriolis vers la côte ouest entre le cap Béar et le cap Creus où le niveau de la mer est donc plus élevé que celui près du cap d'Agde. Un courant côtier vers le nord le long de la côte Roussillon induit par le gradient

de pression, qui rejoint le courant vers le large, peut créer un tourbillon anti-
cyclonique. Ce dernier peut perdurer tant que les coups de vent du nord-ouest
sont présents. L'effet combiné de ces deux facteurs nous a permis d'expliquer
aussi la présence de tourbillons transitoires et de tourbillons de longue durée
de vie. Ce travail fait l'objet d'un article soumis au *Journal of geophysical
research* dont le texte est reproduit ci-après.

Numerical study of eddy generation in the western part of the Gulf of Lion

Abstract

A realistic numerical model is used to investigate the generation process of anticyclonic eddies located in the western part of the Gulf of Lion. During 8 years of simulations from 2001 to 2008, 8 anticyclonic coastal eddies with a life duration longer than 15 days have been observed in the study area between July and early October. The formation process of eddies is investigated by examining the changes in wind forcing and in stratification conditions. These factors alone or combined are discussed regarding eddy's formation processes. These eddies need two conditions to be generated : a persistent and strong northwest wind and a strong stratification. The Ekman transport associated to such a wind and the coastline characterized by the presence of capes can create a pressure gradient generating an anticyclonic circulation, precursor of the eddy. At the same time, a strong stratification condition allows a better transfer of wind-induced potential energy to eddy kinetic energy. Persistent

wind bursts are also required to sustain the eddy in size and intensity.

4.1   Introduction

The Gulf of Lion (hereafter GoL) is a large continental shelf located in the northwestern Mediterranean Sea (Fig. 4.1). As described by *Millot* [1990], the hydrodynamics of the GoL are complex and highly variable, influenced by three main forcings coexisting in this area :

i) strong continental winds : Tramontane (northwesterly/NW, sometimes westerly) and Mistral (northerly/N). The up- and downwelling phenomena generated by the wind along the coast are well-known [*Millot* 1979, 1982; *Hua and Thomasset* 1983] ;

ii) a mesoscale quasi-geostrophic current, the Northern Current (NC) [*Millot* 1991], flowing along the GoL continental slope from the Ligurian Sea to the Catalan Sea (Fig. 4.1). The hydrodynamics of the NC have been well investigated by previous studies [*Millot* 1990; Millot 1999; *Albérola et al.* 1995; *Sammari et al.* 1995; Petrenko 2003; *Flexas et al.* 2002; *Echevin et al.* 2003] ;

iii) fresh water inputs from the Rhône river, bringing nutrients that enhance primary productivity on the shelf [e.g. *Minas and Minas* 1989; *Ludwig et al.* 2009]. The river plume extends offshore towards the southwest part of the GoL under certain meteorological conditions [*Estournel et al.* 1997].

A mesoscale anticyclonic circulation in the western part of the GoL has been first observed by *Millot* [1979, 1982] in the currents and SST images. In the latter, it was partly identified as a tongue of cold water upwelled south
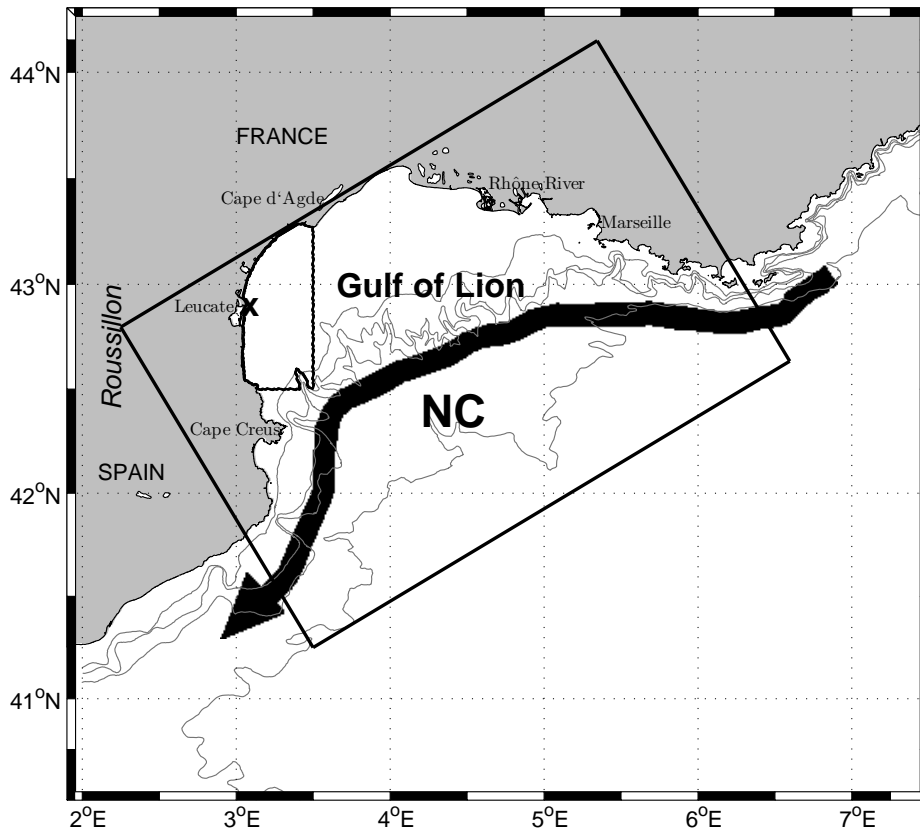
FIG. 4.1 – Map of the Gulf of Lion. The rectangle represents the model domain. The contour indicates the study area where eddies are often observed. The big cross indicates the location of meteorological station at Leucate. Isobaths at 100, 200, 500 and 2000 m are plotted with gray lines.

of Cape d'Agde. Its signature can also be observed in SeaWiFs chlorophyll maps with a high chlorophyll *a* plume on its northern edge circling around the eddy [*Hu et al.* 2009]. *Hu et al.* [2010] also observed an anticyclonic eddy in the western part of the GoL and suggested that the radius of the eddy is estimated to be 15-20 km. The maximum life duration of these anticyclonic eddies is estimated to be up to about 2 months [*Hu et al.* 2009; *Hu et al.* 2010]. The spatial and temporal scales of these coastal eddies are distinct from those

of the large eddies observed in the open ocean like the Gulf Stream rings and the Agulhas rings. They are also smaller than those of the eddies observed in the Mediterranean sub-basin, such as the Algerian eddies which can have lifetimes up to ~3 years and can reach diameters larger than ~250 km [*Millot* 2003; *Ruiz et al.* 2002]. However, eddies are among the physical processes that can have an important role over the continental shelf edge listed by [*Huthnance* 1995]. Indeed, these coastal eddies can be considered as a link between the coastal water and the open sea and could have an important influence on the coast-offshore transport of nutrients and phytoplankton, as well as heat and energy.

Hence, it is important to understand the physical dynamics of these eddies and in particular, their generation process. Various dynamical processes can contribute to eddy generation [*McWilliams* 1985]. For instance, current instabilities are important mechanisms for eddies of the Gulf Stream [e.g. *Robinson and Pinardi* 1988], or in the Gulf of Mexico [e.g. *Hurlburt and Thompson* 1980]. The topographical influence is also an important contributor to the Meddies (eddies of Mediterranean Water) formed near Cape Saint Vincent [*Pichevin and Nof* 1996] and in general, to all the eddies formed around capes and around headlands [e.g. *Signell and Geyer* 1991; *Doglioli et al.* 2004; *Magaldi et al.* 2010]. The eddies in the lee of the Hawaiian islands are formed as a result of combined wind forcing, topography and instabilities associated with current flow [*Lumpkin* 1998; *Chavanne et al.* 2002; *Kersalé et al.* 2010].

In the Northwestern Mediterranean basin, *Pascual et al.* [2002] suggested that an eddy observed in the Balearic Sea is created by wind curl stress. Coastal anticyclonic eddies observed in the eastern part of the GoL [*Allou et al.* 2010] and in the Catalan Sea [*Rubio et al.* 2005; *Rubio et al.* 2009] are created by a separating branch of the NC due to the topography. *Schaeffer* [2010] also showed that the generation mechanism of anticylonic eddies in the eastern part of the GoL are related to the local wind conditions. In our study area, *Millot* [1979, 1982] suggested that anticyclonic circulation and eddies may arise in the surface layer in the western part of the GoL to compensate offshore water following an upwelling phenomena in this area. Estournel et al. [2003] and Petrenko et al. [2008] also show that the wind curl over the GoL can create an anticyclonic eddy circulation over the shelf of the gulf by using academic simulations. However, the precise generation mechanism of the eddy located in the western part of the GoL is still not clear. Starting from the hypothesis of *Millot* [1979, 1982], we investigate the generation process of anticyclonic eddies, especially of the ones with long duration.

The present work is carried out within the framework of the LAgrangian Transport EXperiment (LATEX) projet (2008-2011) initiated to study the role of mesoscale eddies on shelf-offshore exchanges in the GoL.

The paper is organized as follows : Section 2 describes the numerical modeling ; section 3 investigates eddy formation process regarding various wind forcing and stratification conditions ; the results are discussed in Section 4 and

summary and conclusions are presented in section 5.

4.2 Numerical modeling

For the present study, we use Symphonie, a 3-D primitive equation model, with a free surface, hybrid sigma coordinates, based on Boussinesq and hydrostatic approximations [*Marsaleix et al.* 2006; Marsaleix et al. 2008]. Symphonie has already been used in the area, for example to study the wind-induced circulation in the GoL [Auclair et al. 2003; Estournel et al. 2003; Petrenko et al. 2005, 2008] and dense-water formation and/or cascading phenomena over the continental shelf [*Dufau-Julliand et al.* 2004; *Ulses et al.* 2008a,b] and deep convection in the northwestern Mediterranean Sea [*Herrmann and Somot* 2008; *Herrmann et al.* 2008]. A C-grid is used for spatial discretization [*Arakawa and Suarez* 1982]. The second-order closure scheme of Gaspar et al. [1990] is used to estimate vertical turbulence. *Hu et al.* [2009] developed and validated an upwind-type advection-diffusion scheme to improve the ability of the model to reproduce coastal mesoscale eddies. In application, the model domain extends throughout the whole GoL with a horizontal resolution of 1 km and 40 σ-hybrid vertical levels (Fig. 4.1). Surface atmospheric forcings are provided by the meteorological model Aladin of Météo-France with high spatial (0.1° x 0.1°) and temporal (3h) resolutions. Initial and open boundary conditions are provided by the Mediterranean Forecasting System (MFS) ge-

neral circulation model [*Pinardi et al.* 2003] with a resolution of $1/8°$. The original forcing data are bilinearly interpolated in the Symphonie model grid, and linearly interpolated in time. Daily fluxes of fresh water from major rivers (Rhône, Hérault, Aude and Orb), provided by the *Compagnie Nationale du Rhône*. A previous sensitivity study [*Hu et al.* 2009] shows that this model configuration is very appropriate for simulating realistic anticyclonic eddies in the GoL.

We simulate 8 years from January 2001 to December 2008. The daily outputs of current components, salinity, temperature and density are averaged over 24 hours of simulation for filtering diurnal and/or inertial oscillation (frequency is of 17.5 hours in the GoL corresponding to latitudes around 43° N). A wavelet technique, developed by *Doglioli et al.* [2007], is used to analyze the modeled horizontal relative vorticity in order to identify eddy structures in the simulations and to track the localized structures in time. Backward (forward) tracking finds the 'birth' ('death') of the eddy respectively. Hence we can deduce the life duration of the eddy. In the present work, analysis is performed at 20-m depth because, during the stratified season, it is about half the mixed layer depth over which the eddies extend.

In order to study the generation process in response to changes in wind forcings, we use the meteorological wind data used in our numerical simulations. Measured meteorological data are available at terrestrial stations around the GoL, among other at Leucate (Fig. 4.1). We have compared the Aladin wind

with the available measurements and have found a good agreement. In sake of conciseness we do not show this comparison. For this study, we have decided to use the Aladin model data at the grid point near the position of the meteorological Leucate station to illustrate the wind variability in the western part of the GoL. Indeed, this location, systematically being in the path of the NW wind whether this extends spatially or exhibits a strong wind stress curl, represents quite well the changes in the wind forcing in the western part of the GoL. In the following we consider that the wind is a 'strong NW wind event' when its amplitude is larger than (or equal to) 8 m.s^{-1} and its direction between 270°and 360°. When the wind amplitude exceeds 14 m.s^{-1}, we define it as an 'extreme strong wind'.

4.3 Results

Modeling results show that, in the western part of the GoL, anticyclonic features can be observed all year around. However, the anticyclonic features formed during winter-spring are very small in size, weak in intensity, last generally only 2-3 days and finish like filaments before disappearing. In contrast, coherent anticyclonic eddy structures occur between May and October. These anticyclonic eddies generally consist of warm, less salty buoyant water with a positive sea-surface height anomaly (SSHA) comparing to the ambient waters. The eddies size vary from 20 to 80 km in diameter. The application of the

wavelet analysis on all observed eddies in the simulations shows that their life durations vary from several days to a couple of months. In the present work, we define as 'long-life' eddies the anticyclonic eddies which last at least 15 days, in opposition to the other ones that we call 'transient' eddies. It is important to note that 'long-life' is relative to 'transient' for the eddy structures in the study area, and hence can not be compared to the eddies' lifetimes in the open-sea. In the 8 years of simulations, 8 long-life anticyclonic eddies have been observed (Table 1). These long-life eddies occur during a three-month period, between July and early October. No long-life eddy was detected in 2004 and in 2007. The first or the unique eddy generally appears in July (in the following indicated with A1 followed by the year), as it occurs 5 years out of the 6 during which eddies are present (2001, 2002, 2003, 2005 and 2008). The life durations of these first eddies range from 38 to 76 days, except for the 2006 eddy, which starts at the beginning of August and disappears at the end of that month lasting only 22 days. In 2003 and 2005, two long-life eddies have been detected successively during the three-month period. Both second eddies (indicated as A2 followed by the year) begin around mid-September and disappear early October lasting 15 to 22 days. Hence they generally last a shorter time than their July counterparts. Over the 8 years of simulations, we observe long-life eddies 5 times in July, 6 times in August, 5 times in September and 3 times in early October. In summary, the period when a long-life anticyclonic eddy is more likely to be encountered in the western part of the GoL extends

Year	number of eddies	A1	lifetime days	A2	lifetime days
2001	1	10/07→06/10	67	-	-
2002	1	07/07→13/08	38	-	-
2003	2	07/07→18/08	43	12/09 →7/10	26
2004	0	-	-	-	-
2005	2	10/07→04/09	57	20/09 →04/10	15
2006	1	04/08→31/08	22	-	-
2007	0	-	-	-	-
2008	1	15/07→26/09	67	-	-

TAB. 4.1 – Information on the long-life anticyclonic eddies present in the 2001-2008 modeling of the circulation in the western part of the GoL.

from July to early October with the highest probability in August.

These coastal eddies are rarely round in shape and have generally an elliptic form (Fig. 4.2). The irregular contour edge like the small 'tail' in the south edge of the eddy A1_2001 (Fig. 4.2-a) suggests the interaction of the eddy with the NC or surrounding currents. Eddy A1_2002 (Fig. 4.2-b) is smaller than the other eddies and is quite close to the coast. Eddy A2_2003 (Fig. 4.2-d) and eddy A2_2005 (Fig. 4.2-f) are located more off-shore than the others. These eddies are all generated in the same area near the Roussillon coast at around 43°N, 3°15'E. The diameter [1] of the eddies ranges from 10-20 km when they are newborn to 50-80 km when they are well-developed. After their generation, the eddies have slight meridional or off-shore displacement to end up where they are shown on Fig. 4.2. The NC located at their south-southeast edge (Fig. 4.1), combined with the presence of Cape Creus, plays the role of a barrier, and constrains the eddies within the western part of the GoL.

---

[1]Elliptical diameter defined as the mean of the minor and major axes.
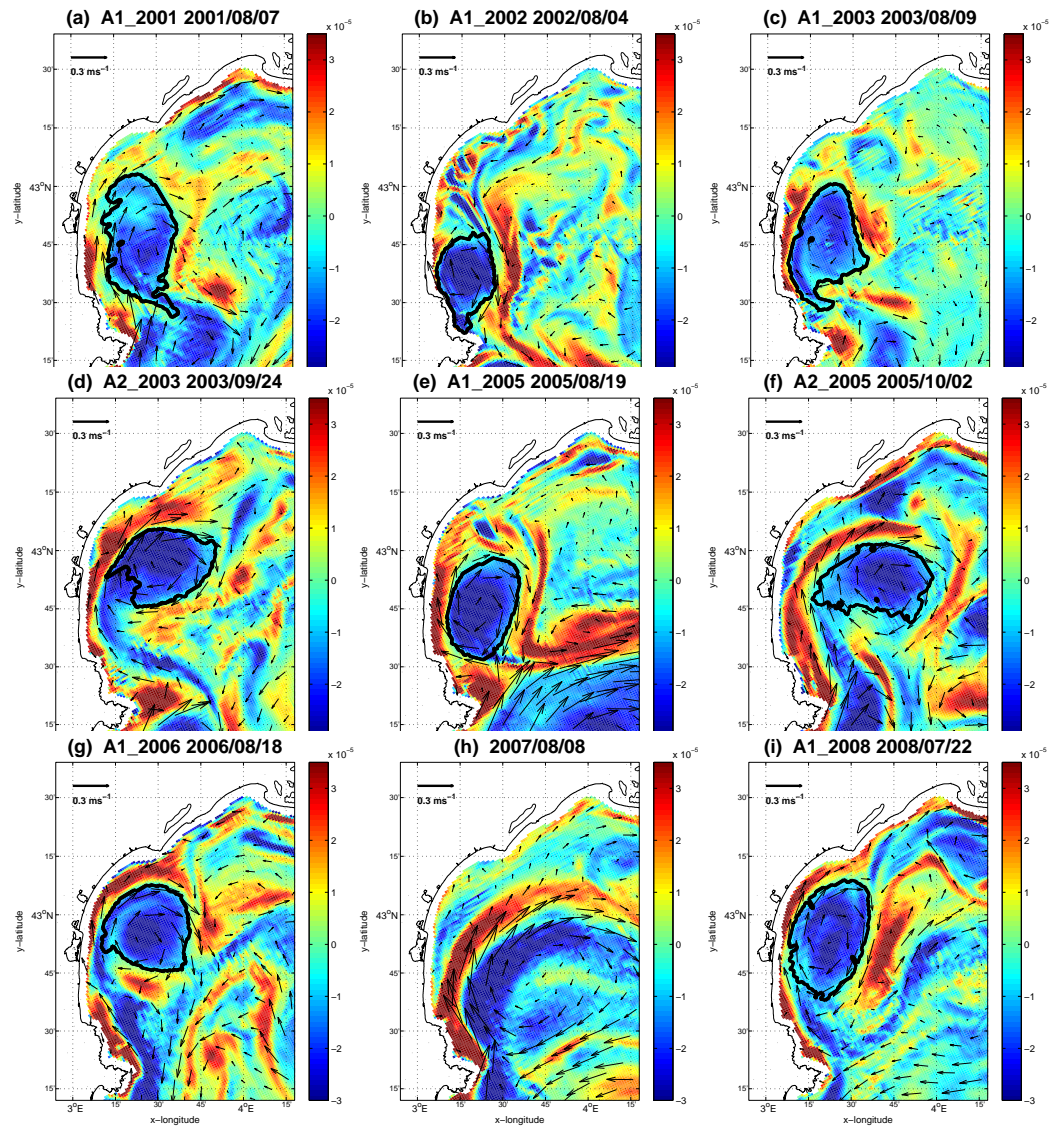
FIG. 4.2 – Snapshot of the modeled relative vorticity [s⁻¹] and current velocity at 20 m depth. The black contours issued from the wavelet analysis show the 8 long-life anticyclonic eddies once they are well-developed : a) A1_2001, b) A1_2002, c) A1_2003, d) A2_2003, e) A1_2005, f) A2_2005, g) A1_2006, i) A1_2008 ; and the circulation over the western part of the shelf is displayed in h).

No long-life eddies have been detected in 2004 and 2007. However, the circulations over the shelf during these two years are quite different. In 2004, only transient anticyclonic features occur. In 2007, a large anticyclonic circulation, but not a closed anticyclonic eddy, occupies the whole west part of the GoL from late May till late October (Fig. 4.2-h). The south-east edge of this circulation consists of the NC along the continental slope.

4.3.1 Influence of wind forcing

The numerical simulations show that, in all cases, the formation of the anticyclonic eddies is associated with strong NW wind events in the western part of the GoL. Since the NW wind is quite frequent in this area, in order to investigate the eddy generation in response to wind forcing, we have tried to avoid the years with numerous successions of NW wind events. Hence, we have chosen to first concentrate on 2005 and show the simple case of the A1_2005 eddy. Following a quiet period with no wind, the wind starts blowing on June 30, 2005. It lasts until July 13 (with one day of recession on July 4). It creates the long-life eddy A1_2005 observed from July 10 till September 4, hence lasting 57 days. The figures selected in Fig. 4.3 illustrate different stages during the eddy's formation.

As we mentioned earlier, from June 26 to 28, there is no strong wind in the western part of the GoL (Fig. 4.3, a-1). On June 28, the currents along the Roussillon coast are southward over the entire water column with a decrease
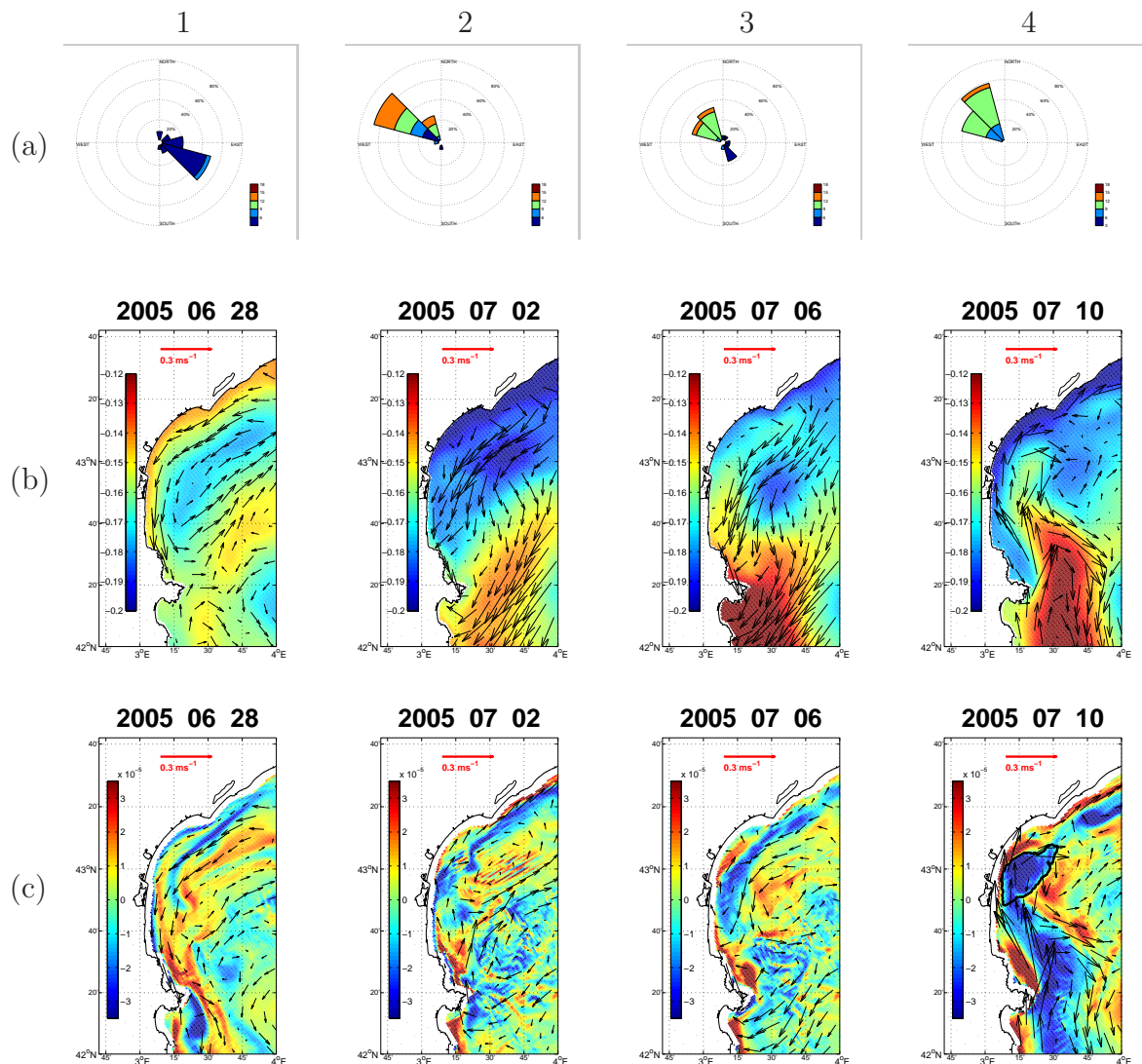
FIG. 4.3 – Time sequences of the generation process of the eddy A1(2005) with 4 days of interval. a) : 3 days wind rose representation at station Leucate ; the location and extension of the fan sector indicating of a wind direction and its percentage ; colors representing wind intensity. b) : sea surface height and current velocity field at 5 m depth. c) : relative vorticity computed at 20 m depth and current velocity fields corresponding to the same depth ; black contours showing the eddy identification issued from the wavelet analysis.
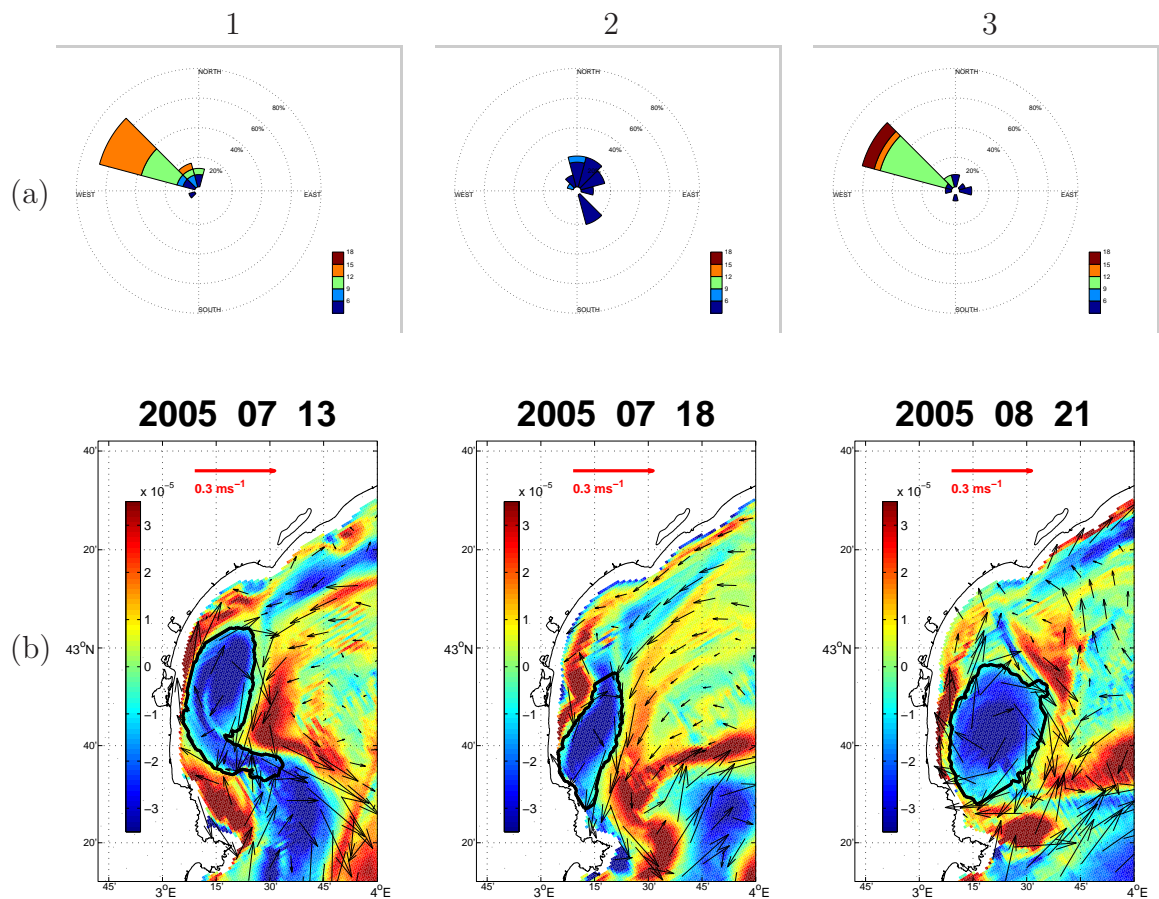
FIG. 4.4 – Time sequences of the evolution of the eddy A1(2005). a) : 3 days wind rose representation at station Leucate ; the location and extension of the fan sector indicating of a wind direction and its percentage ; colors representing wind intensity. b) : relative vorticity computed at 20 m depth and current velocity fields corresponding to the same depth ; black contours showing the eddy identification issued from the wavelet analysis.

(1) 2001

(2) 2002

(3) 2003

(4) 2004

(5) 2005

(6) 2006

(7) 2007

(8) 2008
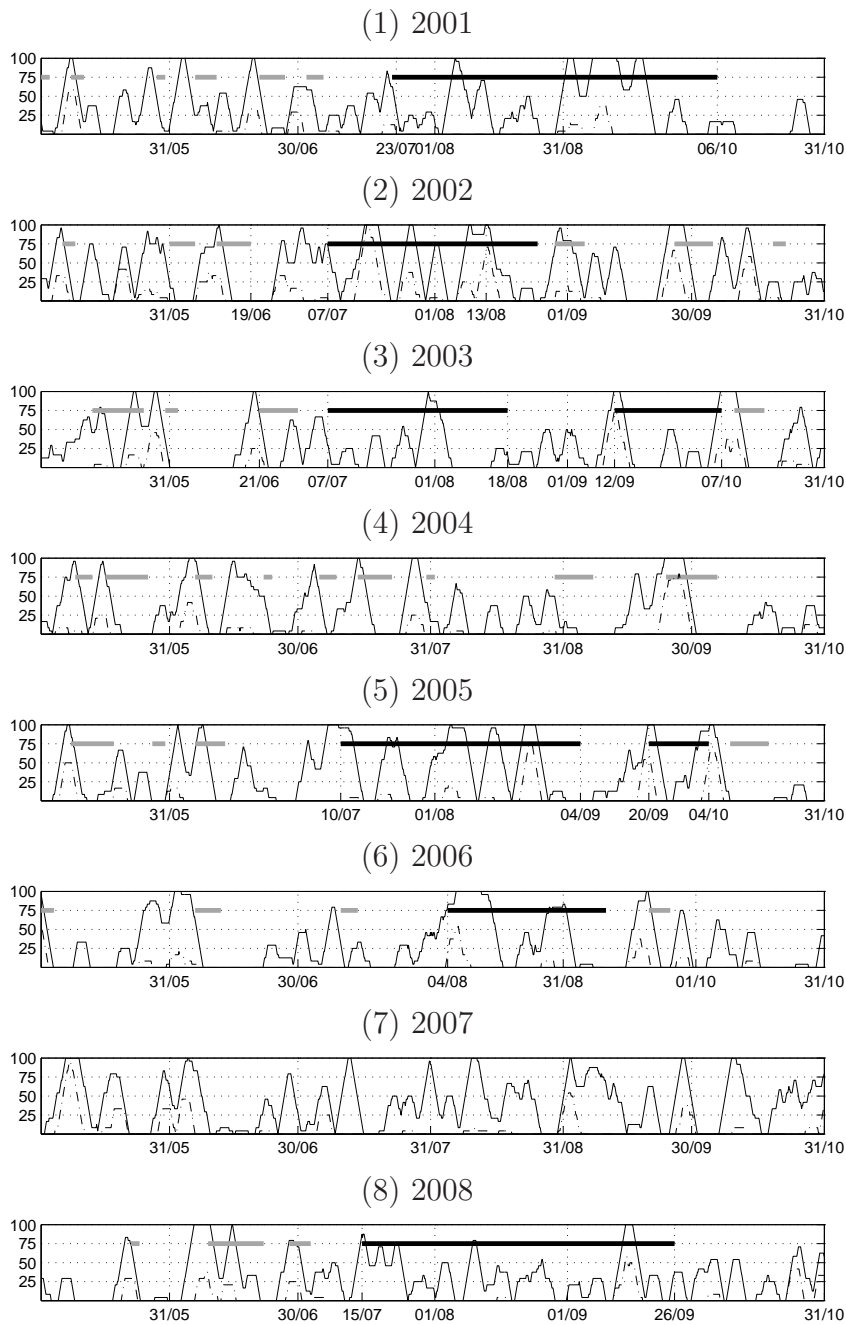
FIG. 4.5 – Temporal evolution of NW wind expressed as a percentage of all wind, with a moving 3 days average, (continuous line : NW wind intensity $\geq$ 8 ms^{-1}; dotted line : $\geq$ 14 ms^{-1}) from May 1 to October 31 for each year. The presence of long-life eddies is indicated by a horizontal black thick line and the transient eddies' presence is indicated by a gray thick line.

in magnitude with depth (Fig. 4.3, b-1, c-1). A strong NW wind blows almost persistently from June 30 to July 2 through the whole shelf with a maximum wind intensity of 15 ms^{-1} (Fig. 4.3, a-2). Offshore, the surface water over the shelf near the north and north-east coast around the Cape d'Agde is advected south-southwestward in response to Ekman transport perpendicular to the wind direction (Fig. 4.3, b-2). The sea surface level close to the north coast is depressed in consequence. An on-shore current is observed at deeper depth to compensate for the upwelled waters (Fig. 4.3, c-2). The surface southwestward Ekman transport is reinforced and constrained by the inner edge of the NC surface layer. Reciprocally, the NC itself is accelerated by the wind-derived circulation and becomes an even stronger barrier preventing the outlet of the southwestward Ekman transport into the Catalan sea. The water piles close to Cape Creus and creates a high SSHA around the cape. The NW wind is absent on July 4 but rises again the day after. The same process repeats itself and the SSHA near the west coast increases. On July 6, the north-south surface pressure gradient starts to create a northward current along the Roussillon coast (Fig. 4.3, c-3). This northward coastal current follows the curved shape of the Roussillon coast. It then turns to the open sea near the Cape d'Agde and joins the southwestward off-shore current. This creates an anticyclonic structure while the surface current is still governed by the wind and keeps its southwestward on-shore movement and keeps on accumulating near the coast. On July 10, the wavelet analysis detects the 'birth' of the eddy. The shape

of this eddy identified by the wavelet analysis at 20 m depth corresponds well with the relative high SSHA at the surface associated with the eddy structure. The eddy is about 20-30 km in diameter and extends through the mixed layer. The advected warm water from the shelf surface accumulated near the western coast are the source waters for this anticyclonic eddy. The strong NW wind persists for 9 days until July 13. The eddy, fed continually under the same process by the coastal northward jet current, increases in size and intensity. At the end of this persisting NW wind event, the eddy has an approximate north-south elliptical shape and is about 30-40 km in diameter (Fig. 4.4-1). The 'tail' at its southern edge reveals its interaction with the NC. The eddy location is more south than its initial location. The eddy weakens when the supply process of wind-driven energy stops. From July 14 to 18, the NW wind disappears for 5 days. By the end of this no wind period, the eddy size has reduced to almost half. The eddy has slightly moved southward to the coast (Fig. 4.4-2) following the relaxation of the surface pressure gradient. The eddy intensity has also decreased and its shape has become more elongated. Afterwards, several strong NW wind events occur in succession with little gaps between them until August 20. At this time, the eddy has become a quite intense structure, less elongated and is about 50 km in diameter (Fig. 4.4-3).

The same work has been performed on all the simulated anticyclonic structures in the western part of the GoL for the 8 years of simulations. It shows that the wind-driven generation mechanism of the eddy A1_2005 is valid for

all other eddies, long-life eddies as well as transient ones. A systematic analysis is done calculating the percentage of the strong NW wind events, with two thresholds (one ≥ 8 ms^{-1} and the other one ≥ 14 ms^{-1}) during the last three days at Leucate station from May 1 to October 31 for the 8 years simulations (Fig. 4.5). The presences of long-life anticyclonic eddies (black thick lines) and transient anticyclonic features (gray thick lines) within this period reveal very clearly the correlation between the persistent NW wind event and the eddies' generation. In general, a strong NW wind event persisting more than about 75% during 3 days is a necessary condition to have an anticyclonic structure formed in the study zone. A sensitivity analysis has been done on the percentage of the NW wind varying the period from 1 to 5 days. The results show that the period of 3 days has the best correlation with the eddy's formation. If the percentage does not reach 75%, but the wind persists for more than 3 days, the cumulative effects of the wind can also generate eddies like the transient eddies in early July 2001 (Fig. 4.5-1) and early May 2003 and like the long-life eddy A1_2003 (Fig. 4.5-3). Moreover, strong NW wind is also necessary after the eddy's formation to sustain the structure. For instance, in 2006, only one persistent NW wind event occurs around July 7 and creates an eddy structure (Fig. 4.5-6). No more persistent NW wind occurs after its formation ; hence the eddy disappears after existing only 5 days and hence is not a 'long-life' eddy. While in early August, the NW wind, persisting for more than half a month, creates the long-life eddy A1_2006.

4.3.2   Influence of stratification conditions

The high probability of observing a long-life anticyclonic eddy during the summer season suggests that the stratification condition probably plays a role on the eddy's generation dynamics. In order to investigate the annual variation of the stratification, the potential energy anomaly ϕ is chosen as the indication of the stability of the water column. This parameter is defined by *Simpson* [1981] and *Simpson and Bowers* [1981] as :

$$\phi = \frac{1}{D} \int_{-H}^{\eta} gz(\bar{\rho} - \rho)dz \qquad (4.1)$$

with the depth-mean density $\bar{\rho}$ defined as :

$$\bar{\rho} = \frac{1}{D} \int_{-H}^{\eta} \rho dz \qquad (4.2)$$

where ρ is the density, H the bathymetry, η the sea surface elevation, $D = H + \eta$ the water column depth and g the gravitational acceleration. For a given density profile, ϕ represents the amount of mechanical energy required to instantaneously homogenize the water column. This parameter has been used successfully as a criterion to study the phenomena concerning stratification [*Burchard and Burchard* 2008; *De Boer et al.* 2008; *Schaeffer* 2010]. The value of ϕ decreases with the level of homogeneity through the water column. Higher values of ϕ indicate a stronger stratification.
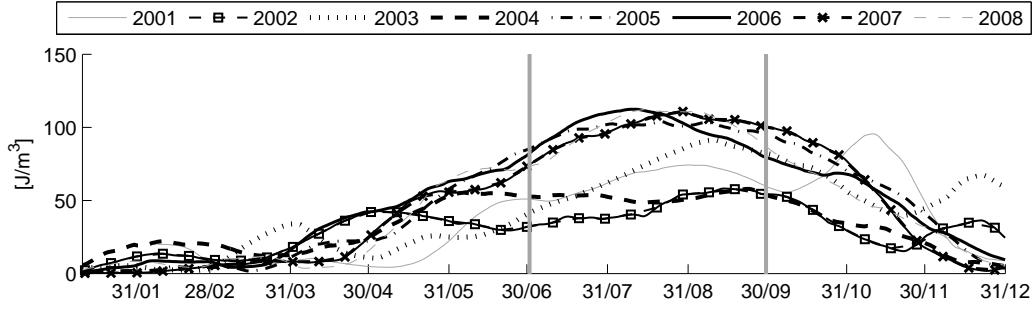
FIG. 4.6 – Time series of averaged monthly moving average potential energy anomaly [Jm^{-3}] over the western part of the GoL for the upper 100 m depth for the years 2001-2008.

In this work, ϕ is calculated for the upper 100 m depth over the western part of the GoL, as indicated by the contour in Fig. 4.1, and horizontally averaged over the studying area.

During winter-spring season, ϕ is minimum in magnitude with a value less than 20 Jm^{-3}, indicating a weak stratification (Fig. 4.6). In general, the increase of ϕ in early May indicates the establishment of the seasonal stratification variation. ϕ reaches a maximum value late June, stays at this level about 3 months till late September and then diminishes with the fall/winter mixing. July, August and September are the months with the maximum value ϕ of about 100 Jm^{-3}. The most stratified conditions are observed during these months and coincidence with the occurrence of all the long-life eddies. We note that ϕ is relatively smaller in 2002 and 2004 with a value of about 60 Jm^{-3} during July-September compared with the value of ϕ of all the others years. Hence, three stratified conditions can be defined by the range of the ϕ

FIG. 4.7 – Left : relative vorticity at 20 m depth, current velocity fields and eddy contour ; black line marks the eddy cross-section ; Middle : Vertical transect of current intensity $[\text{ms}^{-1}]$; Right : Vertical transect of density for (a) : May 12 and (b) : August 19, in 2005.

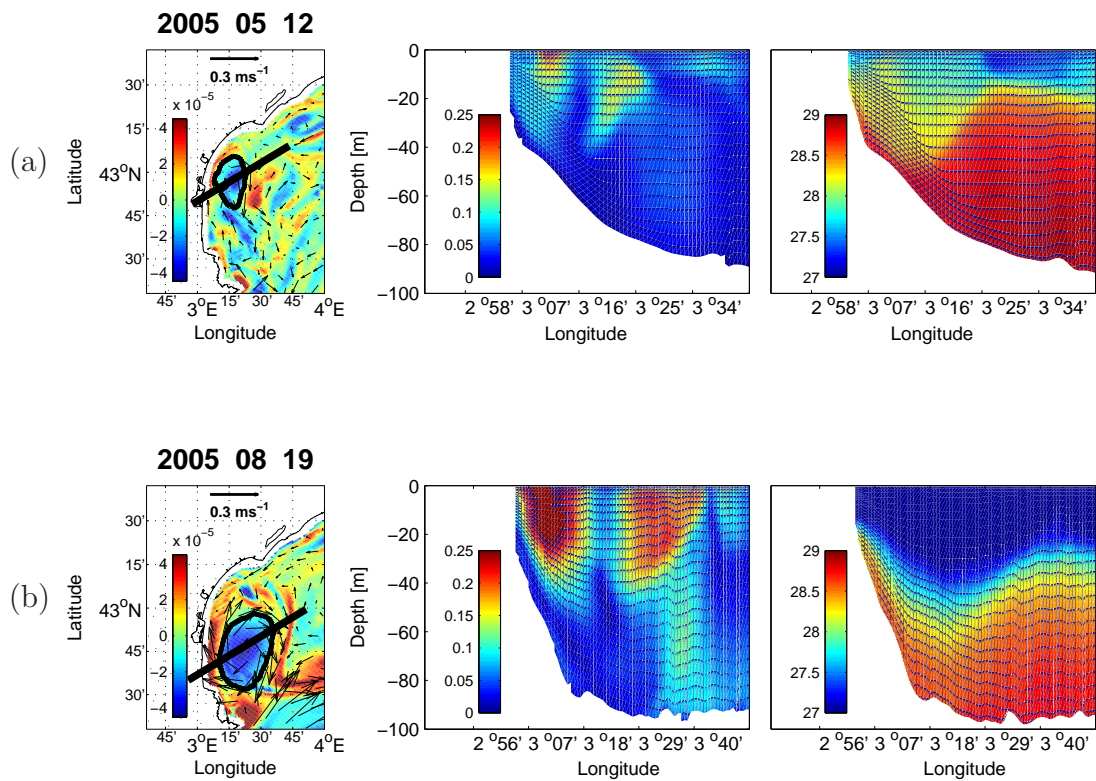value : 1) a weak stratification with a value ϕ below 20 Jm^{-3}, as the one in winter-spring season ; 2) an intermediate stratification with a value ϕ around 60 Jm^{-3} ; as the one in early May and late October of all years and during the summer season in 2002 and 2004 ; 3) a strong stratification with a value ϕ reaching 100 Jm^{-3}, as during all summer seasons except 2002 and 2004. In 2004, no long-life eddy ever occurs despite the successive NW wind events. We think that this is due to the too weak stratification of that summer. The year 2005 is used again to demonstrate the influence of stratification. A transient eddy, referred as A0_2005, is present in early May. Eddy A0_2005 is born on May 8 and disappears on May 18, lasting only 11 days. The strength and horizontal size of this transient eddy are almost one third the ones of long-life eddy A1_2005 (Fig. 4.7-Left) that lasts 57 days from July 10 till September 4. The vertical extent of both anticyclonic eddies is clearly revealed by the areas with high magnitude of current intensity associated with the eddy rotation, and is about 30-35 m depth (40-50 m) for the eddy A0_2005 (A1_2005) (Fig. 4.7-Middle). Vertical transects of density show that both eddies are vertically constrained by the thermocline and hence have baroclinic characteristics (Fig. 4.7-Right). The deepening of the pycnocline in both vertical sections is due to the eddy-induced downwelling within an anticyclonic structure. Excluding the eddy deepening effect, the mixing layer depth ($\sim$ 20m) in early May is shallower than the one in mid-August ($\sim$ 40m). The density gradient between the surface mixed layer and the deeper layer is also less in May than

in August. Both differences indicate that the stratification in early May is weaker than in August, in accordance with the evolution of ϕ. The long-life eddy A1_2005 is hence deeper in vertical extent and has more buoyant water within its core compared to the transient eddy A0_2005.

The differences of eddy characteristics between A0_2005 and A1_2005 can be observed between the other transient and long-life eddies. Such differences, combined with the evolution of the density stratification, suggest that the eddy's size, vertical extent, strength and life duration increase with the stratification condition. During winter-spring, the vertical water column is almost homogenous, and hence is not favorable to eddy generation. The July to September period exhibits the most stratified condition, and hence all the long-life eddies occur within this period. May, June and October have a stratification stronger than the winter-spring one, but smaller than the July-September one. The structures occurring during these 3 months are therefore intermediate in nature, more stable than the filaments observed in winter-spring, but smaller, shallower and less intense than the long-life eddies of July-September. To have a long-life anticyclonic eddy in the western part of the GoL, the second necessary condition, in addition to strong NW wind events, is a strong stratification.

4.4   Discussion

Year	2001	2002	2003	2004	2005	2006	2007	2008	8 years averaged
Percentage of NW wind (%)	55	59	50	53	53	47	62	54	54
Max. NW wind Amplitude(ms^{-1})	16	20	19	17	19	17	19	18	18
Avg. NW wind Amplitude (ms^{-1})	8.9	10	8.7	8.8	9.4	8.8	9.6	8.6	9.1

TAB. 4.2 – Table of percentage of NW wind event and the corresponding maximum and average wind amplitude for the period May-October.

We have shown that, to have a long-life anticyclonic eddy in the western part of the GoL, both persistent strong NW wind events and a well-stratified water column are necessary conditions. If we consider the energy cycle as presented by *Böning and Budich* [1992], the injection of energy by the NW wind can be transferred into potential energy (PE) when the wind-driven Ekman transport pushes the buoyant surface water to the west coast near Cape Creus and downward locally. The eddy generation is driven primarily through the release of PE by baroclinic process [*Holland and Haidvogel* 1980; *Ferrari and Wunsch* 2009]. The mean field PE can also be converted into eddy PE by baroclinic process [*Böning and Budich* 1992]. In other words, in our case, strong wind events are the source of energy, and a well-stratified condition favors the transfer of this wind-induced energy to eddy kinetic energy. The percentage of

the NW wind presence and its maximum and average amplitude from May 1 till October 31 is computed for the 8 years of simulations in order to quantitatively estimate the wind forcing (Table 2). The combined effect of both factors with different levels, resulting in differences of eddy's formation, is discussed in the following six cases : i) When no persistent NW wind event is present, whether stratification is strong or not, no eddy formation occurs. ii) Instead, when a persistent NW wind event occurs while stratification is weak, anticyclonic filaments are generated like the ones formed during winter-spring. iii) When a persistent NW wind event occurs with an intermediate stratification, eddy structures can arise but they possess a short life duration, small size, shallow depth and weak intensity. They correspond to the transient eddies formed in May, June and late October. In 2004, stratification during July-September is not as strong as during the other years (Table 2). Only several persistent NW wind events occur in July, creating transients eddies, but are absent from August to late September (Fig. 4.5-2) and no long-life structures have been detected in 2004. iv) When extremely strong persistent NW wind events occur, long-life eddies can exist despite the intermediate stratification. The long-life eddy A1_2002 is generated in this situation. Indeed, the stratification during summer 2002 is similar to the one in 2004 (Fig. 4.6), implying that summer 2002 is not favorable to long-life eddies. Nonetheless, in 2002, NW wind has the maximum average intensity (20 ms^{-1}) over 8 years (Table 2). Moreover its percentage of 59% is the second highest one after 2007. In fact

the strong wind bursts are also especially concentrated from July to August (Fig. 4.5-2). Despite the stratification but thanks to the strong energy injection, the long-life anticyclonic eddy A1_2002 is formed but with a size smaller than the ones of the other long-life ones (Fig. 4.2). v) When persistent NW wind events and a strong stratification coexist, intense, long-life eddy can be generated. The other 7 long-life eddies : A1_2001, A1_2002, A1_2003, A2_2003, A1_2005, A2_2005 and A1_2008 are generated in this case. In 2006, the long-life eddy lasts only 22 days. 2006 is the year with the least presence of long-life eddy (Table 1). This can be explained by the fact that 2006 has the minimum percentage of the NW wind (47%) of all the 8-year periods. Moreover, the wind has a weak intensity, comparable with the one in 2004. However, the strong stratification in 2006 compensates for the weak wind forcing hence the long-life eddy A1_2006 exists but with a shorter duration. vi) When extremely strong persistent NW wind events occur with a strong stratification, the anticyclonic eddy increases in scale and becomes an anticyclonic circulation like the one observed in 2007 (Fig. 4.2-h). Indeed, on one hand, the stratified condition in 2007 present from late June till late October, is quite strong as shown in Fig. 4.6. On the other hand, the NW wind in 2007 has the largest percentage (62%) of all years and its intensity is the seconder highest. Both conditions for eddy formation are more than satisfied ; hence such anticyclonic circulation can be considered as an extreme case of an eddy-like structure.

4.5 Summary and conclusion

A realistic numerical model has been used in the present work to study the generation of mesoscale anticyclonic eddies located in the western part of the GoL between January 2001 and December 2008. Eddy's life duration varies from several days to several months. 8 long-life anticyclonic eddies with a life duration longer than 15 days have been detected from July to early October. Compared with the transient structures occurring in May, July and late October, the long-life eddies have a bigger size, a deeper vertical extension and are more intense. Indeed, the simulated long-life eddies have dimension of the same order of the Rossby radius of this area suggested to be 15 km by *Grilli and Pinardi* [1998]. The eddies' vertical section of density reveal that the depth of the eddy structures are limited by the thermocline layer. The simulated eddies are hence baroclinic, as the *in situ* anticyclonic eddy observed in early September 2008 in the study area during the Latex08 cruise [*Hu et al.* 2010].

The formation process can be described schematically by Fig. 4.8. A strong NW wind persisting at least 75% of the previous 3 days induces an Ekman transport piling the water close to Cape Creus (Fig. 4.8-1). A northward current along the Roussillon coast is created (Fig. 4.8-2). This current turns to its right approaching Cape d'Agde and generates an anticyclonic circulation (Fig. 4.8-3) that is the precursor of an anticyclonic eddy. After this initial
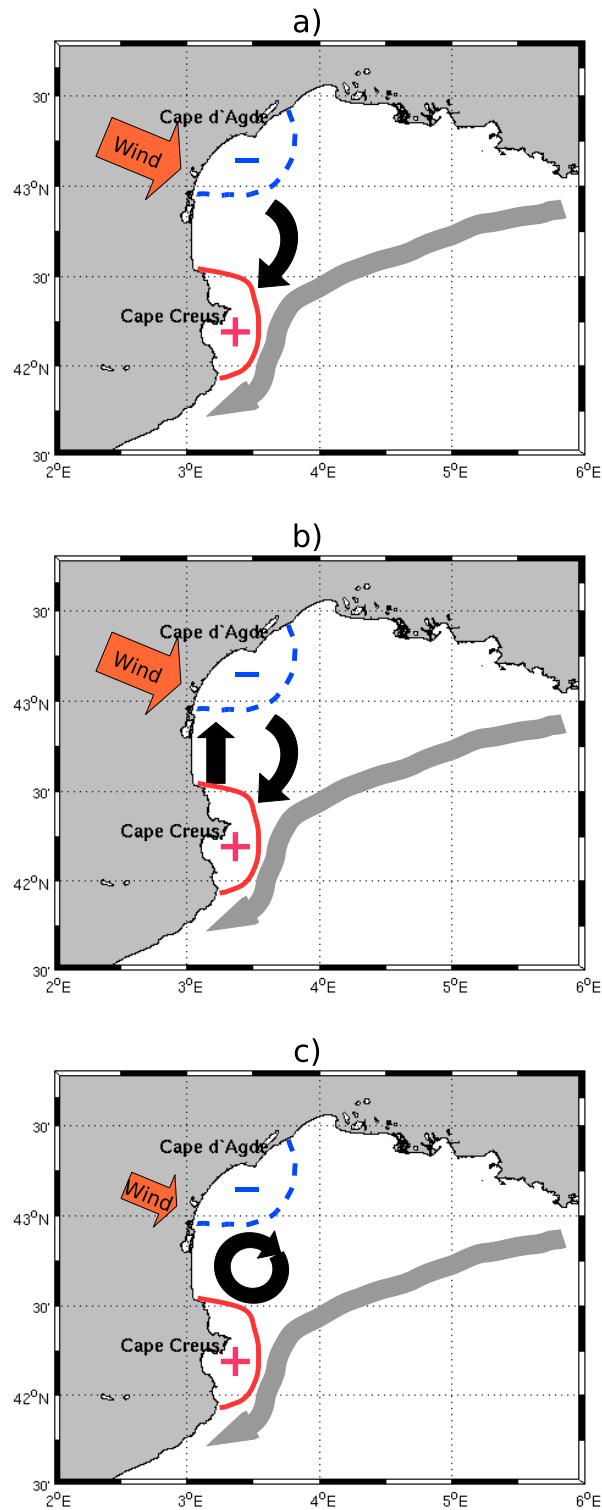
FIG. 4.8 – Schematic of anticyclonic eddy generation process. Wind forcing is indicated by the orange arrows ; sea surface level (+/red or -/blue sign/zone) ; surface currents (black thick arrow) ; NC (gray thick line).

generation phase, the results show that persistent NW wind and a strong stratification guarantee the generation of a long-life eddy in the western part of the GoL. Different cases can be found varying the combination of these two conditions, hence leading to situations from transient eddies to extended anticyclonic circulation. Understanding in detail this generation process may allow in the future the short-term predictability of eddy development.

4.6   Acknowledgments

Conclusions et Perspectives

Les objectifs du présent travail de thèse étaient de caractériser et de comprendre les processus de génération des tourbillons anticycloniques à l'ouest du Golfe du Lion. Ces objectifs ont pu être atteints en utilisant conjointement la modélisation numérique et les mesures *in situ* collectées durant la campagne en mer *Latex08*.

Conclusions

Afin de simuler de façon réaliste les tourbillons côtiers dans la partie ouest du Golfe du Lion nous avons tout d'abord étudié, en effectuant un certain nombre de simulations numériques, la sensibilité du modèle à la résolution du modèle et à la diffusion horizontale. Une configuration du modèle SYM-PHONIE avec une résolution spatiale horizontale de 1 km et un coefficient d'atténuation de 0.8 dans le terme de diffusion horizontale a été retenue suite à des comparaisons avec les données satellitales. L'application de la technique d'analyse en ondelettes sur les résultats du modèle a permis d'identifier les tourbillons, de les suivre et d'estimer leur durée de vie. La simulation numérique pour l'année 2001 montre que des tourbillons anticycloniques se développent à l'ouest du Golfe du Lion pendant la période allant de juillet à début octobre. A la lumière des caractéristiques générales de ces tourbillons, nous avons effectué une campagne en mer *Latex08* dans la zone d'intérêt la première semaine de septembre 2008. Pendant cette campagne un tourbillon anticyclonique a été observé à l'ouest du Golfe du Lion à

partir des données d'ADCP de coque du *TéthysII*, de flotteurs lagrangiens et d'images satellitales. Les caractéristiques du tourbillon observé *in situ* sont bien comparables avec celui présent dans les résultats du modèle. L'analyse de ces données, conjointement avec les résultats de simulation numérique, a permis d'améliorer notre connaissance des tourbillons anticycloniques qui apparaissent à l'ouest du Golfe du Lion.

En général ils sont générés près de la côte du Roussillon pendant la saison estivale-automnale. Ils ont une durée de vie allant de quelques jours jusqu'à plus qu'un mois. Nous qualifions les tourbillons présents plus de 15 jours de structures 'de longue durée de vie'. Sinon, nous les appelons tourbillons 'transitoires'. Ces tourbillons côtiers sont rarement circulaires et ont plus souvent une forme elliptique avec un diamètre [1] allant de $\sim$20 kilomètres, au début de leur génération, à $\sim$80 kilomètres lorsqu'ils sont pleinement développés. Ils présentent des eaux plus chaudes, moins salées et génèrent une anomalie positive de la surélévation par rapport aux eaux ambiantes. Leur vitesse tangentielles maximales peut atteindre 0.6 ms^{-1}, ce qui indique que ce sont des tourbillons côtiers intenses. Leur extension verticale, limitée par la thermocline, peut atteindre jusqu'à $\sim$40 mètres en été. Après leur génération, les tourbillons résident à l'ouest du golfe avec une vitesse de dérive très faible. Pendant leur durée de vie, ils peuvent interagir avec le

---

[1]Diamètre représentant la dimension de la structure elliptique, non assimilable à celui d'un cercle

Courant Nord et dans ce cas on constate soit un renforcement de la partie sud-est du tourbillon, soit sa disparition.

Une simulation pluri-annuelle a été réalisée pour la période 2001 - 2008. Elle a permis d'étudier la reproductibilité et la variabilité des tourbillons, et d'appréhender leur processus de génération en reprenant les idées fondamentales proposées par *Millot* [1982]. Les résultats de simulation ont montré que, pour chaque année de 2001 à 2008, des tourbillons anticycloniques se produisent régulièrement, de mai à octobre, à l'ouest du Golfe du Lion avec des caractéristiques similaires à celles présentées précédemment.

Nous avons effectué des études systématiques sur tous les tourbillons générés au cours des 8 ans de simulation numérique de 2001 à 2008 et nous avons détecté 8 tourbillons anticycloniques de longue durée, tous ayant lieu entre le début juillet et le début octobre. Les années 2004 et 2007 se révèlent être anormales par rapport aux autres six années. En effet, en 2004 aucun tourbillon de longue durée de vie ne se développe, tandis qu'en 2007, une grande circulation anticyclonique, à la place d'un tourbillon cohérent, est observé à l'ouest du golfe de début mai jusqu'à fin octobre. Pour les autres six années, au moins un tourbillon de longue durée de vie est présent. En 2003 et 2005, deux tourbillons de longue durée de vie sont développés.

Il a été montré que le processus de génération des tourbillons anticycloniques à l'ouest du Golfe du Lion, qu'il soit de type transitoire ou de longue

durée de vie, est le suivant : lorsqu'un fort vent du nord-ouest souffle durant 2-3 jours à l'ouest du golfe, il génère un upwelling au sud de cap d'Agde où le niveau de la mer baisse. L'eau de surface au voisinage du cap d'Agde est entraînée par le vent, s'éloigne de la côte nord et se dirige, par transport d'Ekman, vers la côte ouest entre le cap Béar et le cap Creus où elle s'y accumule. Par suite, le niveau de la mer dans cette zone se trouve être plus élevé par rapport à celui au voisinage du cap d'Agde induisant un gradient de pression entre ces deux zones. Lors de la relaxation du vent, ce gradient de pression crée un courant vers le nord le long de la côte du Roussillon qui suit la morphologie curviligne de la côte, et qui, sous l'effet des forces de Coriolis, tourne sur sa droite pour compléter la boucle de circulation anticyclonique.

En fait il est constaté que deux conditions sont nécessaires pour qu'un tourbillon de longue durée de vie se développe : la présence d'un vent du nord-ouest fort et persistant et d'une forte stratification de la masse d'eau. Au plus le vent du nord-ouest est fort et persistant et au plus la stratification est intense, au plus un tourbillon anticyclonique se crée et est résistant. En analysant l'effet combiné de ces deux facteurs en fonction de leur différents degrés d'intensité, nous avons pu expliquer l'existence des tourbillons transitoires et des tourbillons de longue durée de vie, mais également les situations particulières constatées en 2004 et 2007.

Perspectives

Afin de conforter l'ensemble des résultats obtenus au cours de ce travail de thèse, de nouvelles observations *in situ* ont été réalisées. Ainsi trois mouillages de courantomètres ADCP ont été déployés en août 2009 afin de mesurer les courants horizontaux dans la zone d'étude à l'ouest du Golfe du Lion jusqu'en septembre 2010. Les séries temporelles en continu, acquises à l'aide de ces mouillages, permettront d'étudier les variations spatiales et temporelles des courants à l'ouest du golfe. Deux autres campagnes en mer *Latex09* et *Latex10* ont été mises en œuvre dans la même zone d'intérêt que *Latex08* respectivement pendant la dernière semaine d'août 2009 et pendant septembre 2010. Au cours de ces deux campagnes, des données hydrologiques ont été acquises avec une bathysonde, ce qui n'avait pas été possible au cours de la campagne *Latex08* à cause des mauvaises conditions de mer. L'exploitation de ces données de terrain permettra d'avoir une meilleur vision de la structure verticale des tourbillons ainsi que des circulations dans la partie ouest du plateau. L'extention des simulations numériques jusqu'en 2010 devra être menée conjointement de sorte à couvrir temporellement les périodes correspondant aux campagnes *Latex09* et *Latex10*. L'ensemble de ces travaux permettra de tester les hypothèses concernant la génération des tourbillons et leur développement.

Nous avons également noté que les tourbillons pouvaient interagir avec le Courant Nord. Une perspective intéressante pourrait être alors d'évaluer quantitativement cette interaction. Différents outils sont disponibles dans la communauté scientifique et ont été adaptés dans le cadre du projet LATEX.

L'outil diagnostique lagrangien Ariane, mis au point par *Blanke and Raynaud* [1997] au LPO à Brest, a deux modes de calculs : un mode qualitatif de suivi lagrangien de particules individuelles et un mode quantitatif pour le calcul de la fonction de courant. En le couplant à SYMPHONIE de façon autonome (off-line), cet outil permettra d'estimer le temps de résidence des eaux sur le plateau, influencé par la présence des tourbillons, et d'estimer les échanges des masses d'eau, enrichies par l'inclusion du panache distal du Rhône ou par les eaux de l'upwelling près du Cap d'Agde, via les tourbillons présents à l'ouest du Golfe du Lion.

L'application de la méthode des Exposants de Lyapunov aux sorties du modèle SYMPHONIE que nous avons obtenus dans le Golfe du Lion permettra de comparer les résultats de *Nencioli et al.* [en préparation] obtenus à partir de données satellitales d'altimétrie dans l'identification des structures Lagrangiennes cohérentes, qui sont des barrières hydrodynamiques pour le transport de matière sur le plateau.

Le modèle hydrodynamique a été couplé avec un module Lagrangien pour étudier l'influence des processus hydrodynamiques sur le transport et les distributions du zooplankton dans le nord-ouest de la Méditérrannée [*Qiu et al.*

2010, Annexe 2]. Cette étude, basée sur la simulation de l'année 2001, pourra être étendue à l'ensemble de la série temporelle de cette présente thèse afin d'étudier la variabilité interannuelle du processus.

Enfin, pour étudier le rôle des tourbillons anticycloniques simulés dans la partie ouest du Golfe du Lion sur les processus biogéochimiques, le couplage du modèle hydrodynamique avec le modèle biogéochimique Eco3M [*Baklouti et al.* 2006a,b] est actuellement en cours dans le cadre d'une thèse au sein du laboratoire et les premiers résultats montrent une influence des tourbillons sur la structure du réseau trophique [*Campbell et al.* en préparation, 2009, Annexe 3].

L'ensemble de ces études permettra de mieux comprendre et de quantifier l'impact des tourbillons sur les échanges de matière et d'énergie côte-large dans le Golfe du Lion.

Bibliographie

Albérola, C., and C. Millot (2003), Circulation in the French Mediterranean coastal zone near Marseilles : the influence of the wind and the Northern Current, *Cont. Shelf Res.*, *23*, 587–610. 11, 12, 34, 58

Albérola, C., C. Millot, and J. Font (1995), On the seasonal and mesoscale variabilities of the Northern Current during the PRIMO-0 experiment in the western Mediterranean Sea, *Oceanol. Acta*, *18*, 163–192. 11, 46, 72

Allou, A., P. Forget, and J. Devenon (2010), Submesoscale vortex structures at the entrance of the Gulf of Lions in the Northwestern Mediterranean Sea, *Cont. Shelf Res.*, *30*(7), 724 – 732, doi :DOI:10.1016/j.csr.2010.01.006. 14, 15, 63, 75

Arakawa, A., and M. Suarez (1982), Vertical Differencing of the Primitive Equations in Sigma Coordinates, *Mon. Wea. Rev.*, *111*, 34–45, doi :10.1175/ 1520-0493(1983)111. 76

Auclair, F., P. Marsaleix, and C. Estournel (2001), The penetration of the Northern Current over the Gulf of Lion (Mediterranean) as a downscaling problem, *Oceanol. Acta*, *24*, 529–544. 4, 27, 136

Auclair, F., P. Marsaleix, and P. De Mey (2003), Space-time structure and dynamics of the forecast error in a coastal circulation model of the Gulf

of Lions, *Dyn. Atmos. Oceans*, *36*, 309–346, doi :10.1016/S0377-0265(02)
00068-4. 4, 27, 76, 136, 152, 160

Baklouti, M., F. Diaz, C. Pinazo, V. Faure, and B. Quéguiner (2006a), Investigation of mechanistic formulations depicting phytoplankton dynamics for models of marine pelagic ecosystems and description of a new model, *Prog. Oceanogr.*, *71*(1), 1–33. 107

Baklouti, M., V. Faure, L. Pawlowski, and A. Sciandra (2006b), Investigation and sensitivity analysis of a mechanistic phytoplankton model implemented in a new modular numerical tool (Eco3M) dedicated to biogeochemical modelling, *Prog. Oceanogr.*, *71*(1), 34–58. 107

Benitez-Nelson, C. R., et al. (2007), Mesoscale Eddies Drive Increased Silica Export in the Subtropical Pacific Ocean, *Science*, *316*(5827), 1017–1021, doi :10.1126/science.1136221. 45

Blanke, B., and S. Raynaud (1997), Kinematics of the Pacific Equatorial Undercurrent : An Eulerian and Lagrangian approach from GCM results, *J. Phys. Oceanogr.*, *27*, 1038–1053. 106

Böning, C. W., and R. G. Budich (1992), Eddy dynamics in a primitive equation model : sensitivity to horizontal resolution and friction, *J. Phys. Oceanogr.*, *22*, 361–381. 94

Bouffard, J., S. Vignudelli, M. Herrmann, F. Lyard, P. Marsaleix, Y. Ménard,

and P. Cipollini (2008), Comparison of ocean dynamics with a regional circulation model and improved altimetry in the North-western Mediterranean, *19*, 117–133, doi :10.3319/TAO.2008.19.1-2.117. 25, 138

Broche, P., J. L. Devenon, P. Forget, J. De Maistre, J. J. Naudin, and G. Cauwet (1998), Experimental study of the Rhone plume. Part I : physics and dynamics, *Oceanol. Acta*, *21*, 725–738. 9, 10

Burchard, H., and R. Burchard (2008), A dynamic equation for the potential energy anomaly for analysing mixing and stratification in estuaries and coastal seas, *Estuarine, Coastal Shelf Science.*, *77*(4), 679 – 687, doi :DOI: 10.1016/j.ecss.2007.10.025. 89

Campbell, R., F. Diaz, C. Ulses, Z. Y. Hu, C. Estournel, A. Petrenko, A. Doglioli, and I. Dekeyser (2009), Impact of a mesoscale eddy on the structure of the trophic foodweb in the Gulf of Lions (NW Mediterranean), *ASLO Aquatic Sciences Meeting, Nice, France.* 107

Campbell, R., F. Diaz, Z. Y. Hu, A. Doglioli, A. Petrenko, and I. Dekeyser (en préparation), Eddy induced coastal plankton community changes in a coupled numerical model of the Gulf of Lion. 107

Chavanne, C., P. Flament, R. Lumpkin, B. Dousset, and A. Bentamy (2002), Scatterometer observations of wind variations induced by oceanic islands :

implications for wind-driven ocean circulation., *Canadian Journal of Remote Sensing*, *28*(3), 466–474. 74

Conan, P., and C. Millot (1995), Variability of the Northern Current off Marseilles, western Mediterranean Sea, from February to June 1992., *Oceanol. Acta*, *182*, 193–205. 11, 34

Crépon, M., L. Wald, and M. Monget (1982), Low-frequency waves in the ligurian sea during december 1977, *J. Geophys. Res.*, *87*, 595 – 600. 64

De Boer, G. J., J. D. Pietrzak, and J. C. Winterwerp (2008), Using the potential energy anomaly equation to investigate tidal straining and advection of stratification in a region of freshwater influence, *Ocean Model.*, *22*, 1–11. 89

Doglioli, A., A. Griffa, and M. Magaldi (2004), Numerical study of a coastal current on a steep slope in presence of a cape : The case of the Promontorio di Portofino, *J. Geophys. Res.*, *109*, C12033, doi :10.1029/2004JC002422. 74

Doglioli, A. M., B. Blanke, S. Speich, and G. Lapeyre (2007), Tracking coherent structures in a regional ocean model with wavelet analysis : application to Cape Basin Eddies, *J. Geophys. Res.*, *112*, C05043, doi : 10.1029/2006JC003952. 31, 77

Dufau-Julliand, C., P. Marsaleix, A. Petrenko, and I. Dekeyser (2004), Three-dimensional modeling of the Gulf of Lion's hydrodynamics (northwest Me-

diterranean) during January 1999 (MOOGLI3 Experiment) and late winter 1999 : Western Mediterranean Intermediate Water's (WIW's) formation and its cascading over the shelf break, *J. Geophys. Res.*, *109*, C11002, doi : 10.1029/2003JC002019. 4, 11, 27, 30, 76

Echevin, V., M. Crepon, and L. Mortier (2003), Interaction of a coastal current with a gulf : application to the shelf circulation of the Gulf of Lions in the Mediterranean Sea, *J. Phys. Oceanogr.*, *33*, 188–206. 12, 72

Estournel, C., V. Kondrachoff, P. Marsaleix, and R. Vehil (1997), The plume of the Rhône : numerical simulation and remote sensing, *Cont. Shelf Res.*, *17*(8), 899–924, doi :DOI:10.1016/S0278-4343(96)00064-7. 3, 9, 46, 72

Estournel, C., P. Broche, P. Marsaleix, J. L. Devenon, F. Auclair, and R. Vehil (2001), The rhone river plume in unsteady conditions : Numerical and experimental results, *Estuarine, Coastal and Shelf Science*, *53*(1), 25 – 38, doi :DOI:10.1006/ecss.2000.0685. 4, 27

Estournel, C., X. Durrieu de Madron, P. Marsaleix, F. Auclair, C. Julliand, and R. Vehil (2003), Observation and modeling of the winter coastal oceanic circulation in the Gulf of Lions under wind conditions influenced by the continental orography (FETCH experiment), *J. Geophys. Res.*, *108*(C3), 7–18, doi :10.1029/2001JC000825. 4, 12, 13, 24, 27, 46, 75, 76, 133, 136, 161

Estournel, C., F. Auclair, M. Lux, C. Nguyen, and P. Marsaleix (2007), "Scale oriented" embedded modeling of the North-Western Mediterranean in the frame of MFSTEP, *Ocean Science Discussions, Volume 4, Issue 1, 2007, pp.145-187*, *4*, 145–187. 25, 28, 30, 136

Ferrari, R., and C. Wunsch (2009), Ocean Circulation Kinetic Energy : Reservoirs, Sources, and Sinks, *Annu. Rev. Fluid Mech.*, *41*, 253–282, doi : 10.1146/annurev.fluid.40.111406.102139. 94

Flexas, M. M., X. Durrieu de Madron, M. A. Garcia, M. Canals, and P. Arnau (2002), Flow variability in the Gulf of Lions during the MATER HFF experiment (March-May 1997), *J. Mar. Sys.*, *33-34*, 197 – 214, doi : DOI:10.1016/S0924-7963(02)00059-3. 11, 15, 17, 63, 72

Garçon, V. C., A. Oschlies, S. C. Doney, D. McGillicuddy, and J. Waniek (2001), The role of mesoscale variability on plankton dynamics in the north atlantic, *Deep-Sea Res. II*, *48*(10), 2199 – 2226, doi :DOI:10.1016/S0967-0645(00)00183-1. 45

Gaspar, P., Y. Grégoris, and J.-M. Lefevre (1990), A simple eddy kinetic energy model for simulations of the oceanic vertical mixing : Tests at Station Papa and long-term upper ocean study site, *J. Geophys. Res.*, *95*, 179–193. 27, 76, 137

Gatti, J. (2008), Intrusions du Courant Nord Méditérranée sur la partie est

du plateau continental du Golfe du Lion, Ph.D. thesis, Université de la
Méditéerranée. 8, 27

Gatti, J., A. Petrenko, J.-L. Devenon, Y. Leredde, and C. Ulses (2006), The
Rhone river dilution zone present in the northeastern shelf of the Gulf of
Lion in December 2003, *Cont. Shelf Res.*, *26*, 1794–1805, doi :10.1016/j.csr.
2006.05.012. 4, 9, 12, 136

Ginzburg, A. I., A. G. Kostianoy, V. G. Krivosheya, N. P. Nezlin, D. M.
Soloviev, S. V. Stanichny, and V. G. Yakubenko (2002), Mesoscale eddies
and related processes in the northeastern black sea, *J. Mar. Sys.*, *32*(1-3),
71 – 90, doi :DOI:10.1016/S0924-7963(02)00030-1. 64

Grilli, F., and N. Pinardi (1998), The computation of Rossby radii dynamical
processes of deformation for the Mediterranean Sea, *MTP News*, *6*, 4. 28,
60, 97

Guénard, V. (2004), Etude du Mistral en zone côtière : approches théoriques et
observationnelles appliquées aux campagnes MAP et ESCOMPTE, Ph.D.
thesis, Université du Sud Toulon Var. 10

Herrmann, M., S. Somot, F. Sevault, C. Estournel, and M. Déqué (2008),
Modeling the deep convection in the northwestern Mediterranean Sea using
an eddy-permitting and an eddy-resolving model : Case study of winter

1986-1987, *J. Geophys. Res.*, *113*, C04011, doi :10.1029/2006JC003991. 27, 76

Herrmann, M. J., and S. Somot (2008), Relevance of ERA40 dynamical downscaling for modeling deep convection in the Mediterranean Sea, *Geophys. Res. Lett.*, *35*, L04607, doi :10.1029/2007GL032442. 27, 76

Holland, W. R., and D. B. Haidvogel (1980), A parameter study of the mixed instability of idealized ocean currents, *Dyn. Atmos. Oceans*, *4*(3), 185 – 215, doi :DOI:10.1016/0377-0265(80)90014-7. 94

Hu, Z. Y., A. A. Doglioli, A. M. Petrenko, P. Marsaleix, and I. Dekeyser (2009), Numerical simulations of eddies in the Gulf of Lion, *Ocean Model.*, *28*(4), 203–208, doi :DOI:10.1016/j.ocemod.2009.02.004. 46, 47, 48, 60, 61, 63, 65, 73, 76, 77

Hu, Z. Y., A. A. Petrenko, A. M. Doglioli, and I. Dekeyser (2010), Study of coastal eddies : application in the Gulf of Lion, *J. Mar. Sys.*, *submitted*. 73, 97

Hua, B., and F. Thomasset (1983), A Numerical Study of the Effects of Coastline Geometry on Wind-Induced Upwelling in the Gulf of Lions, *J. Phys. Oceanogr.*, *13*, 678–694. 72

Hurlburt, H. E., and J. D. Thompson (1980), A numerical study of Loop

Current intrusions and eddy shedding in Gulf of Mexico, *J. Phys. Oceanogr.*, *10*, 1611–1631. 74

Huthnance, J. M. (1995), Circulation, exchange and water masses at the ocean margin : the role of physical processes at the shelf edge, *Prog. Oceanogr.*, *35*(4), 353 – 431, doi :DOI:10.1016/0079-6611(95)80003-C. 2, 74

James, I. (1996), Advection schemes for shelf sea models, *J. Mar. Sys.*, *8*, 237–254, doi :10.1016/0924-7963(96)00008-5. 28

Jameson, L., and T. Miyama (2000), Wavelet analysis and ocean modeling : A dynamically adaptive numerical method "WOFD-AHO", *Mon. Wea. Rev.*, *128*, 1536–1548, doi :10.1175/1520-0493(2000)128⟨1536:WAAOMA⟩2.0.CO; 2. 31

Kersalé, M., A. M. Doglioli, and A. A. Petrenko (2010), Sensitivity study of the generation of mesoscale eddies in a numerical model of Hawaii islands, *Ocean Sci.*, *submitted.* 74

Langlais, C. (2007), Etude de la variabilité interannuelle des échanges côte-large. Simulation haute résolution de la dynamique du Golfe du Lion, Ph.D. thesis, Université du Sud Toulon Var, France. 12

Leredde, Y., C. Denamiel, E. Brambilla, C. Lauer-Leredde, F. Bouchette, and P. Marsaleix (2007), Hydrodynamics in the Gulf of Aigues-Mortes, NW

Mediterranean Sea : in situ and modelling data, *Cont. Shelf Res.*, *77*, 2389–2406. 12

Ludwig, W., E. Dumont, M. Meybeck, and S. Heussner (2009), River discharges of water and nutrients to the Mediterranean and Black Sea : Major drivers for ecosystem changes during past and future decades ?, *Prog. Oceanogr.*, *80*(3-4), 199–217, doi :10.1016/j.pocean.2009.02.001. 3, 8, 46, 72

Lumpkin, C. F. (1998), Eddies and currents in the Hawaii islands, Ph.D. thesis, University of Hawaii. 74

Luo, J., and L. Jameson (2002), A wavelet-based technique for identifying, labeling, and tracking of ocean eddies, *J. Atmos. Ocean. Technol.*, *19*(3), 381–390, doi :10.1175/1520-0426(2002)019⟨0381:AWBTFI⟩2.0.CO;2. 31

Magaldi, M., T. Özgökmen, A. Griffa, and M. Rixen (2010), On the response of a turbulent coastal buoyant current to wind events : the case of the Western Adriatic Current, *Ocean Dynam.*, *60*, 93–122, 10.1007/s10236-009-0247-9. 74

Marsaleix, P. (1998), A numerical study of the formation of the Rhône River plume, *J. Mar. Sys.*, *14*, 99–115, doi :10.1016/S0924-7963(97)00011-0. 4, 27

Marsaleix, P., F. Auclair, and C. Estournel (2006), Considerations on Open

Boundary Conditions for Regional and Coastal Ocean Models, *J. Atmos. Ocean. Technol.*, *23*, 1604–1613, doi :10.1175/JTECH1930.1. 27, 76

Marsaleix, P., F. Auclair, J. Floor, M. Herrmann, C. Estournel, I. Pairaud, and C. Ulses (2008), Energy conservation issues in sigma-coordinate free-surface ocean models, *Ocean Model.*, *20*, 61–89, doi :10.1016/j.ocemod.2007.07.005. 27, 29, 76, 136

McGillicuddy, J., D.J., et al. (2007), Eddy/Wind Interactions Stimulate Extraordinary Mid-Ocean Plankton Blooms, *Science*, *316*(5827), 1021–1026, doi :10.1126/science.1136256. 45

McWilliams, J. C. (1985), Submesoscale, coherent vortices in the ocean, *Rev. Geophys*, *23*(2), 165–182, doi :10.1029/RG023i002p00165. 74

Millot, C. (1979), Wind induced upwellings in the Gulf of Lions, *Oceanol. Acta*, *2*, 261–274. 10, 16, 24, 45, 46, 47, 72, 75

Millot, C. (1982), Analysis of upwelling in the Gulf of Lions, *Hydrodynamics of semi-enclosed seas : Proceedings of the 13th International Liège Colloquium on Ocean Hydrodynamics. Elsevier Oceanogr. Ser.*, *34*, 143–153. 16, 24, 25, 34, 46, 47, 62, 72, 75, 103

Millot, C. (1990), The Gulf of Lions' hydrodynamics, *Cont. Shelf Res.*, *10*, 885–894, doi :10.1016/0278-4343(90)90065-T. 10, 24, 34, 45, 72

Millot, C. (1991), Mesoscale and seasonal variabilities of the circulation in the western Mediterranean, *Dynamics of Atmospheres and Oceans*, *15*, 179–214, doi :10.1016/0377-0265(91)90020-G. 11, 72

Millot, C. (1999), Circulation in the Western Mediterranean Sea, *J. Mar. Sys.*, *20*, 423–442, doi :10.1016/S0924-7963(98)00078-5. 45, 64, 72, 133

Millot, C. (2003), Circulation in the Mediterranean Sea and consequences on the water quality, *EGS - AGU - EUG Joint Assembly, Abstracts from the meeting held in Nice, France, 6 - 11 April 2003*. 74

Millot, C., and M. Crépon (1981), Inertial Oscillations on the Continental Shelf of the Gulf of Lions, *jpo*, *11*, 639–657, doi :10.1175/1520-0485(1981) 011. 10

Millot, C., and L. Wald (1980), The effect of Mistral wind on the Ligurian current near Provence, *Oceanol. Acta*, *3*, 399–402. 12, 133, 152

Millot, C., and L. Wald (1981), Upwelling in the Gulf of Lions, *Coastal Upwelling Research, Richards Ed.*, pp. 160–166. 16

Minas, M., and H. Minas (1989), Primary production in the Gulf of Lions with considerations to the Rhône River input, *Water Pollution Research Reports*, *32*(5), 112–125. 3, 46, 72

Mémery, L., G. Reverdin, J. Paillet, and A. Oschlies (2005), Dintroduction to the pomme special section : Thermocline ventilation and biogeochemical

tracer distribution in the northeast atlantic ocean and impact of mesoscale dynamics, *J. Geophys. Res.*, *110*(4), C07S01, doi :10.1029/2005JC002976. 3

Nencioli, F., V. S. Kuwahara, T. D. Dickey, Y. M. Rii, and R. R. Bidigare (2008), Physical dynamics and biological implications of a mesoscale eddy in the lee of Hawaii : Cyclone Opal observations during E-Flux III, *Deep-Sea Res. II*, *55*, 1252–1274, doi :10.1016/j.dsr2.2008.02.003. 51

Nencioli, F., F. d'Ovidio, A. M. Doglioli, and A. A. Petrenko (en préparation), Direct observations of an hyperbolic point in the Gulf of Lion. 106

Nof, D. (1999), Strange encounters of eddies with walls, *J. Mar. Res.*, *57*(5), 739–761. 39

Olson, D. (1980), The Physical Oceanography of Two Rings Observed by the Cyclonic Ring Experiment. Part II : Dynamics., *J. Phys. Oceanogr.*, *10*, 514–528. 55

Pascual, A., B. Buongiorno Nardelli, G. Larnicol, M. Emelianov, and D. Gomis (2002), A Case of An Intense Anticyclonic Eddy In The Balearic Sea (w Mediterranean), *J. Geophys. Res.*, *107*, 3183, doi :10.1029/2001JC000913. 75

Petrenko, A. A. (2003), Variability of circulation features in the Gulf of Lion

NW Mediterranean Sea. Importance of inertial currents, *Oceanol. Acta*, *26*, 323–338. 10, 11, 12, 34, 46, 72, 133, 151, 152, 160

Petrenko, A. A., Y. Leredde, and P. Marsaleix (2005), Circulation in a stratified and wind-forced Gulf of Lions, NW Mediterranean Sea : *in situ* and modeling data, *Cont. Shelf Res.*, *25*, 7–27, doi :10.1016/j.csr.2004.09.004. 4, 12, 27, 34, 49, 64, 76, 133, 136, 152, 160

Petrenko, A. A., C. Dufau, and C. Estournel (2008), Barotropic eastward currents in the western Gulf of Lion, northwestern Mediterranean Sea, during stratified conditions, *J. Mar. Sys.*, *74*(1-2), 406–428, doi :DOI: 10.1016/j.jmarsys.2008.03.004. 4, 12, 17, 27, 75, 76, 136

Pichevin, T., and D. Nof (1996), The eddy cannon, *Deep-Sea Res. I*, *43*(9), 1475 – 1507, doi :DOI:10.1016/S0967-0637(96)00064-7. 74

Pinardi, N., et al. (2003), The Mediterranean ocean forecasting system : first phase of implementation (1998-2001), *Ann. Geophys.*, *21*, 3–20. 77

Qiu, Z., A. Doglioli, Z. Hu, P. Marsaleix, and F. Carlotti (2010), The influence of hydrodynamic processes on zooplankton transport and distributions in the north western mediterranean : Estimates from a lagrangian model, *Ecological Model.*, *221*(23), 2816 – 2827, doi :DOI:10.1016/j.ecolmodel.2010.07. 025. 106

Robinson, M. A. S., A. R., and N. Pinardi (1988), Gulf Stream simulations

and the dynamics of ring and meander processes, *J. Phys. Oceanogr.*, *18*, 1811–1853. 74

Rubio, A., P. Arnau, M. Espino, M. Flexas, G. Jordà, J. Salat, J. Puig-defàbregas, and A. S.-Arcilla (2005), A field study of the behaviour of an anticyclonic eddy on the Catalan continental shelf (NW Mediterranean), *Prog. Oceanogr.*, *66* (2-4), 142–156, doi :10.1016/j.pocean.2004.07.012. 15, 63, 75

Rubio, A., B. Barnier, G. Jordà, M. Espino, and P. Marsaleix (2009), Origin and dynamics of mesoscale eddies in the Catalan Sea (NW Mediterranean) : Insight from a numerical model study, *J. Geophys. Res.*, *114* (C06009), 0148–0227, doi :10.1029/2007JC004245. 15, 75

Ruiz, S., J. Font, M. Emelianov, J. Isern-Fontanet, C. Millot, J. Salas, and I. Taupier-Letage (2002), Deep structure of an open sea eddy in the Algerian Basin, *J. Mar. Sys.*, *33-34*, 179–195, doi :10.1016/S0924-7963(02)00058-1. 74

Sammari, C., C. Millot, and L. Prieur (1995), Aspects of the seasonal and mesoscale variabilities of the Northern Current inferred from the PROLIG-2 and PROS-6 experiments, *Deep-Sea Res. I*, *42*, 893–917. 11, 46, 64, 72

Schaeffer, J. (2010), Impact du vent sur la circulation hydrodynamique dans

le Golfe du Lion : modélisation haute résolution., Ph.D. thesis, Université du Sud Toulon-Var. 15, 75, 89

Signell, R., and W. Geyer (1991), Transient eddy formation around headlands, *J. Geophys. Res.*, *96*(C2), 2561–2575. 74

Simpson, J. (1981), The Shelf-Sea Fronts : Implications of their Existence and Behaviour, *Philosophical Transactions of the Royal Society of London. Series A, Mathematical and Physical Sciences*, *302*(1472), 531–546. 89

Simpson, J., and D. Bowers (1981), Models of stratification and frontal movement in shelf seas, *Deep-Sea Res. I*, *28*(7), 727 – 738, doi :DOI: 10.1016/0198-0149(81)90132-1. 89

Spall, M. A., and W. R. Holland (1991), A Nested Primitive Equation Model for Oceanic Applications, *J. Phys. Oceanogr.*, *21*, 205–220, doi :10.1175/ 1520-0485(1991)021. 28

Stanev, E. (2005), Understanding black sea dynamics : An overview of recent numerical modeling, *Oceanography.*, *18*, 56–75. 64

Stanev, E. V., J. M. Beckers, C. Lancelot, J. V. Staneva, P. Y. L. Traon, E. L. Peneva, and M. Gregoire (2002), Coastal-open ocean exchange in the black sea : Observations and modelling, *Estuarine, Coastal Shelf Science.*, *54*(3), 601 – 620, doi :DOI:10.1006/ecss.2000.0668. 64

Taupier-Letage, I., I. Puillat, C. Millot, and P. Raimbault (2003), Biological response to mesoscale eddies in the algerian basin, *J. Geophys. Res.*, *108*, C8, doi :10.1029/1999JC000117. 45

Thill, A., S. Moustier, J. M. Garnier, C. Estournel, J. J. Naudin, and J. Y. Bottero (2001), Evolution of particle size and concentration in the Rhône river mixing zone : : influence of salt flocculation, *Cont. Shelf Res.*, *21*(18-19), 2127 – 2140, doi :DOI:10.1016/S0278-4343(01)00047-4. 8

Ulses, C., C. Grenz, P. Marsaleix, E. Schaaff, C. Estournel, S. Meulé, and C. Pinazo (2005), Circulation in a semi enclosed bay under the influence of strong fresh water input, *J. Mar. Sys.*, *56*, 113–132. 28

Ulses, C., C. Estournel, J. Bonnin, X. Durrieu de Madron, and P. Marsaleix (2008a), Impact of storms and dense water cascading on shelf-slope exchanges in the Gulf of Lion (NW Mediterranean), *J. Geophys. Res.*, *113*, C02010, doi :10.1029/2006JC003795. 4, 11, 27, 76

Ulses, C., C. Estournel, P. Puig, X. Durrieu de Madron, and P. Marsaleix (2008b), Dense shelf water cascading in the northwestern Mediterranean during the cold winter 2005 : Quantification of the export through the Gulf of Lion and the Catalan margin, *Geophys. Res. Lett.*, *35*, L07610, doi : 10.1029/2008GL033257. 4, 11, 27, 76

Annexe

Forçages Météorologiques

SSR : urface solar radiation ; Signe + ; Unité w/m².

SNSF : surface longwave flux ; Signe + si downward ; Unité w/m².

UWIND : composante Ox du vent à 10m ; Unité (m/s)

VWIND : composante Oy du vent à 10m ; Unité (m/s)

PSS : pression niveau mer en Pascals

θ_2 : temperature potentielle à 2m en Kelvin (Celsius+273.15)

Q2 : Humidité spécifique à 2m ; (kg_{eau}/kg_{air})

PRECIPI : precipitation en mètres (de hauteur d'eau) par secondes

<u>SSR</u> *Temperature.F*

Variable	Unité dans Aladin	Unité dans Symphonie	Conversions
SSR	Joule/m^2	W/m^2	Désintégration
SNSF	Joule/m^2	W/m^2	Désintégration
U_{wind}	$m \cdot s^{-1}$	$m \cdot s^{-1}$	-
V_{wind}	$m \cdot s^{-1}$	$m \cdot s^{-1}$	-
PSS	Pascale	Pascale	-
θ_2	Kelvin	Kelvin	-
Q_2	%	%	-
PRECIPI	$kg \cdot m^2$	$m \cdot s^{-1}$	$kg \cdot m^2 s^{-1}$ (désintégrer)
			$\downarrow$
			$m \cdot s^{-1}$ (* $1/\rho$)

Dans les équations de conservation qui concernent le tranport des quantités telles que la température T et la salinité S :

$$\frac{\partial T}{\partial t} + u\frac{\partial T}{\partial x} + v\frac{\partial T}{\partial x} + w\frac{\partial T}{\partial x} = -\frac{\partial(\overline{T'w'})}{\partial z} + \frac{Q_c}{\rho_0 \cdot C_p}\frac{\partial I}{\partial z} \qquad (1.1)$$

Q_c est le flux solaire incident (SSR_Z).

<u>SNSF</u> *Temperature.F*

Les conditions aux limites à la surface libre (en z = η) :

$$\upsilon_t\frac{\partial T}{\partial z} = Q_e + Q_s + Q_l + (1 - T_r) \cdot Q_c \qquad (1.2)$$

Q_e est le flux de chaleur latente (SLHF_Z) ;

Q_s est le flux de chaleur sensible (SSHF_Z) ;

Q_c est le flux radiatif dans les courtes longueurs d'onde (SSR_Z - flux solaire incident) ;

Q_l est le flux radiatif dans les grandes longueurs d'onde (SNSF_Z) ;

bulk_formulae.f

Q_l **SLHF_Z : surface latent heat flux**

$$Q_l = \rho_{air} \cdot L_v \cdot C_e \cdot U_{10} \cdot (Q_{10} - Q_0) \qquad (1.3)$$

ρ_{air} : la masse volumique de l'air (1.226 kgm^{-3}) ;

L_v : Chaleur latente de vaporisation $2.5 \cdot 10^6$;

C_e : the Dalton number (valeur calculée) ;

U_{10} : vitesse du vent à 10 mètres ;

Q_{10}, Q_0 : Delta d'humidité spécifique (valeur calculée) ;

$$Q_0 = \frac{0.98 * 640380}{\rho_{air} * exp\frac{-5107.4}{(T+273.15)}} \tag{1.4}$$

Q_s **SSHF_Z : surface sensible heat flux**

$$Q_s = \rho_{air} \cdot Cp_{air} \cdot C_h \cdot U_{10} \cdot (\theta_{10} - \theta_0) \tag{1.5}$$

Cp_{air} : capacité calorifique de l'air 1000.5 ;

C_h : Stanton number (valeur calculée) ;

$\theta_{10} - \theta_0$: delta temp potentielle 10m-0m ;

U(V)WIND

La tension de surface $\vec{\tau_s}$ (WSTRESS_Z dans *Symphonie*) est calculée à partir de :

$$\vec{\tau_s} = \rho_{air} \cdot C_v \cdot \|\vec{V}_{vent}\| \cdot \vec{V}_{vent} \tag{1.6}$$

ρ_{air} : la masse volumique de l'air ($1.226 \ kgm^{-3}$) ;

$\vec{V}_{vent}$:la vitesse du vent à 10 m d'altitude ;

C_v : le coefficient de tranînée ;

$$UV_{10} = \sqrt{(UWIND^2 + VWIND^2)} \qquad (1.7)$$

PSS

$$\Delta T_p = T_{p10} - (T + 273.15) * (\frac{10^5}{PSS})^{0.286} \qquad (1.8)$$

ΔT_p : Delta de temperature potentielle entre les niveaux 10m et 0m ;

T_{p10} : Température potentielle à 10m ;

$$R_0 = \frac{0.622 * PVS_0}{PSS - PVS_0} \qquad (1.9)$$

R_0 : rapport de melange saturant à 0 metre

PVS_0 : 0.622 * Pression Vapeur Saturante 0 metre

Dans Salinity.F :

L'eau evaporée ou condensée est calculée a partir du flux de chaleur latente

$$\frac{SHLF}{A} \qquad (1.10)$$

$SHLF$: Flux chaleur latente de condensation (W/m^2 / $J/s \cdot m^2$) ; A : Constante, la chaleur latente de condensation ($2.47 \cdot 10^6$ J/s)

Le volume evaporé ou condensé par maille dv (horizontal) :

$$dv = \frac{SHLF \cdot dt}{\rho_{eau} \cdot A} \cdot dx \cdot dy \qquad (1.11)$$

The influence of hydrodynamic processes on zooplankton transport and distributions in the North Western Mediterranean : estimates from a Lagrangian model

Qiu, Z. F., Doglioli, A. M., Hu, Z. Y. Marsaleix, P., Carlotti, F., 2009 : **The influence of hydrodynamic processes on zooplankton transport and distributions in the North Western Mediterranean : estimates from a Lagrangian model**. Ecological Model. 221 (23), 2816 - 2827.

2.1   abstract

A Lagrangian module has been developed and coupled with the 3D circulation model Symphonie to study the influence of hydrodynamic processes on zooplankton transport and distributions in the North Western Mediterranean (NWM). Individuals are released every 3 days from March to August 2001 in two initial areas : around the DYFAMED sampling station in the central Ligurian Sea and in the Rhône river plume. Then the individuals are tracked for 40 days either as passive particles or with a simple diel vertical migration (DVM) pattern. The simulations suggest strong seasonal patterns in the distributions of the individuals released around the DYFAMED sampling station. Individuals spread all over the NWM basin after 40 days but different patterns occur depending on the season, the initial depths of release and the capacity of DVM. Offshore-shelf transport only occurs in April and May with particles ending up in the Gulf of Lions (GoL) in low concentrations. In other months, the Northern Current (NC) can be considered as a barrier for particles entering the GoL from the offshore sea. A quarter to a half of passive individuals released in the Rhône river plume remain in the GoL. The rest is transported by the NC towards the Catalan Sea. Applying a simple DVM scheme does not increase the retention of particles on the shelf.

2.2   Introduction

Over the past few decades, it has become clear that physical processes are important drivers of population dynamics in the oceans [Miller et al. 1998; Batchelder et al. 2002]. Zooplankton organisms are critically dependent on their physical environments but they are not necessarily passive particles [Batchelder et al. 2002; Cianelli et al. 2007; Sentchev and Korotenko 2007; Carr et al. 2008]. They swim vertically which influences their spatio-temporal distributions. At each phase of their development, they have to find prey and avoid predators. At the adult stage they will seek mates and reproduce. Therefore, zooplankton transport in a variety of physical conditions can be considered as the combination of two closely linked processes. The first is zooplankton transport by non-stationary flow fields and the second is the behavioural response of zooplankton, mainly by swimming, to the changes of environmental conditions.

When investigating the relationships between particle distribution and physical processes, researchers often used bio-physical models [e.g. Levy et al. 2000; Oschlies 2002]. Lagrangian particle tracking models coupled with hydrodynamic models are particularly efficient tools to examine the role played by various physical processes, to study transport processes over an entire basin and to simulate complex and interactive processes acting at different scales [e.g. Miller et al. 1998; Blanke et al. 1999; Falco et al. 2000; Guizien et al.

2006; Speirs et al. 2006; Lett et al. 2007].

Recent developments of Lagrangian modeling have highlighted the links between physical structures, zooplankton behaviour and marine productivity in regions such as the Benguela ecosystem [Mullon et al. 2003; Lett et al. 2007] or the Georges Bank [Miller et al. 1998]. Cianelli et al. [2007] simulated the particle exchange in the Gulf of Lions (GoL) using a Lagrangian approach coupled with a three-dimensional (3D) circulation model. They found that particle distributions are strongly related to the mesoscale and sub-mesoscale hydrodynamic structures on the shelf and to the offshore circulation associated with the Northern Current (NC).

In the North Western Mediterranean (NWM) the large-scale circulation is dominated by the NC that forms in the Ligurian Sea where the Western Corsica Current (WCC) merges with the Eastern Corsica Current (ECC) (Fig. 2.1, Palomera et al. [2007]). From the Ligurian Sea the NC flows along the continental shelf to the Catalan Sea. Sometimes a branch of the NC can intrude into the GoL [Millot and Wald 1980; Estournel et al. 2003; Petrenko 2003; Petrenko et al. 2005]. The main hydrodynamic features of the GoL have been previously researched both experimentally and numerically [e.g. Millot 1999; Andre et al. 2005]. The shelf circulation in the GoL is complex due to the combined effects of various forcings, which are mainly the strong winds blowing from the north (Mistral) and from the northwest (Tramontane), the NC, the Rhône river discharges and the complex topography, characterised by several

canyons.

The NWM and particularly the GoL, is an interesting area to study the influence of water circulation and estuarine inputs on biological activity and distribution. The NWM sub-basin is one of the most productive areas in the Mediterranean owing to important river discharges from the Rhône and Ebre rivers, strong wind mixing on the shelf and in the open sea, gyres, upwellings and vertical mixing. Production and phytoplankton stock occurring in favourable zones (fronts, whirlwinds, river plumes) induces production and zooplankton stock dominated by *Calanus helgolandicus*, *Centropages typicus*, *Pseudocalanus* and *Paracalanus sp.* [Champalbert 1996]. Small pelagics (such as sardine and anchovy) and medium size-pelagics (such as mackerel and bonite) are the main contributors to total landings (about 50%). The GoL is a major spawning area for the small pelagic fish in the NWM [Garcia et al. 1996; Palomera et al. 2007], owing to its relative high primary production over the year [Diaz et al. 2001].

Spatial distribution of zooplankton is a key issue to understand regional functioning of pelagic ecosystem. Spatial differences in zooplankton concentrations may be related to advective and mixing transport as well as local production or predation pressure. In this paper, we use a Lagrangian model to simulate the trajectories of passive particles and vertically migrating organisms. Trajectories of zooplankton individuals of average life-time of 40 days (an average values for copepods, jellyfish, fish larvae) from a detailed physical

oceanographic model let us to investigate which part of zooplankton produced on the shelf of the GoL is maintained due to physical retention or concentration mechanisms, and which part is advected outside of the shelf. This is particularly relevant for the fish larvae (anchovy and sardines) produced on the Rhône plume [Palomera 1991], which can stay on the productive shelf or be washed away in the Catalan Sea. Another major issue is the potential exchange of zooplankton from the Ligurian Sea to the GoL and the Catalan Sea. Jellyfish swarms of *Pelagia noctiluca*, a small pelagic jellyfish, start off shore in the Ligurian Sea or at the shelf-slope in the NWM from March to August [Mariottini et al. 2008] and are advected west ward through the northern current and on the coast depending on surface currents. The third major issue is the advection of plankton larvae of benthic species, such as sponge [Mariani et al. 2006] or sea urchins [Pedrotti 1993], which can exchange genotypes between different regions of the NWM.

It is well known that zooplankton organisms are not completely passive and may change their vertical position by active swimming or density changes. Diel vertical migration (DVM) is the most common zooplankton swimming behaviour in which organisms reside in surface or near-surface waters at night and in deeper waters during the day. This behaviour enables zooplankton to feed in relatively productive surface waters at night and avoid visual predators during the day [Haney 1988]. The potential effect of DVM on zooplankton transport has been demonstrated by several researchers [Batchelder et al.

2002; Sentchev and Korotenko 2007; Carr et al. 2008].

Thus our goal is to investigate the influence of advection on zooplankton transport, as well as the combination between advection and DVM, to better evaluate the connections of zooplankton between different regions of the NWM. An outline of the Lagrangian approach is given in the next section. The simulated results, considering zooplankton individuals as passive particles and with active DVM, are presented in section 3 and discussed in section 4. In the following text, the term "particles" will be used to describe these zooplankton individuals.

2.3 Materials and methods

Hydrodynamic model

We use the 3D numerical hydrodynamic model Symphonie to determine current fields. A detailed description of the model is given by Marsaleix et al. [2008] and references therein. During last ten years the model has been successfully used for several studies in the NWM : the NC intrusions on the continental shelf [Auclair et al. 2001; Petrenko et al. 2005; Gatti et al. 2006], wind-forced circulation [Auclair et al. 2003; Estournel et al. 2003; Petrenko et al. 2008] and the Rhône river plume dynamics [Estournel et al. 2001].

In the model, the Arakawa-C grid is used with horizontal mesh of 3km and a hybrid (z-σ) coordinate system [Estournel et al. 2007] with 41 vertical levels.

A minimum depth of 3m is imposed in nearshore areas. Turbulence closure in the vertical direction is achieved through the scheme proposed by Gaspar et al. [1990]. The upwind type advection scheme is described in Hu et al. [2009] and references therein.
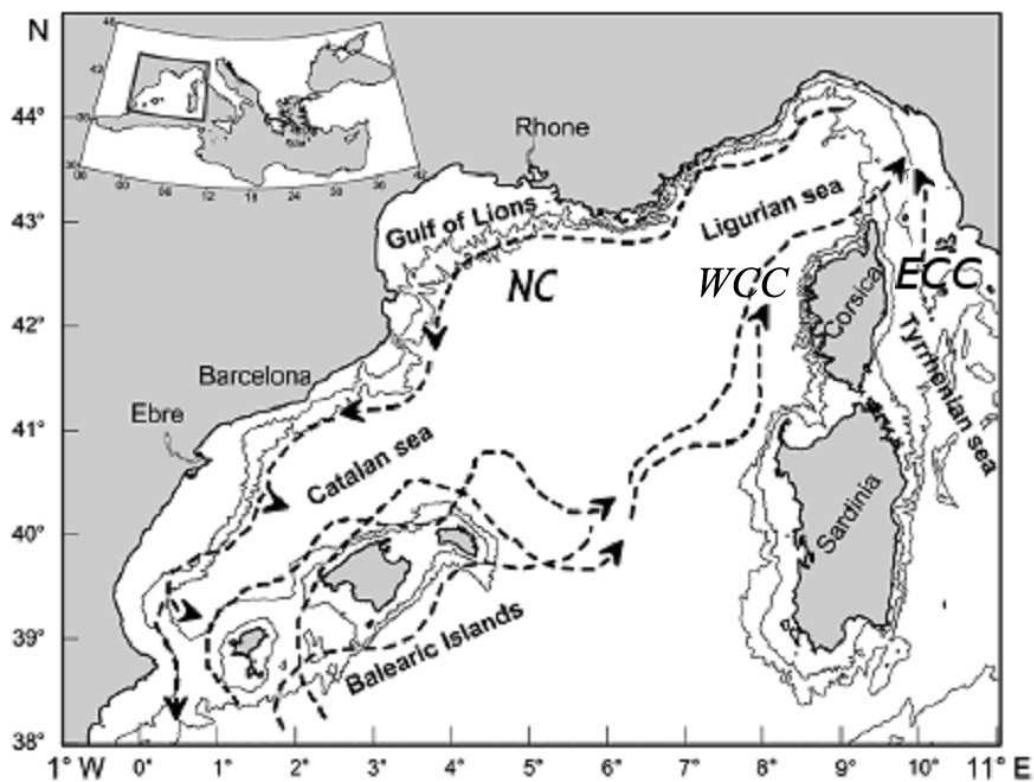

FIG. 2.1 – Major basins and currents in the North Western Mediterranean

The real fresh-water inputs from the Rhône river are provided by the "Compagnie Nationale du Rhône" every day and meteorological forcings are given from the Meteo-France model Aladin at high frequency (3h). The restoring terms of the open boundary scheme allow forcing the model with the features of the general circulation given by the regional-scale model MOM.

Modelling results were recently validated by comparison with the satellite measurements by Bouffard et al. [2008] and Hu et al. [2009].

Particle tracking model

We use a Lagrangian particle tracking code based on the ROMS Offline Floats [ROFF, introduced in details by Carr et al. 2008]. The brief flow chart is shown in Fig. 2.2. The Lagrangian particle tracking algorithm is derived from the following vector equation :

$$\frac{dx}{dt} = \vec{u}(x, t) \tag{2.1}$$

Here x is the particle location and $\vec{u}$ is the particle velocity at the position x. We uses an advanced fourth-order accurate Adams-Bashford-Moulton (ABM hereafter) predictor-corrector scheme to integrate the Equation 2.1 over time. The advanced ABM method is a predictor-corrector method, combining the Adams-Bashford method (the predictor step, Equation 2.2) and the advanced Adams-Moulton method (the corrector step, Equation 2.3).

$$\tilde{x}^{n+1} = x^n + \frac{dt}{24}[55\vec{u}(x^n, t^n) - 59\vec{u}(x^{n-1}, t^{n-1}) + 37\vec{u}(x^{n-2}, t^{n-2}) - 9\vec{u}(x^{n-3}, t^{n-3})] \tag{2.2}$$

$$x^{n+1} = \frac{19}{270}\tilde{x}^{n+1} + \frac{251}{270}\{x^n + \frac{dt}{24}[9\vec{u}(\tilde{x}^{n+1}, t^{n+1}) + 19\vec{u}(x^n, t^n) - 5\vec{u}(x^{n-1}, t^{n-1}) + \vec{u}(x^{n-2}, t^{n-2})]\}$$

$$(2.3)$$

The right-hand side of the Equation 2.1 is comprised by a series of stored 3D velocity fields and zooplankton swimming velocity within their DVM behaviour.

$$\vec{u}(x, t) = \vec{u}_{sym} + \vec{u}_{dvm} \qquad (2.4)$$

The item $\vec{u}_{sym}$ is interpolated in time and space of the daily average velocity fields from the circulation model Symphonie, i.e. the velocity values are linearly interpolated from the eight nearest grid cells.

The item $\vec{u}_{dvm}$ is treated in two ways : (i) zooplankton are considered as passive drifters for which the transport processes are determined uniquely by the velocity fields ; (ii) DVM behaviour has been considered as follows : if a particle is above 50m at 06 :00, it will swim down with the velocity 50mh^{-1} from 06 :00 to 08 :00 ; from 18 :00 to 20 :00 all particles will swim up from deeper depths to near-surface with the velocity 50mh^{-1}. Otherwise the zooplankton transport processes are only determined by the velocity fields. No limits are fixed for the maximum zooplankton depth. The value 50mh^{-1} is suggested by field observations [Mauchline 1998].

We used the z coordinate system in the vertical direction. Moreover, we implemented a particle reflection condition at the model rigid boundaries (the

coastal boundaries and the bottom boundaries) while particles leaving the model domain through the open boundaries are assumed to be lost.

After primary simulations, we release particles at two locations to estimate the exchange between the shelf and the offshore sea. The first one is in the Rhône river plume (position R in Fig. 2.7) and considered as a shelf area. The second one is around the oceanographic sampling station DYFAMED (position D in Fig. 2.7) and considered as an offshore area. Two hundred particles are released at position R in a rectangle area of 60×20km (the center 4.8°E, 43.2°N) and at two different depths, with 100 particles at 5m and 100 particles at 20m. Moreover, two hundred particles are released at position D in a square area of 30×30km (the center 7.87°E, 43.42°N) and at two different depths, with 100 particles at 5m and 100 particles at 100m. Here we fix 200 particles, being a good compromise between the need of computer time saving and of assuring a good statistics.

Particles are released at position D and R every 3 days from March 1st to August 31, 2001 and tracked for 40 days. Although the life spans of different species vary considerably, we use 40 days because they would represent one life duration of many species [Mauchline 1998]. Some experiments, such as releasing individuals every one day and at each time step and so on, have been performed to test a suitable particle release time scale. The results show that simulations with releasing individuals no longer than every 3 days are suitable for statistic analysis. By considering other factors such as computer

ability constrains at the same time, we finally choose releasing individuals every 3 days.

After accurate sensitivity tests and considering computing time constraints we decided to run the particle tracking model with a time-step of 300 seconds.

Simulation analysis

The model domain extends between longitude 1.75°W and 10.90°E and latitude 38.28°N and 45.61°N (Fig. 2.7). In order to classify different zones of the NWM as aggregative or dispersive, we divide the model domain into 9 sectors. Sectors 1 and 2 correspond to shelf areas delimited by the isobath of 200m in the GoL and in the Catalan Sea, respectively; sector 3 marks the shelf area around the Balearic islands; sectors 4, 5 and 6 represent the Ligurian Sea (Here sectors 5 and 6 represent different ecosystems in the Ligurian Sea); sector 7 bounds the center of the NWM gyre; sector 8 is the shelf slope where the main branch of the NC passes; sector 9 represents the offshore zone in the Catalan Sea.

2.4 Results

Fate of passive particles

Particles are transported almost anywhere in the NWM, highlighting a potential high connectivity between the different regions. As an example of particle transport in simulations without DVM, we show some trajectories of particles released at position D on April 30 (Fig. 2.7). It is observed that particles are divided into two parts after being released at position D. Following an anticlockwise circulation some particles drift southwards and then eastwards along the WCC. After reaching the area northeast to the Corsica Island, these particles enter the NC then flow northwards along the continental slopes and finally go back at position D. At the end of the simulation, these particles remain in the Ligurian Sea. Similar trajectories in the Ligurian Sea are also observed in the drifter measurements by Poulain [2008]. Other particles firstly drift westwards, then follow the NC along the shelf slope and finally flow into the Catalan Sea. Along the path, some of them leave the NC towards the NWM gyre and the GoL.

The final distribution patterns of particles released at positions D and R are shown in Fig. 2.3 and Fig. 2.4, respectively. The release locations are also included. The percentages of particles reaching different sectors after 40 days are reported in Table 2.1 and Table 2.2. In both the figures and the tables particles released during one month have been considered as a whole.

Particles released at position D spread almost anywhere in the NWM but with notable differences depending on the month and the initial depths of release (Fig. 2.3). In March (Fig. 2.3A) the majority of particles released at both 5m and 100m remain in the Ligurian Sea, while a minority of them follow the NC. More of particles released at 100m than those released at 5m reach the Catalan Sea. In April (Fig. 2.3B) the situation changes significantly with an increase in the number of particles released at 5m reaching the shelf slope and the Catalan Sea. The distribution patterns of particles released at 100m in the Catalan Sea are similar to those in March. In May (Fig. 2.3C) practically all of particles released at both 5m and 100m reach the Catalan Sea and only a few of them remain in the Ligurian Sea. Compared to the earlier months, a substantial number of particles released at 5m enter the GoL. In June (Fig. 2.3D) few particles end up in the Ligurian Sea, which is similar to that in May. The particles released at 5m are divided in two groups, either trapped in the NWM gyre or advected to the Catalan Sea. The particles released at 100m are channelled into the NC, along the shelf and in the Catalan Sea. At the east edge of the GoL, some particles released at 100m are located in water shallower than 200m. In July (Fig. 2.3E) we observe a big difference in final distribution patterns of particles released at both 5m and 100m, in a similar way as that in March. Most of particles released at 100m reach the Catalan Sea while those released at 5m remain essentially in the Ligurian Sea. Finally, in August (Fig. 2.3F) the situation is similar to that of

July for the particles released at 100m. However, more particles released at 5m spread in the Ligurian Sea and in the NWM gyre.

These results are summarized in Table 2.1, where percentages of particles reaching different sectors are calculated considering particles released at both 5m and 100m as a whole. In March over 60% of particles stay in the Ligurian Sea (sectors 4 to 6) while only 9% of them enter the Catalan Sea (sectors 2, 3 and 9). Most particles are concentrated in the superficial layer of the eastern Ligurian Sea (41% in sector 5A). In April the maximum particle percentage of 39% is found on the shelf slope (sector 8). In May and June the maximum percentages of particles (43% and 35% respectively) are observed in the Catalan Sea. In July about 47% of particles remain in the Ligurian Sea and 33% of them are located on the shelf slope while 20% reach the Catalan Sea. Finally, in August the maximum particle percentage of 39% is found in the Catalan Sea. Furthermore, Table 2.1 shows that only a few of particles released at position D enter the GoL and finally stay there (the maximum of 3% in June).

Particles released at position R spread mainly southwestwards and none are able to reach the Ligurian Sea (Fig. 2.4). Monthly differences in final distribution patterns of particles are observed while the initial depths of release (5m and 20m) do not seem to affect the final distribution patterns. Two main distribution patterns of particles might be distinguished in the whole set of simulations (from March to August). In the first case (March and April,

TAB. 2.1 – Percentages of particles reaching different sectors in simulations without DVM (particles released at both 5m and 100m around the DYFAMED station)

sector	GoL 1	Catalan Sea				Ligurian Sea					NWM gyre		shelf slope	
		2	3	9A	9B	4	5A	5B	6A	6B	7A	7B	8A	8B
March	≤ 1	≤ 1	1	6	2	10	41	1	12	≤ 1	4	0	21	2
April	2	≤ 1	≤ 1	19	2	4	15	2	5	1	11	0	25	14
May	2	1	2	32	11	3	7	1	5	1	6	0	20	8
June	3	1	3	32	3	≤ 1	3	≤ 1	9	3	13	0	24	7
July	≤ 1	0	≤ 1	20	≤ 1	2	27	≤ 1	17	0	2	0	28	5
August	≤ 1	≤ 1	≤ 1	30	9	3	18	0	14	0	8	0	16	1

Fig. 2.4A), particles out of the GoL mostly scatter in the northeastern Catalan Sea and in the western NWM gyre. A certain number of particles reach the southern open boundary. In the second case (from May to August, Fig. 2.4B), the situation changes with particles out of the GoL being mainly located in the path of the NC. A decrease in the number of particles reaching the southern open boundary is also observed. In both cases a large number of particles remain in the GoL (Fig. 2.4). Differences in final distribution patterns of particles according to the month of release are summarized in Table 2.2. In March about 24% of particles remain in the GoL and 16% in the NWM gyre. Most particles are located on the shelf slope with the percentage of 38%. In April and May an increase in the number of particles is observed in the GoL and the total percentages of particles are 47% and 56%, respectively. On the other hand, less than 15% of particles reach the Catalan Sea. The percentage of particles in the NWM gyre is 12% in April and only 2% in May. From June

TAB. 2.2 – Percentages of particles reaching different sectors in simulations without DVM (particles released at both 5m and 20m in the Rhône river plume)

sector	GoL 1	Catalan Sea				Ligurian Sea					NWM gyre		shelf slope	
		2	3	9A	9B	4	5A	5B	6A	6B	7A	7B	8A	8B
March	24	3	5	14	≤1	0	0	0	0	0	16	0	38	≤1
April	47	1	1	12	≤1	0	0	0	0	0	12	0	26	0
May	56	4	≤1	10	0	0	0	0	0	0	2	0	29	0
June	35	2	2	28	0	0	0	0	0	0	7	0	27	0
July	34	1	3	32	0	0	0	0	0	0	5	0	25	0
August	36	7	3	30	0	0	0	0	0	0	≤1	0	23	0

to August the percentages of particles in the GoL and on the shelf slope do not change (around 35% and 25%, respectively). More particles scatter in the NWM gyre in June (7%) than in July and August (5% and 1%, respectively), but less in the Catalan Sea (32% compared to 36% and 40%, respectively).

Fate of particles with DVM

The final distribution patterns of particles released at positions D and R are shown in Fig. 2.5 and Fig. 2.6, respectively. For the sake of simplicity we show final distribution patterns of particles for several months representative of the whole set of simulations (from March to August). We calculate differences between percentages of particles reaching combined regions (as introduced in section 2.3) in simulations with DVM and those without DVM (Table 2.3 and Table 2.4). The tables also show the percentages of particles reaching combined regions in simulations with DVM.

Regarding particles released at position D, differences in final distribution patterns are observed depending on the month and the initial depths of release. In March (Fig. 2.5A) a large number of particles concentrate in the Ligurian Sea. Other particles follow the NC and a few of them reach the Catalan Sea. Differences in final distribution patterns of particles for both initial depths of release are small. In June (Fig. 2.5B) very few of particles released at both 5m and 100m remain in the Ligurian Sea. Most of particles released at 100m accumulate in the path of the NC along the shelf slope. The majority of particles released at 5m are channelled into the path of the NC in the Catalan Sea. In August (Fig. 2.5C) some particles released at 5m are located in the Ligurian Sea and the NWM gyre. Moreover, some particles released at 5m and the majority of particles released at 100m end up in the path of the NC along the shelf slope and in the Catalan Sea.

Compared to simulations without DVM (Fig. 2.3), simulations with DVM show less spreading of particles, particularly for the particles released at 5m. In Table 2.3 we can observe an increase in the number of particles on the shelf slope in simulations with DVM compared to those without DVM, whereas other regions lose particles except for the Catalan Sea in June.

Regarding particles released at position R, monthly differences in final distribution patterns are observed, whereas the effect of initial depths of release could be neglected. In March (Fig. 2.6A) some particles are located in the central and southwestern GoL. Some particles reach the Catalan Sea and two

Tab. 2.3 – Percentages of particles reaching combined sectors (as referred in the text) in simulations with DVM and differences (in brackets) in particles of simulations with DVM and those without DVM (particles released at both 5m and 20m around the DYFAMED station)

sector	GoL (1)	Catalan Sea (2,3,9)	Ligurian Sea (4,5,6)	NWM gyre (7)	shelf slope (8)
March	≤1 (0)	4 (-4)	59 (-6)	3 (-1)	33 (+10)
April	2 (0)	21 (0)	23 (-4)	2 (-9)	52 (+13)
May	≤1 (-1)	42 (-4)	15 (-2)	2 (-4)	40 (+12)
June	2 (-1)	43 (+4)	11 (-4)	1 (-12)	41 (+10)
July	≤1 (0)	10 (-11)	41 (-4)	2 (0)	47 (+14)
August	≤1 (0)	27 (-12)	17 (-18)	7 (-1)	48 (+31)

different distribution patterns appear. These patterns are separated appropriately along the latitude 40.5°N and a connection for the two patterns is observed in the area north to the Mallorca Island. In April (Fig. 2.6B) some particles are located in the northeastern and southwestern GoL. Other particles mainly accumulate in the central and southern Catalan Sea. In June (Fig. 2.6C) particle distribution patterns in the GoL are similar to those in March, but more particles out of the GoL concentrate in the path of the NC.

Compared to simulations without DVM (Fig. 2.4), simulations with DVM decrease the spread of the final distribution patterns and the number of particles reaching the open boundary. In general (Table 2.4), simulations with DVM increase the number of particles in the Catalan Sea (except in May and July) and on the shelf slope (except in April), but decrease them in the GoL and in the NWM gyre. No changes are observed in the Ligurian Sea.

Tᴀʙ. 2.4 – Percentages of particles reaching combined sectors (as referred in the text) in simulations with DVM and differences (in brackets) in particles of simulations with DVM and those without DVM (particles released at both 5m and 20m in the Rhône river plume)

sector	GoL (1)	Catalan Sea (2,3,9)	Ligurian Sea (4,5,6)	NWM gyre (7)	shelf slope (8)
March	10 (-14)	43 (+20)	0 (0)	$\leq$1 (-15)	46 (+8)
April	32 (-15)	39 (+24)	0 (0)	6 (-6)	22 (-3)
May	42 (-14)	6 (-8)	0 (0)	$\leq$1 (-1)	51 (+23)
June	16 (-19)	36 (+5)	0 (0)	0 (-7)	47 (+21)
July	23 (-11)	28 (-8)	0 (0)	$\leq$1 (-5)	49 (+24)
August	20 (-16)	40 (0)	0 (0)	0 (-1)	39 (+17)

2.5 Discussion

Fate of particles released around the DYFAMED station

To discuss the relationship between particle distribution and currents, we plot the monthly average circulation patterns in March, June and August from the circulation model Symphonie (Fig. 2.8).

In March (Fig. 2.8(A,B)) the WCC, the ECC and the NC form a cyclonic circulation in the Ligurian Sea. In the particle release area and the central Ligurian Sea, low velocity currents are observed. After being released, most particles are advected by the low velocity currents towards the central Ligurian Sea. Some of them are advected in the cyclonic circulation. That explains why over 60% of particles stay in the Ligurian Sea, especially 10% in sector 4, which is the largest percentage in all months. In the final distribution patterns of particles, more particles released at 5m remain in the Ligurian Sea than

those released at 100m. One reason is that one southeast branch of the NC is observed west of 8°E at 5m instead of at 100m. This branch carries particles back to the Ligurian Sea. This is also a reason that more particles released at 100m reach the Catalan Sea than those released at 5m. Furthermore, it explains why more particles released at 5m reach the shelf slope and the Catalan Sea in simulations with DVM than those without DVM.

In June (Fig. 2.8(C,D)) a northwestward current is observed at position D. This current drives particles directly in the NC and few particles remain in the Ligurian Sea. This explains why lower than 5% of particles remain in sectors 4 and 5. Furthermore, the NC velocity is higher at 5m than that at 100m. Consequently the particles released at 5m drift further than those released at 100m when reaching the Catalan Sea. The variability of surface currents explains why some particles released at 5m flow into the NWM gyre. In simulations with DVM, a large decrease in spread is observed for the final distribution patterns of the particles released at 5m, especially in the NWM gyre, because currents in deeper water prevent particles from escaping from the NC.

In August (Fig. 2.8(E,F)) a northwestward current is still observed at 100m while it does not exist at 5m. This pattern explains why the particles released at 5m spread in the Ligurian Sea while those released at 100m are channeled into the NC and quickly transported out of the Ligurian Sea. It also explains why a decrease in the number of particles released at 5m is observed in the

Ligurian Sea and the NWM gyre in simulations with DVM, compared to those without DVM. Furthermore, it is the reason why the percentages of particles in the Ligurian Sea are lower than those in March and higher than those in June.

Rubio et al. [2009] showed that drifting buoys launched at the southeastern part of the GOL and tracked by the ARGOS satellite system in the NWM Sea during summer 2005 were never entering on the shelf of the GOL but drifted in the NC over the shelf slope, however temporary trapped in mesoscale structures associated with the NC. Our simulations in June, July and August are consistent with their observations and simulations.

The NC plays a clear role as vector from the Ligurian Sea to the Catalan Sea. According to several campaigns performed in the NWM [Alberola et al. 1995; Petrenko 2003], the NC flux varies throughout the year, with a maximum flux 1.5-2 Sv (down to 700 dbar) during the winter and spring seasons (roughly from December to May). The NC velocity is higher in June than that in August (Fig. 2.8). Thus particles released in June flow faster and further accordingly, which is shown in the final distribution patterns of particles in the Catalan Sea. In addition, the NC flows southwards in the area north to the Mallorca Island (east of 2°E) in March and flows southwestwards further along the continental slope of the Catalan Sea (up to 0.5°E) in June and August (Fig. 2.8). This explains why more particles are located in the northeastern Catalan Sea in March than those in June and August.

Under specific wind and stratification conditions, surface waters of the NC tend to penetrate onto the shelf at the eastern entrance of the GoL [Millot and Wald 1980; Auclair et al. 2003; Echevin et al. 2003; Petrenko 2003; Petrenko et al. 2005]. Consequently, the penetration will carry particles onto the shelf. However in our simulations, offshore-shelf transport is rare and the particles end up in the GoL in low concentrations. Most of the time, the NC flows southwestwards along the shelf break delimiting the GoL and acts as a barrier which separates the shelf circulation from the regional circulation. Moreover, even though particles move occasionally into the GoL advected by the penetrating branch of the NC, some of them will be washed out of the GoL by the southwestern branch of currents in the Rhône river plume.

Different percentages of particles reaching combined regions are shown in the previous sections for particles released around the DYFAMED station between simulations with DVM and those without DVM. The differences are relate to combined influence of currents and swimming behaviours. Swimming behaviours in simulations with DVM deduce a different vertical distribution pattern of particles from those without DVM. Despite the effect of vertical currents one particle released at 5m will remain in the depth of 5m on a whole day. However when swimming behaviours considered the particle will stay at the surface and in the depth about 100m almost half a day, respectively. The situations for simulations with particles released at 100m may be deduced by analogy. As shown in Fig. 2.8 currents at 5m differ from those at 100m,

stronger but more divergent at the surface than in the deeper layer. Our simulations with DVM show that some particles will reduce durations in the currents at the surface and increase those in deeper layer compared to those without DVM. That is a reason to explain the results shown in Table 2.3. An increase in the number of particles on the shelf slope is observed, whereas other regions lose particles except for the Catalan Sea in June.
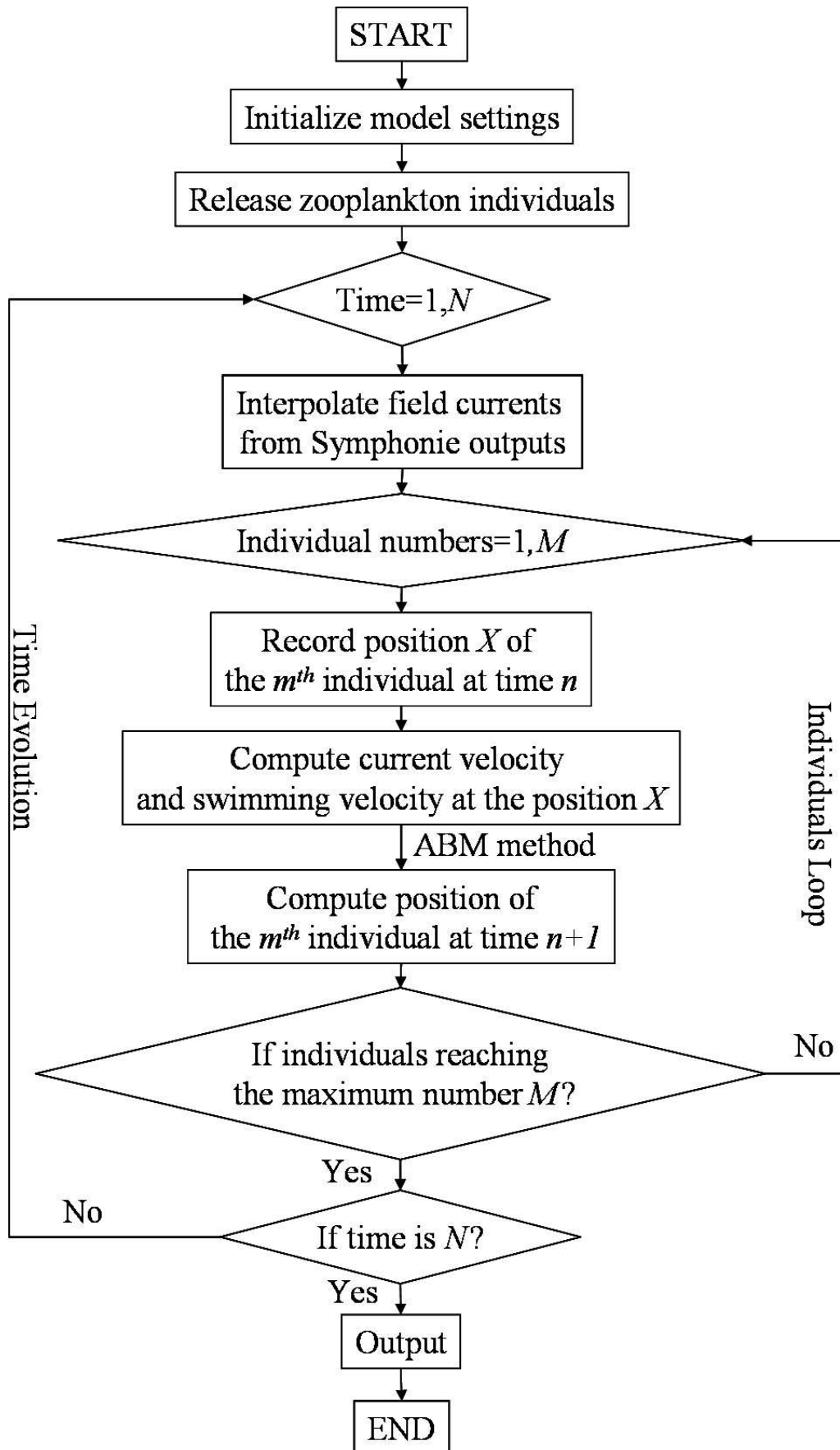
FIG. 2.2 – Flow-chart of the Lagrangian particle tracking model
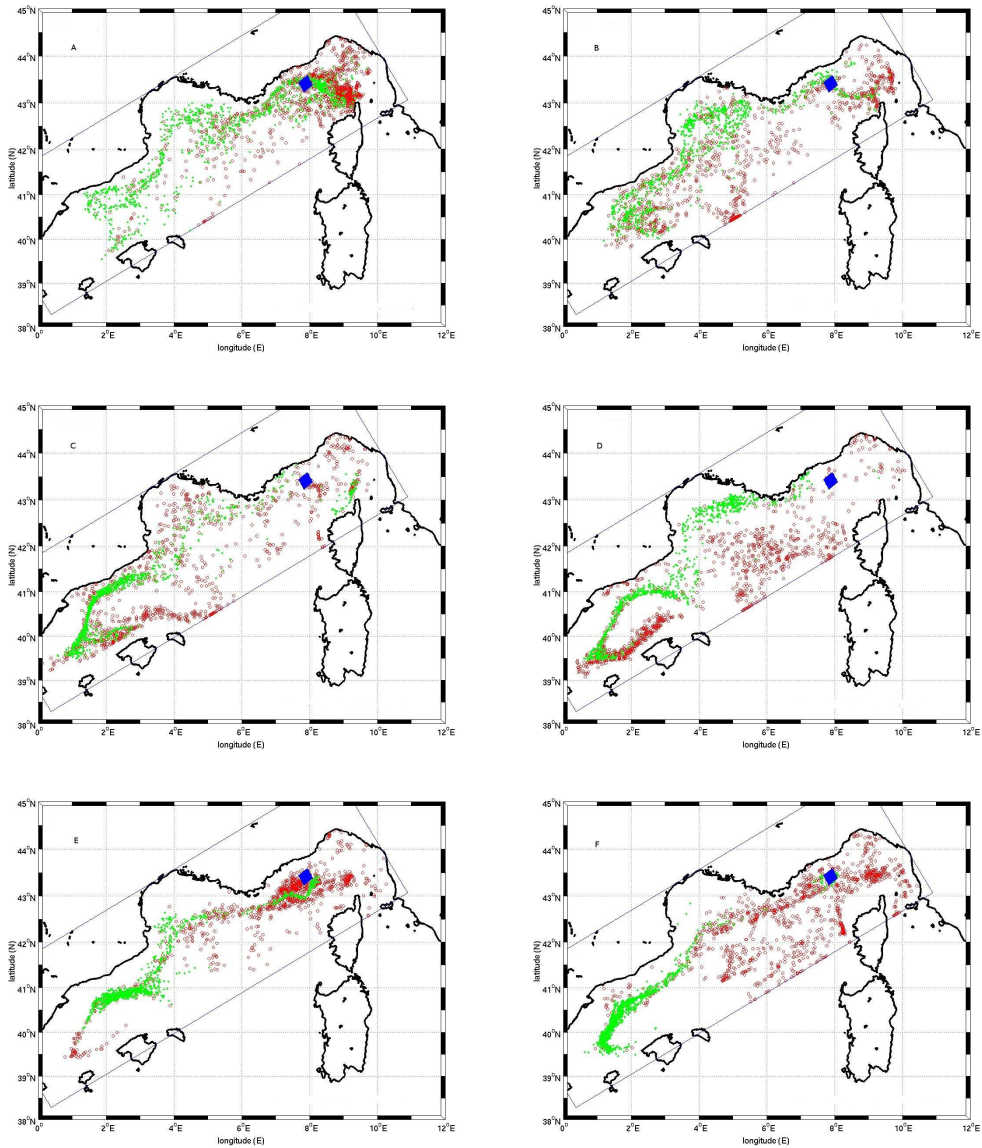
Fɪɢ. 2.3 – Final distribution patterns of passive particles released around the DYFAMED station (blue square) in different months : (A) March, (B) April, (C) May, (D) June, (E) July and (F) August. Empty red circles represent final positions of particles released at 5m ; full green lozenges represent final positions of particles released at 100m.
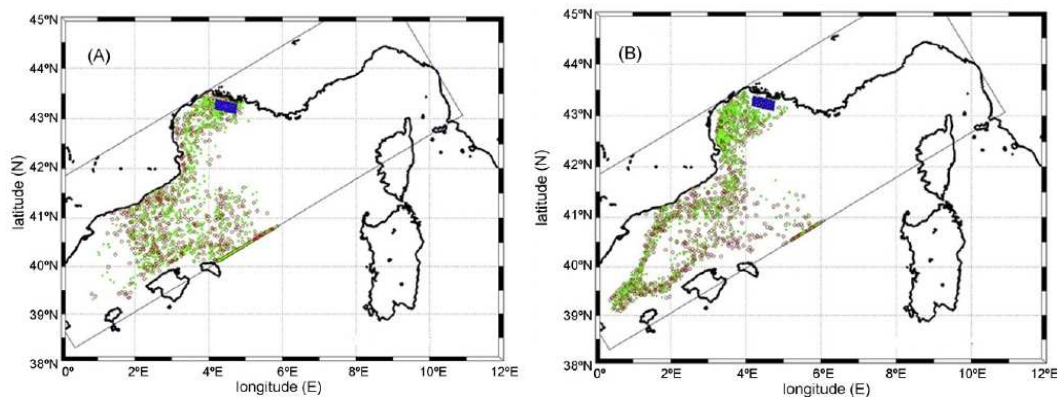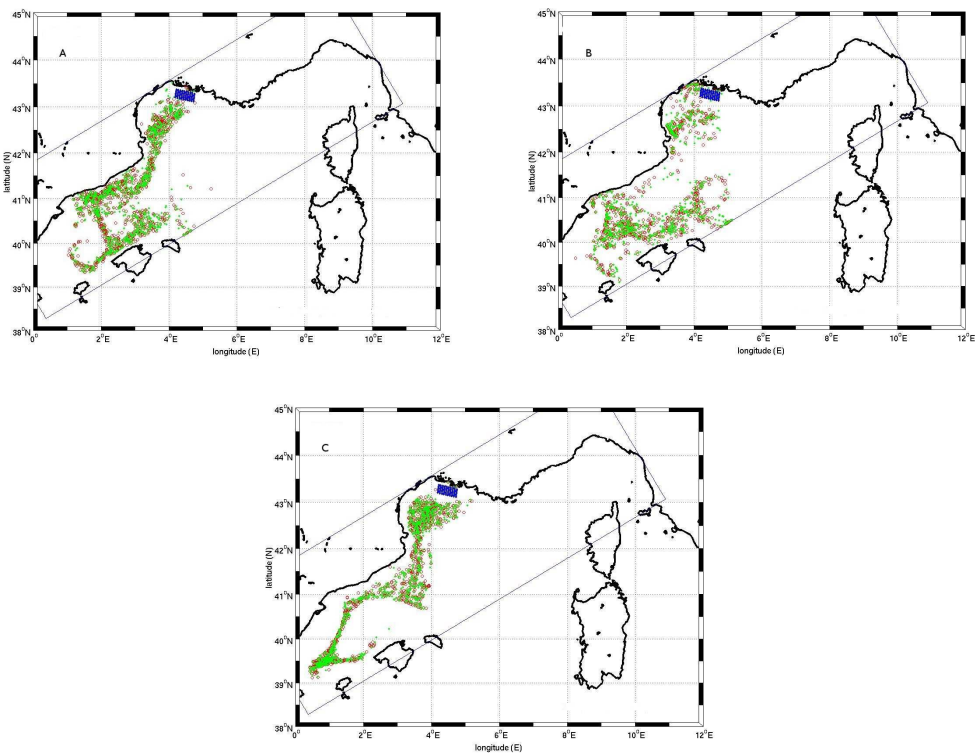
FIG. 2.4 – Final distribution patterns of passive particles released in the Rhône river plume (blue square) in two months : (A) March and (B) June. Empty red circles represent final positions of particles released at 5m ; full green lozenges represent final positions of particles released at 20m.
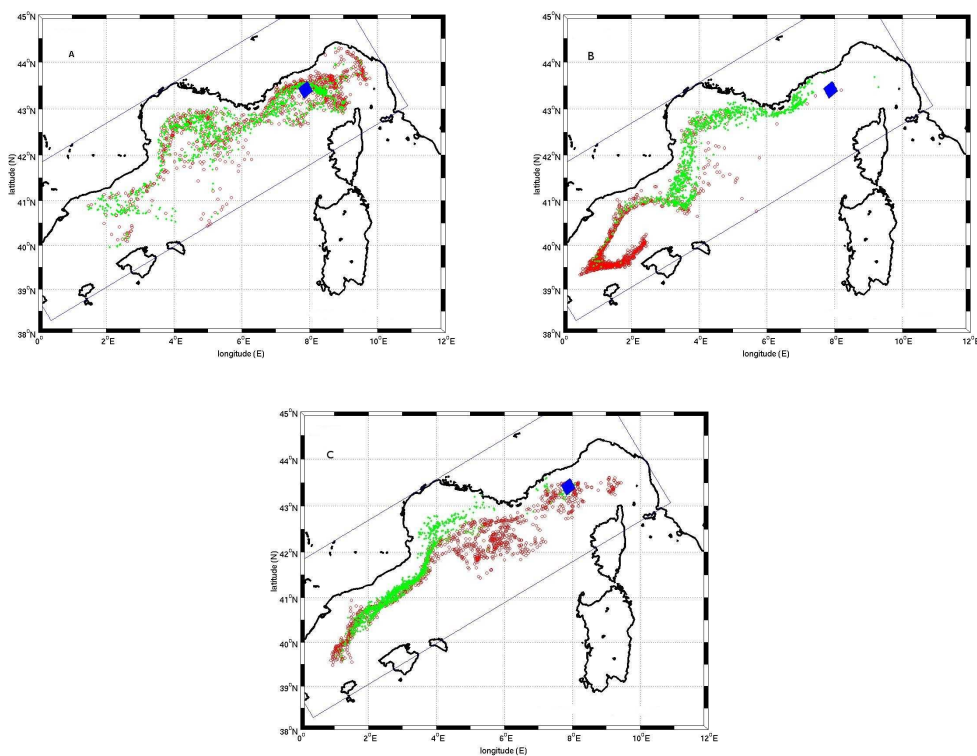
FIG. 2.5 – Final distribution patterns of particles released around the DYFA-MED station (blue square) in simulations with DVM in three months : (A) March, (B) June and (C) August. Empty red circles represent final positions of particles released at 5m ; full green lozenges represent final positions of particles released at 100m.

FIG. 2.6 – Final distribution patterns of particles released in the Rhône river plume (blue square) in simulations with DVM in three months : (A) March, (B) April and (C) June. Empty red circles represent final positions of particles released at 5m ; full green lozenges represent final positions of particles released at 20m.
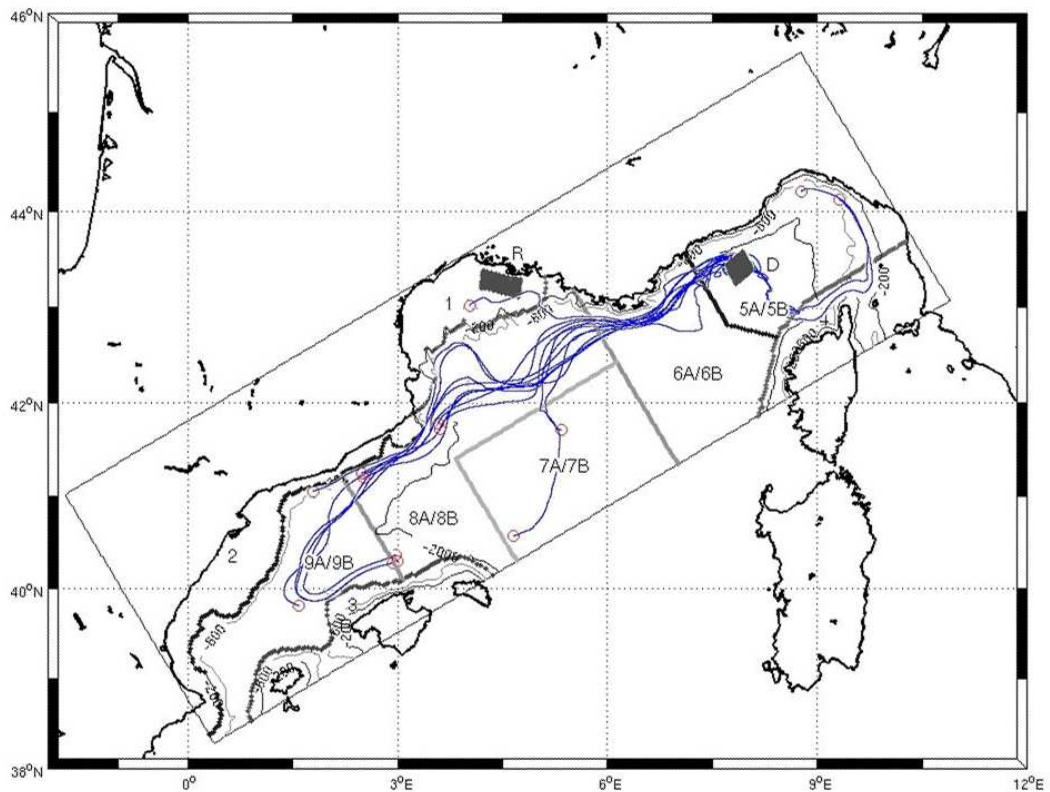
Fig. 2.7 – Model domain (dashed rectangle) and the corresponding bathyme-try (thin contours). Black filled rectangles represent the release locations of particles (see text). The model domain is divided into 9 sectors (thick lines) for the analysis of particle distribution. Sectors indicated with A/B considered the layer upper 200m depth (A) and the layer below 200m depth (B). Trajec-tories are also shown in blue lines for the passive particles released on April 30, 2001 around the DYFAMED station. Red circles represent final positions of particles after 40-day transport. For graphical purposes only a subset of particles is shown.
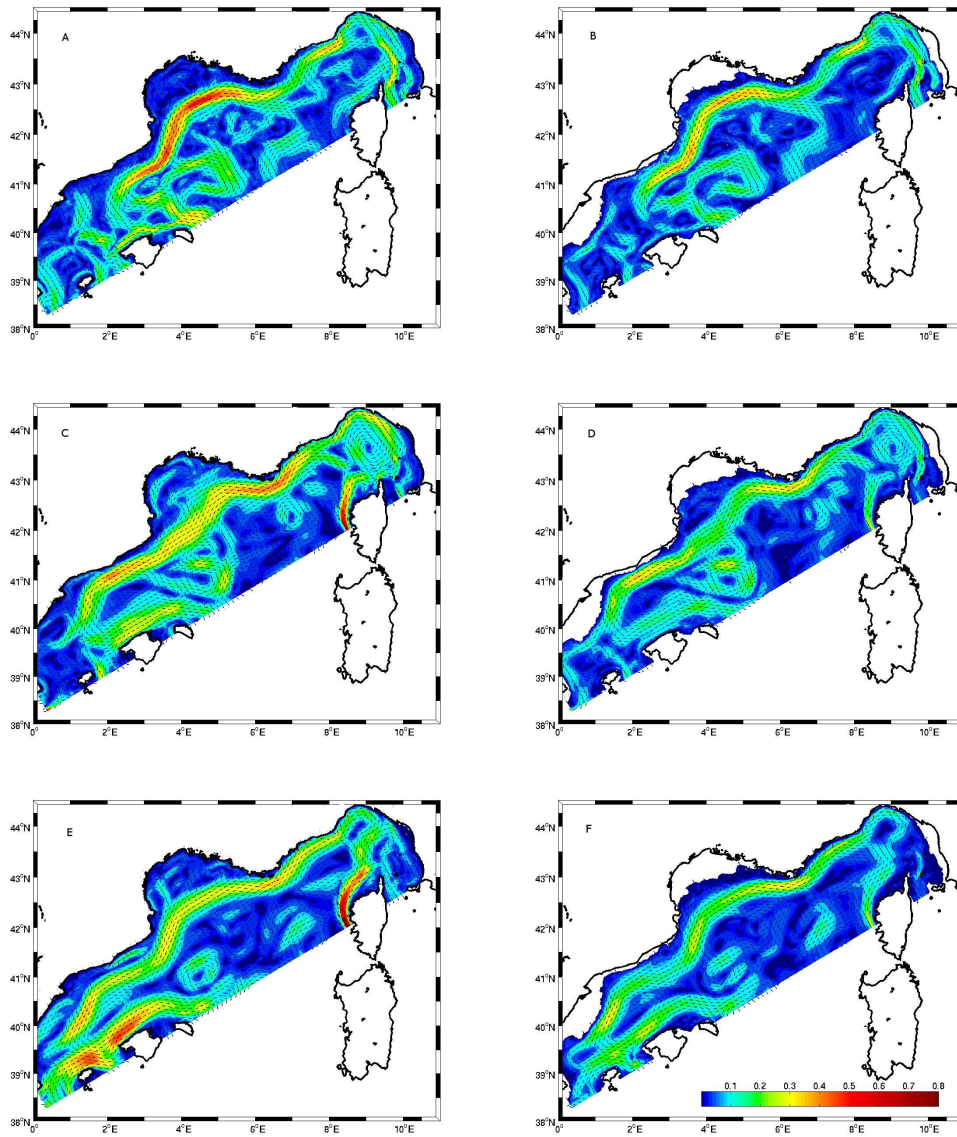
FIG. 2.8 – The intensity of the monthly average currents [ms^{-1}] at 5m (left column) and 100m (right column) in three months : (A,B) March, (C,D) June and (E,F) August. Black arrows represent directions of currents.

Fate of particles released in the Rhône river plume

A quarter to a half of particles released at position R remain in the GoL in simulations without DVM. One reason is that the shelf circulation is weak in the main areas of the GoL (Fig. 2.8). Thus the transport speed of particles is small. Another reason is due to gyres and eddies on the shelf [Hu et al. 2009]. When particles enter in, they are prevented escaping from the GoL.

Two different distribution patterns of particles out of the GoL are due to the variability of the NC. The path of the NC changes in the Catalan Sea in different months, as discussed in the previous section. In several simulations, particles were trapped in the Balearic Current and then aggregated in the associated North Balearic Front. In their application to the transport in the NWM region, Mancho et al. [2008] identified the North Balearic Front as a Lagrangian barrier. The region has been identified as a key spawning are for the bluefin tuna, as well as a feeding area for anchovy and sardines [Tugores et al. 2010].

In our simulations, particles can drift out to the offshore sea in all months all along the south boundary of the GoL (data not shown). On the contrary, an offshore-shelf particle exchange only appears when the NC penetrates into the GoL under specific wind and stratification conditions [Auclair et al. 2003; Petrenko 2003; Petrenko et al. 2005]. Thus our simulations show that physical processes favour the shelf-offshore particle exchange.

DVM behaviour reduces transport of particles away from the regions where there are offshore currents at the surface and onshore currents at deeper depths [Botsford et al. 1994; Batchelder et al. 2002]. This effect of DVM has been observed in the upwelling regions and river plumes of the GoL (data not shown). However, in most of our simulations, DVM behaviour does not increase the number of particles remaining in the GoL because of complex currents on the shelf. The upwelling phenomenon of the GoL displays a very large spatio-temporal variability due to the coastline geometry and the high variability of winds. Andre et al. [2005] found that the upwellings along the northeastern coasts of the GoL and south of Cape d'Agde are wind-driven, the former by the Mistral and the latter by the Tramontane.

Moreover, currents in the GoL vary vertically owing to the combined effects of various forcings. For instance, the hydrological structures in the central GoL are complex, with the influence of the Rhône river's freshwater plume in the first 40m of the water column and, closer to the bottom, with the confrontations of downwelled coastal cold water and upwelled warmer and saltier slope water [Estournel et al. 2003]. The current direction changes largely in depth, inducing an increase in the number of particles either remaining in or escaping from the GoL. Our results show that most of the simulations with DVM do not favour an increase in the number of particles remaining in the GoL.

Compared to simulations without DVM, simulations with DVM induce a

large increase in the number of particles in the Catalan Sea (in March and April) and on the shelf slope (from May to August), as described before. One reason is that the NC velocity is higher in March and April than that from May to August. Another reason could be that DVM behaviour reduces particles escaping from the NC. In March (Fig. 2.8(A,B)) an anti-cyclonic circulation is located close to the NC path in sector 7 (between 4°E and 6°E). When tracked passively, about 16% of particles flow in this circulation to the NWM gyre from the NC. When tracked with DVM, most of these particles continue to flow in the NC and enter the Catalan Sea. The same situation occurs in June.

Ecological relevance

The objective of our study was to quantify and to model zooplankton transport and Lagrangian modelling can be an effective way to investigate dynamic transport patterns of invertebrates. However we have no way to validate such model, because little is known about zooplankton (including ichthyoplankton) distribution and transport in the NWM, data being very scarce. Agostini and Bakun [2002] noted as final conclusion for the understanding of anchovy stock dynamics in the NWM that "fully testing these ideas would require a greater sampling effort than heretofore undertaken, so as to be able to assemble and make available basic information on the spatial distribution of spawning. This information is surprisingly lacking for such an ocean area which is bordered by

a number of relatively affluent and technologically advanced states that have very important interests in marine resource management and marine ecosystem conservation." Our simulations show that any study of plankton dispersal for organisms of life duration larger than the week should be addressed at the regional scale.

It is clear that such "transport studies" will probably increase in the next decade using satellite-tracked drifters, and by guiding the vertical position of the drifter might help to mimic zooplankton transport. Several key issues in the NWM related to fisheries, jelly fish swarms, and ecosystem functioning requires such integrated approaches.

2.6 Conclusions

We have developed a Lagrangian tool to simulate the transport and distributions of particles coupled with the 3D circulation model Symphonie. The particles could be zooplankton, sediment or other passive suspended matter. A primary DVM scheme has been considered and successfully used for zooplankton. The Lagrangian tool has been used to estimate the influence of hydrodynamic processes on zooplankton transport and distributions in the NWM.

Our results suggest that the particle transport and distributions are strongly related to the hydrodynamic structures on the shelf and the offshore circu-

lations associated with the NC. On the regional scale, particles spread almost anywhere in the NWM after being transported for 40 days, when released around the DYFAMED station. In the spring and summer conditions, the current fields in the NWM favour a shelf-offshore particle exchange, whilst offshore-shelf transport is nearly inhibited. The NC can be considered as a barrier for particles entering the GoL from the offshore sea. Most of particles released in the Rhône river plume either stay in the GoL or end up in the Catalan Sea.

The biological processes associated with particles have been considered using a simple DVM scheme. Our DVM scheme is overly simple and does not increase the number of particles remaining on the shelf. As a next step, we will include more biological processes during the life time of particles, such as growth, development and associated changes in swimming velocity [see Carlotti and Wolf 1998, as an example]. In order to do this, we will consider the phytoplankton and micro-zooplankton distributions in the NWM and couple our Lagrangian model with the biogeochemical model Eco3M [Baklouti et al. 2006].

2.7   Acknowledgements

Bibliographie

Agostini, V.N., Bakun, A., 2002. 'Ocean triads' in the Mediterranean Sea : physical mechanisms potentially structuring reproductive habitat suitability (with example application to European anchovy, *Engraulis encrasicolus*). Fish. Oceanogr. 11(3), 129-142. 162

Alberola, C., Millot, C., Font, J., 1995. On the seasonal and mesoscale variabilities of the Northern Current during the PRIMO-0 experiment in the western Mediterranean Sea. Ocean. Acta. 18 (2), 163-192. 151

Andre, G., Garreau, P., Garnier, V., Fraunie, P., 2005. Modelled variability of the sea surface circulation in the North-western Mediterranean Sea and in the Gulf of Lions. Ocean. Dyn. 55, 294-308. 133, 161

Auclair, F., Marsaleix, P., Estournel, C., 2001. The penetration of the northern current over the Gulf of Lion (western Mediterranean Sea) as a downscaling problem. Ocean. Acta. 24, 529-544. 4, 27, 136

Auclair, F., Marsaleix, P., De Mey P., 2003. Space-time structure and dynamics of the forecast error in a coastal circulation model of the Gulf of Lions. Dyn. Atmos. Oceans. 36, 309-346. 4, 27, 76, 136, 152, 160

Baklouti, M., Faure, V., Pawlowski, L., Sciandra, A., 2006. Investigation and sensitivity analysis of a mechanistic phytoplankton model implemented in a

new modular numerical tool (Eco3M) dedicated to biogeochemical modelling. Progr. Oceanogr. 71, 34-58 164

Batchelder, H., Edwards, C., Powell, T., 2002. Individual-based models of copepod population in coastal upwelling regions : implications of physiologically influenced diel vertical migration on demographic success and nearshore retention. Progr. Oceanogr. 53, 307-333. 132, 135, 161

Blanke, B., Arhan, M., Madec, G., Roche, S., 1999. Warm water paths in the equatorial Atlantic as diagnosed with a general circulation model. J. Phys. Oceanogr. 29, 2753-2768. 132

Botsford, L.W., Moloney, C.L., Hastings, A., et al., 1994. The influence of spatially and temporally varying oceanographic conditions on meroplanktonic metapopulations. Deep-Sea. Res. II. 41,107-145. 161

Bouffard, J., Vignudelli, S., Herrmann, M., Lyard, F., Marsaleix, P., Menard, Y., Cipollini, P., 2008. Comparison of ocean dynamics with a regional circulation model and improved altimetry in the North-western Mediterranean. Terr. Atmos. Ocean. Sci. 19, 117-133. 25, 138

Carlotti, F., Wolf, K.U., 1998. A Lagrangian ensemble model of Calanus finmarchicus coupled with a 1-D ecosystem model. Fish. Oceanogr. 7(3-4), 191-204. 164

Carr, S.D., Capet, X.J., Mcwilliams, J.C., Pennington, J.T., Chavez, F.P., 2008. The influence of diel vertical migration on zooplankton transport and

recruitment in an upwelling region : estimates from a coupled behavioral-physical model. Fish. Oceanogr. 17(1), 1-15. 132, 136, 138

Champalbert, G., 1996. Characteristics of zooplankton standing stock and communities in the western Mediterranean Sea : relations to hydrology. Sci. Mar. 60 (Suppl. 2), 97-113. 134

Cianelli, D., Diaz, F., Leredde, Y., Marsaleix, P., Carlotti, F., 2007. Particle exchange and residence times in the North Western Mediterranean. Nuovo. Cimento. C. 30, 139-148. 132, 133

Diaz, F., Raimbault, P., Boudjellal, B., Garcia, N., Moutin, T., 2001. Early phosphorus limitation during spring in the Gulf of Lions. Mar. Ecol., Prog. Ser. 211, 51-62. 134

Echevin, V., Crepon, M., Mortier, L., 2003. Interaction of a coastal current with a gulf :application to the shelf circulation of the Gulf of Lions in the Mediterranean Sea. J. Phys. Oceanogr. 33, 188-206. 152

Estournel, C., Broche, P., Marsaleix, P., Devenon, J.L., Auclair, F., Vehil, R., 2001. The Rhone river plume in unsteady conditions : numerical and experimental results. Est. Coast. and Shelf Sci. 53, 25-38. 136

Estournel, C., Durrieu, X., Marsaleix, P., Auclair, F., Julliand, C., Vehil, R., 2003. Observation and modelisation of the winter coastal oceanic circulation in the Gulf of Lions under wind conditions influenced by the continental

orography (FETCH experiment). J. Geophys. Res. 108 (C3), pages 7-1 to 7-18. 4, 12, 13, 24, 27, 46, 75, 76, 133, 136, 161

Estournel, C., Auclair, F., Lux, M., Nguyen, C., Marsaleix, P., 2007. "Scale oriented" embedded modeling of the North-Western Mediterranean in the frame of MFSTEP. Ocean Sci. Discuss. 4, 145-187. 25, 28, 30, 136

Falco, P., Griffa, A., Poulain, P.M., Zambianchi, E., 2000. Transport properties in the Adriatic Sea as deduced from drifter data. J. Phys. Oceanogr. 30, 2055-2071. 132

Garcia, L.E., Castellon, A., Font, J., Tintore, J., 1996. The Balearic current and volume transports in the Balearic basin. Ocean. Acta. 19, 489-497.

134

Gaspar, P., Gregoris, Y., Lefevre, J.M., 1990. A simple eddy kinetic energy model for simulations of the oceanic vertical mixing : Tests at station Papa and long-term upper ocean study site. J. Geophys. Res. 95, 16179-16193. 27, 76, 137

Gatti, J., Petrenko, A., Devenon, J.L., Leredde, Y., Ulses, C., 2006. The Rhone river dilution zone present in the northeastern shelf of the Gulf of Lion in December 2003. Continent. Shelf. Res. 26, 1794-1805. 4, 9, 12, 136

Guizien, K., Brochier, T., Duchne, J.C., Koh, B.S., Marsaleix, P., 2006. Dispersal of owenia fusiformis larvae by wind-driven currents : turbulence, swim-

ming behaviour and mortality in a three-dimensional stochastic model. Mar. Ecol., Prog. Ser. 311, 47-66. 132

Haney, J., 1988. Diel patterns of zooplankton behavior. Bull. Mar. Sci. 43, 583-603. 135

Hu, Z.Y., Doglioli, A.M., Petrenko, A.A., Marsaleix, P., Dekeyser, I., 2009. Numerical simulations of eddies in the Gulf of Lion, Ocean Modell. 28 (4), 203-208. 137, 138, 160

Lett, C., Veitch, J., van der Lingen, C.D., Hutchings, L., 2007. Assessment of an environmental barrier to transport of ichthyoplankton from the southern to the northern Benguela ecosystems. Mar. Ecol., Prog. Ser. 347, 247-259. 133

Levy, M., Memery, L., Madec, G., 2000. Combined effects of mesoscale processes and atmospheric high-frequency variability on the spring bloom in the MEDOC area - a mathematical model. Deep-Sea Res. I. 47, 27-53. 132

Mancho, A.M., Hernandez-Garcia, E., Small, D., Wiggins, S. Fernandez, V., 2008. Lagrangian transport through an ocean front in the Northwestern Mediterranean Sea. J. Phys. Oceanogr. 38, 1222-1237. 160

Mariani, S., Uriz, M.J., Turon, X., Alcoverro, T., 2006. Dispersal strategies in sponge larvae : integrating the life history of larvae and the hydrologic component. Oecologia 149(1), 174-184. 135

Mariottini, G.L., Giacco, E., Pane, L., 2008. The mauve stinger *Pelagia noctiluca* (Forsskal, 1775). Distribution, ecology, toxicity and epidemiology of stings. A review. Mar. Drugs 6(3), 496-513. 135

Marsaleix, P., Estournel, C., Kondrachoff, V., Vehil, R., 1998. A numerical study of the formation of the Rhone River plume. J. Mar. Syst. 14 (1-2), 99-115. 4, 27

Marsaleix, P., Auclair, F., Floor, J.W., Herrmann, M.J., Estournel, C., Pairaud, I., Ulses, C., 2008. Energy conservation issues in sigma-coordinate free-surface ocean models. Ocean. Mod. 20 (1), 61-89. 27, 29, 76, 136

Mauchline, J., 1998. The biology of calanoid copepods. Adv. Mar. Biol 33, 710 pp. 139, 140

Miller, C.B., Lynch, D.R., Carlotti, F., Gentleman, W., Lewis, C.V.W., 1998. Coupling of an Individual-Based Population Dynamic Model of Calanus finmarchicus to a Circulation Model for the Georges Bank Region. Fish. Oceanogr. 7, 219-234. 132, 133

Millot, C., Wald, L., 1980. The effect of Mistral wind on the Ligurian current near Provence. Ocean. Acta. 3, 399-402. 12, 133, 152

Millot, C., 1999. Circulation in the Western Mediterranean Sea. J. Mar. Syst. 20, 423-442. 45, 64, 72, 133

Mullon, C., Freon, P., Parada, C., Van der lingen, C., Huggett, J., 2003. From particles to individuals : modelling the early stages of anchovy (*Engraulis*

capensislencrasicolus) in the southern Benguela. Fish. Oceanogr. 12(4-5), 396-406. 133

Oschlies, A., 2002. Nutrient supply to the surface waters of the North Atlantic : A model study. J. Geophys. Res. 107 (C5), 3046. 132

Palomera, I., 1991, Vertical distribution of eggs and larvae of *Engraulis encrasicolus* in stratified waters of the western Mediterranean. Mar. Biol. 111, 37-44. 135

Palomera, I., Olivar, M.P., Salat, J., Sabates, A., Coll, M., Garca A., Morales-Nin, B., 2007. Small pelagic fish in the NW Mediterranean Sea : An ecological review. Progr. Oceanogr. 74 (2-3), 377-396. 133, 134

Pedrotti, M.L., 1993. Spatial and temporal distribution and recruitment of echinoderm larvae in the Ligurian Sea. J. Mar. Biol. Assoc. U.K. 73, 513-530. 135

Petrenko, A., 2003. Variability of the circulation features in the Gulf of Lion NW Mediterranean Sea. Importance of inertial currents. Ocean. Acta. 26, 323-338. 10, 11, 12, 34, 46, 72, 133, 151, 152, 160

Petrenko, A., Leredde, Y., Marsaleix, P., 2005. Circulation in a stratified and wind-forced Gulf of Lions, NW Mediterranean Sea : in-situ and modeling data. Continent. Shelf. Res. 25, 7-27. 4, 12, 27, 34, 49, 64, 76, 133, 136, 152, 160

Petrenko, A., Dufau, C., Estournel, C., 2008. Barotropic eastward currents in the western Gulf of Lion, north-western Mediterranean Sea, during stratified conditions. J. Mar. Syst. 74, 406-428. 4, 12, 17, 27, 75, 76, 136

Poulain, P.M., 2008. Integration of Lagrangian observations into a Mediterranean Marine Observatory, Towards an integrated system of Mediterranean marine observatories. N° 34 in *CIESM Workshop Monographs* [F. Briand, Ed.], 144 pages, Monaco. 142

Rubio, A., Taillandier, V., Garreau, P., 2009. Reconstruction of the Mediterranean Northern Current variability and associated cross shelf transports in the Gulf of Lions from satellite tracked drifters and model outputs. J. Mar. Syst. 78(Suppl. 1), s63-s78. 151

Sentchev, A. and Korotenko, K., 2007. Modelling distribution of flounder larvae in the eastern English Channel : sensitivity to physical forcing and biological behaviour. Mar. Ecol., Prog. Ser. 347, 233-245. 132, 136

Speirs, D.C., Gurney, W.S.C., Heath, M.R., Horbelt, W., Wood S.N., Cuevas, B.A., 2006. Ocean-scale modelling of the distribution, abundance, and seasonal dynamics of the copepod *Calanus finmarchicus*. Mar. Ecol., Prog. Ser. 313, 173-192. 133

Tugores, M.P., Iglesias, M., Diaz, N., Onate, D., Miquel, J., Giraldez, A., 2010. Latitudinal and interannual distribution of the European anchovy (*Engraulis encrasicolus*) and sardine (*Sardina pilchardus*) in the western Medi-

terranean, and sampling uncertainty in abundance estimates. ICES J. Mar.

Sci.

160

EGU (2009) Poster : Coastal (sub)Mesoscale Eddies in the Gulf of Lion

Hu, Z.Y., Doglioli, A.M., Petrenko, A., Marsaleix, P., Dekeyser, I. Coastal (Sub)Mesoscale Eddies in the Gulf of Lion. *EGU meeting, Vienna, Austria.* YSOPP Poster Award of the Ocean Sciences Division for EGU 2009.

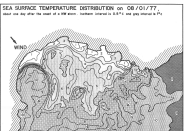# Coastal (sub)Mesoscale Eddies in the Gulf of Lion

Ziyuan Hu[1], Andrea M. Doglioli[1], Anne Petrenko[1], Patrick Marsaleix[2], Ivan Dekeyser[1] and, LATEX group

[1] Aix-Marseille Université; CNRS; LOPB-UMR 6535, OSU/Centre d'Océanologie de Marseille
[2] Laboratoire d'Aérologie – CNRS et Université Paul Sabatier

Introduction
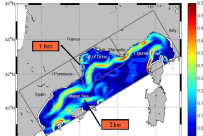
Millot [1982] was pioneer in observing an anticyclonic circulation in the western part of the Gulf of Lion (GoL), following upwelling phenomena and an offshore drift of surface water.

Sea surface temperature (AVHRR) August 1, 1977 at about 09 00 TU. [Millot 1982]

Numerical Modeling

We used the SYMPHONIE numerical model [Marsaleix et al, 2008]. Starting from a regional model (Northwestern Mediterranean, 3-km resolution), we implemented a nested high resolution shelf-scale model (Gulf of Lion, 1-km resolution) and we tested the spatial grid resolution and a new horizontal diffusion scheme.

Horizontal slice of the modeled speed intensity on July 25, 2001 at 20-m depth for 3-km and 1-km (in the GoL). [Hu et al., 2009]

We use the technique developed by Doglioli et al.[2007], based on wavelet analysis of horizontal slices of relative vorticity to identify and follow the eddy structure and to measure its area.
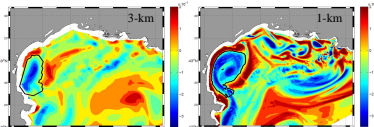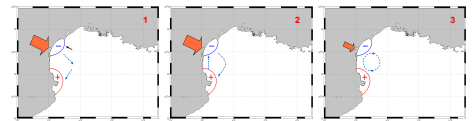

Sensitivity study on the model resolution: Simulated horizontal field of relative vorticity [s^{-1}] of 3-km resolution (left) and of 1-km resolution (right), on July 25, 2001 at 20-m depth. The black contour is the identification of the eddy structure issued from the wavelet analysis [Hu et al., 2009]. For the sensitivity study on the horizontal diffusion, please see [Hu et al., 2009].
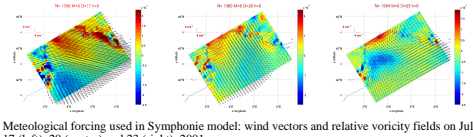
Abstract

The Lagrangian Transport Experiment (LATEX) project (2008-2011) has been initiated in order to study the impact of (sub-) mesoscale eddies interacting with the Northern Current on the evolution of conservative or biogeochemical tracers' distributions with a combined use of satellite data, numerical modeling, and Eulerian and Lagrangian in situ measurements.
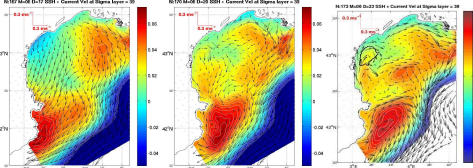
Eddy generation process

Schematic representation of the anticyclonic eddy generation process: wind forcing (orange arrow); sea surface level (red or blue zone); surface current (blue dash arrow) and bottom current (black solid arrow).

Numerical illustration

Meteological forcing used in Symphonie model: wind vectors and relative voricity fields on July 17 (left), 20 (center) and 23 (right), 2001.
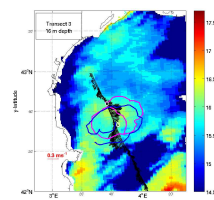

Simulated sea surface height and surface current vectors on July 17 (left), 20 (center) and 23 (right), 2001; the black contour on July 23, issued from the wavelet analysis, identifies the 'birthday' of the eddy.

in situ observations (Cruise Latex08)

The Cruise Latex08 (September 1-6, 2008) was launched in order to confirm and to identify eddies in the western side of the GoL.

Sea surface temperature (AVHRR: Météo-France) on Sept. 2, 2008; horizontal current measured by ADCP along the transect 3 at 16 m depth on Sept. 5, 2008; trajectories of floating buoys from Sept. 5 to 8, 2008 with their inital positions (white o).

The buoys accomplished the complete circle in around 5 days with a displacement velocity of around 30 cm/s. The eddy radius is in the range: 20-30 km.
Nencioli et al. [2008] showed that we can determine the eddy center position by using transect ADCP data.
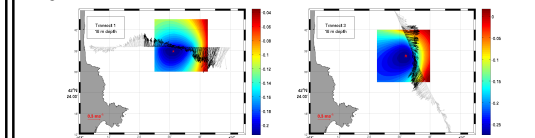
Estimated positions of the center of anticyclonic eddy at 16-m depth (red *) for Transect 1 (left) and Transect 3 (right). The colored areas are divided into a 30x30 grid. Tangential components of the black vectors are computed for each point within the grid. The center of the eddy is defined as the point for which the mean absolute value of tangential velocity is maximal. Isopleths indicate values of equal mean tangential velocity.

Conclusions:

The sensitivity study on model resolution and horizontal diffusion allows us to find the best model setup to reproduce (sub) mesoscale eddies in the GoL.
With this model setup, from the numerical results, we propose a hypothesis for the generation process of this simulated anticyclonic eddy.
The cruise Latex08 confirmed the presence of an anticyclonic eddy.

Perspectives:

Simulations will be run for a long period (2001-2008) to obtain annual variability and statistics on coastal eddies.
Combined with the data from the next cruises (Latex09 and Latex2010), we will quantify the role of these (sub) mesoscale eddies on the shelf-offshore exchanges in the GoL.

Bibliography

Doglioli A.M., Blanke B., Speich S., Lapeyre G. (2007), *Tracking coherent structures in a regional ocean model with wavelet analysis: application to Cape Basin Eddies*, J. Geophys. Res., 112, C05043.
Hu Z.Y., Doglioli A. M., Petrenko A. A., Marsaleix P., Dekeyser I. (2009), *Numerical Simulation of mesoscale eddies in the Gulf of Lion*. Ocean Modelling, 20, 203-208
Millot, C. (1982), *Analysis of upwelling in the Gulf of Lions*, in: Hydrodynamics of semi-enclosed seas, Nihoul (Ed).
Marsaleix P., Auclair F., Floor J. W., Herrmann M. J., Estournel C., Pairaud I., Ulses C. (2008), *Energy conservation issues in sigma-coordinate free-surface ocean models*. Ocean Modelling, 20, 61-89.
Nencioli, F., Kuwahara, V.S., Dickey, T.D., Rii, Y.M., Bidigare, R.R., (2008). *Physical dynamics and biological implications of a mesoscale eddy in the lee of Hawai i: Cyclone Opal observations during E-Flux III*. Deep-Sea Research Part II, 55, 10-13.

ASLO (2009) Poster : Nutrients dynamics and trophic interactions between plankton groups in a submesoscale anticyclonic eddy.

Campbell, R., Diaz, F., Ulses, C., Hu, Z.Y., Estournel, C., Petrenko, A., Doglioli, A.M., Dekeyser, I. Nutrients dynamics and trophic interactions between plankton groups in a submesoscale anticyclonic eddy. *ASLO Aquatic Sciences Meeting, Nice, France.*

Nutrients dynamics and trophic interactions between plankton groups in a submesoscale anticyclonic eddy

R. Campbell [1,2], F. Diaz [2], Z. Hu [2], C. Estournel [3], C. Ulses [3], A. Petrenko [2], A. Doglioli [2], I. Dekeyser [4]

1. ACRI ST, Sophia-Antipolis, France. 2. LOPB, Marseilles, France. 3. LA, Toulouse, France 4. COM, Marseilles, France

Introduction

The coastal ocean represents a key link between large ocean basins and the continent. In order to best understand this zone, we must study the hydrodynamic processes which transfer matter and energy between the coast and the open sea. By using a coupled biogeochemical-physical three-dimensional model, we study an eddy and describe the changes in the planktonic trophic web throughout the eddy's lifespan.
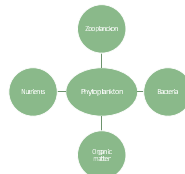
NW Mediterranean

Eddy detection zone
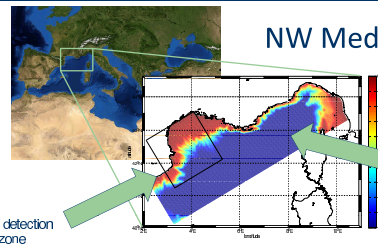
Modeled zone and bathymetry

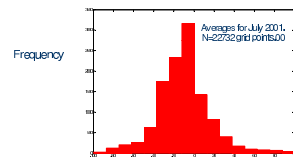## Model descriptions and preliminary validation

Biogeochemical model : Eco3M-NWMED

The biogeochemical model used is Eco3M-NWMED, which is a derivative of Eco3M, details of which are outlined in (Baklouti et al. [2006a,b]). The present model contains more variables and is adapted to the northwestern Mediterranean Sea (Hermann, 2007). The Eco3M-MED model can be considered as a multi-nutrient and multi-plankton functional types [sensu Le Quéré et al., 2005] model since its code simulates the dynamics of several biogeochemical decoupled cycles of biogenic elements and pelagic plankton groups. Taken into account by this model are the following:
- Zooplankton (meso, nano and micro) non-redfieldian ratios.
- Phytoplankton (Synechococcus, heterogeneous nanophytoplankton, diatoms) non-redfieldian ratios.
- Bacteria
- Particulate and dissolved organic matter
- Nutrients (NO_3^-, PO_4^{3-}, NH_4^+, Silicates)

Hydrodynamic model: Symphonie

The hydrodynamic model used was developed at the Pôle d'Océanographie Côtière (Estournel et al., 2005; Marsaleix et al., 2008). This model is used for regional-scale oceanographic modeling (eg Ulses et al, 2008, Petrenko et al 2005). It is based on the following hypotheses: incompressibility, Boussinesq, hydrostatic.

SeaWiFS
Point by point % error frequency: Average model vs SeaWiFS

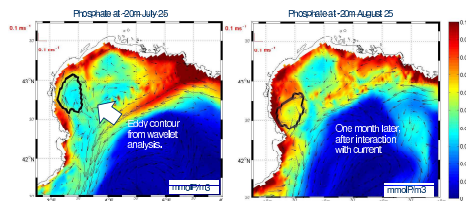Averages for July 2001. N=22732 grid points.00

Frequency

% Error

Monthly average surface chlorophyll concentrations derived from the model are compared to satellite images treated with a chlorophyll-extraction algorithm (Gohin et al, 2002.The error is comparable to the error of the satellite data when compared to in situ data at the regional level (GlobCOLOUR Validation Report, 2007).
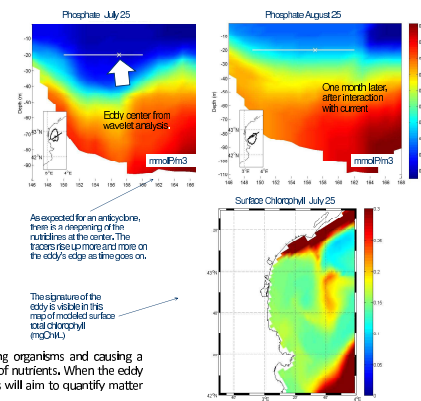
Results and Conclusions

Anticyclonic eddy:
Located using wavelet analysis
July 17 – August 28, 2001
- Diameter 40±8 km
- Salinity: 37.75
- Temperature: 21°C

Previous work (Hu, 2007) has been carried out in order to identify eddy structures in the Gulf of Lions and quantify their location, duration, and physical properties. Wavelet analysis was conducted on a horizontal slice of relative vorticity, which was calculated based on the model velocity outputs.

Vertical Structure

Phosphate July 25

Phosphate August 25

Eddy center from wavelet analysis

One month later, after interaction with current

Phosphate at -20m July 25

Phosphate at -20m August 25

Eddy contour from wavelet analysis.

One month later, after interaction with current

As expected for an anticyclone, there is a deepening of the nutriclines at the center. The tracers rise up more and more on the eddy's edge as time goes on.

The signature of the eddy is visible in this map of modeled surface total chlorophyll (mgChl/L)

Surface Chlorophyll July 25

Conclusions

Within the span of a few days the eddy transforms the zone by trapping organisms and causing a reduction in all classes of phytoplankton and bacteria due to predation and lack of nutrients. When the eddy interacts with the nearby current, there is an exchange of matter. Future studies will aim to quantify matter transported by the eddy.

References

Bassumi, C., Zervakis, V., Marsaleix, P., Papadoconstis, A., Audsir, F., Perlortidelis, L., Tragou, E., 2005. Dense water formation and cascading in the Gulf of Thermaikos (North Aegean), from observations and modelling. Continental Shelf Research 25, 2366–2386.
GlobCOLOUR Validation Report, 2007. www.globcolour.info
Gohin, F., Druon, J.N., and Lampert, L. 2002. A five channel chlorophyll concentration algorithm applied to SeaWiFS data processed by SeaDAS in coastal waters. Intl. J. Rem. Sens., 23(8): 1639 – 1661.
Hu, Z., 2007. Sur les structures tourbillonnaires et filamentaires dans le Golfe du Lion, avec la teoric des ondelettes. Masters thesis, Universite de la Mediterranee, Aix-Marseille II.46p.
Marsaleix, P., Auclair, F., Floor, J.-W., Hermann, M., L., Estournel, C., Pairaud, I., Ulses, C., 2008. Energy conservation issues in sigma-coordinate free-surface ocean models. Ocean Modelling 20, 61-89.
Petrenko et al., 2005. A. Petrenko, Y. Leredde and R Marsaleix. Circulation in a stratified and wind-forced Gulf of Lions, NW Mediterranean Sea: in situ and modeling data. Continental Shelf Research 25 (2005), pp. 7-27
Ulses, C., C. Estournel, P. Puig, X. Durrieu de Madron, and P. Marsaleix, 2008. Dense shelf water cascading in the northwestern Mediterranean during the cold winter 2005: Quantification of the export through the Gulf of Lion and the Catalan margin. Geophysical Research. Letters 35, L07610.

Contact
rose.campbell@univmed.fr
www.com.univ-mrs.fr/~campbell